ACS NANOSCIENCE Au
AN OPEN ACCESS JOURNAL OF THE AMERICAN CHEMICAL SOCIETY

pubs.acs.org/nanoau
Review

Nanocomposites Based on Magnetic Nanoparticles and Metal−Organic Frameworks for Therapy, Diagnosis, and Theragnostics

Darina Francesca Picchi, Catalina Biglione, and Patricia Horcajada*

Cite This: ACS Nanosci. Au 2024, 4, 85−114
Read Online

ABSTRACT: In the last two decades, metal−organic frameworks (MOFs) with highly tunable structure and porosity, have emerged as drug nanocarriers in the biomedical field. In particular, nanoscaled MOFs (nanoMOFs) have been widely investigated because of their potential biocompatibility, high drug loadings, and progressive release. To enhance their properties, MOFs have been combined with magnetic nanoparticles (MNPs) to form magnetic nanocomposites (MNP@MOF) with additional functionalities. Due to the magnetic properties of the MNPs, their presence in the nanosystems enables potential combinatorial magnetic targeted therapy and diagnosis. In this Review, we analyze the four main synthetic strategies currently employed for the fabrication of MNP@MOF nanocomposites, namely, mixing, *in situ* formation of MNPs in presynthesized MOF, *in situ* formation of MOFs in the presence of MNPs, and layer-by-layer methods. Additionally, we discuss the current progress in bioapplications, focusing on drug delivery systems (DDSs), magnetic resonance imaging (MRI), magnetic hyperthermia (MHT), and theragnostic systems. Overall, we provide a comprehensive overview of the recent advances in the development and bioapplications of MNP@MOF nanocomposites, highlighting their potential for future biomedical applications with a critical analysis of the challenges and limitations of these nanocomposites in terms of their synthesis, characterization, biocompatibility, and applicability.

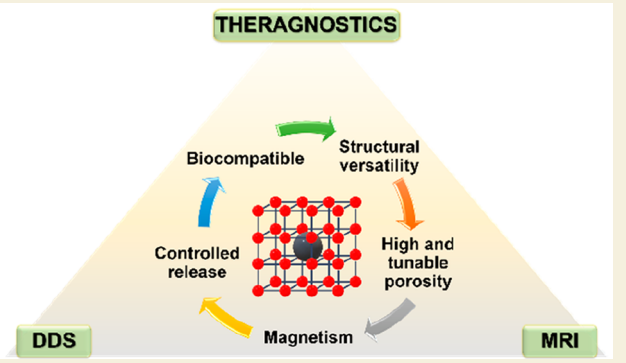

KEYWORDS: *magnetic nanoparticles, metal−organic frameworks, magnetic MOF composites, MNP@MOF, nanomaterials, bioapplication, drug delivery systems, magnetic resonance imaging, theragnostic*

1. INTRODUCTION

Since 2006, metal−organic frameworks (MOFs) have been exponentially investigated in the biomedical field,[1−6] where they have been proposed as imaging agents[7] and drug carriers.[8] These materials are coordinative networks, based on metallic inorganic subunits (e.g., chains, clusters, atoms) and organic bridging ligands (Figure 1), with crystalline architectures, presenting a high and tunable porosity and structural versatility.[9−11] In this sense, their properties make them promising candidates in several biomedical areas such as drug delivery systems (DDSs),[5,12,13] biosensing,[14,15] antimicrobial therapy,[16,17] biomedical imaging,[2] phototherapy,[18,19] and theragnostics,[20,21] among others.[11,22]

An important consideration for the biomedical application of MOFs is their safety; it is crucial to ensure and evaluate the synthetic route and the final chemical composition taking into account that the solvents, metal ions, and organic ligand precursors could possess potential toxicity.[23] Thus, the selection of safe and biocompatible metal and ligand

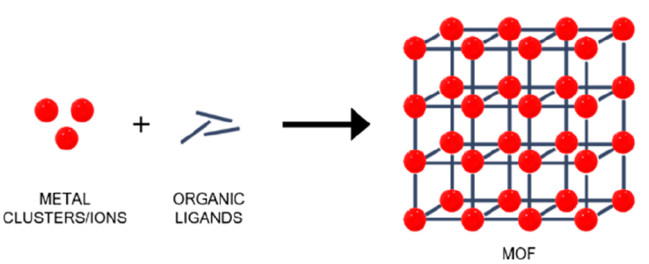

Figure 1. Schematic representation of MOF structure.

Received: August 21, 2023
Revised: November 29, 2023
Accepted: November 29, 2023
Published: December 23, 2023

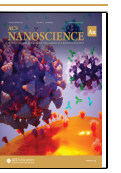

https://doi.org/10.1021/acsnanoscienceau.3c00041
ACS Nanosci. Au 2024, 4, 85−114

precursors is very important.[24] Furthermore, the size, morphology, and surface properties of the MOF are of pivotal relevance both for its biosafety and efficacy.[20,24] Indeed, the main features in MOFs as DDSs are the biocompatibility, porosity available for drug loading, and controlled release at the targeted site, which are closely related to its physicochemical properties and dimensions. For instance, intravenous administration generally necessitates a size below 200 nm; therefore, the nanoscale design, encompassing factors such as size, shape, and surface functionalization, can influence the capacity for cell-specific targeting and subsequent cellular uptake.[25] Furthermore, particles smaller than 250 nm have been reported to exhibit a higher likelihood of extravasation through leaky endothelium via the enhanced permeability and retention (EPR) effect, a characteristic fundamental for deposition in the tumor targeting site.[25,26] Additionally, the clearance route is affected by the size: nanoparticles larger than 200 nm in diameter are preferentially cleared by the reticuloendothelial system, whereas those smaller than 10 nm are eliminated by renal filtration.[25] In this context, nanoscaled MOFs (nanoMOFs) have attracted great attention in this matter because of their optimal size. Moreover, they can be tuned not only to target a particular administration route and safety but also the biodistribution.[27−30]

In addition to the advantageous properties of nanoMOFs, incorporating guest materials into MOFs, thereby forming MOF nanocomposites, presents a promising avenue for enhancing the performance of these structures in the realm of nanomedicine. Currently, there is a growing body of reviews that recognize the importance of improving MOF properties with the integration of organic polymers,[31−33] enzymes,[34,35] metals and metal oxides,[36,37] silica,[38] polyoxometalates,[39] quantum dots,[40,41] and carbons,[42,43] among others.[44] In this regard, MOF nanocomposites are becoming particularly promising as DDSs, by associating nanoMOFs with different nanometric (inorganic, organic) species[44,45] that will provide them with additional relevant properties (targeting, furtivity, therapeutic effect, imaging, etc.).[20,21]

Of particular relevance are the composites based on nanoMOFs and magnetic nanoparticles (MNPs).[46−48] In the biomedical field, MNPs are mainly represented by magnetite (Fe_3O_4), maghemite (γ-Fe_2O_3), and some ferrite colloids which typically have a hydrodynamic size below 100 nm.[49] Given the enormous variability in their synthesis, their physicochemical properties (*e.g.*, size, shape, structure, surface charge, magnetism) are tuned for a multitude of applications, such as magnetically guided nanoparticles for drug delivery,[50,51] magnetofection (gene delivery),[50,52] magnetic hyperthermia,[53,54] magnetic resonance imaging (MRI)[55−57] or magnetic particle imaging (MPI),[58] and magnetic separation (cell separation, cell sensing, biosensing, etc.).[59] Combining these relevant properties with those of MOFs (*e.g.*, porosity, versatility) makes the resulting composites excellent candidates to be used in advanced drug delivery, nanothermometry, biosensing, bioimaging, and MRI contrast agents. A series of iron oxide nanoparticles with biocompatibility and nontoxicity are currently commercialized.[60,61] Despite the noteworthy advancements in MNPs and their significant clinical implications,[61−63] applying a nanocomposite system that harnesses the combined properties of MNPs and nanoMOFs introduces a compelling approach for augmenting the properties of both components while ensuring enhanced biocompatibility and potential efficacy for theragnostic applications.

Thus, here we will review the recent progress in the development of magnetic composites (MNP@MOF) based on MOFs and MNPs, specifically Fe-MNPs, discussing the main synthetic approaches and their challenging characterization with special attention to biomedical-related considerations, considering mainly nanocomposites (<500 nm) and the most significant submicron-sized composites (>500 nm). Further, the most relevant bioapplications of the MNP@MOF composites reported recently will be critically described, identifying their main advantages and limitations.

2. SYNTHETIC APPROACHES FOR MAGNETIC METAL−ORGANIC FRAMEWORK COMPOSITES

To combine MNPs with MOFs, four main strategies have been traditionally employed depending on the synthetic route of the final composite: (1) mixing, where the composite is formed by simply putting in contact previously synthesized magnetic particles and MOF crystals,[64] (2) *in situ* formation of MNPs in the presence of preformed MOFs, (3) *in situ* synthesis of the MOF in the presence of magnetic particles, and (4) layer-by-layer, using functionalized nucleation sites to grow step-by-step the MOF by repeated cycles.[65] Furthermore, it is important to highlight that different morphologies can be obtained such as core−shell and non-core−shell structures (Figure 2). In a

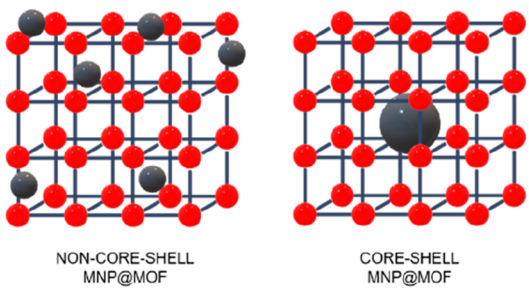

Figure 2. Schematic representation of the non-core−shell and core−shell MNP@MOF composites.

core−shell composite, the MOF acts as the shell surrounding a single nanoparticle core material. Therefore, the core material in the case of MNP@MOF nanocomposites is the MNP and this configuration provides unique properties and synergistic effects between the core and shell components. In contrast, a non-core−shell MOF composite refers to a structure where the MNPs are randomly distributed, resulting in a heterogeneous composite with the MOF and the additional MNPs allocated throughout the composite structure, either within the framework and/or on the outer surface.

Overall, in the following section, the synthetic procedures are illustrated following the above classification, considering their architectural configuration.

2.1. Mixing

The simplest approach is the mixing method, which involves the interaction of both presynthesized MNPs and MOFs (Figure 3). The final composite is thus exclusively based on the stability of the interactions between the two components.[64]

Only a few examples are reported so far, mainly involving mesoporous iron(III) trimesate MIL-100(Fe)[66] or chromium-(III) terephthalate MIL-101(Cr)[67] (MIL, Material Institut Lavoisier) as MOF, selected by their high porosity (up to S_{BET}

https://doi.org/10.1021/acsnanoscienceau.3c00041
ACS Nanosci. Au 2024, 4, 85−114

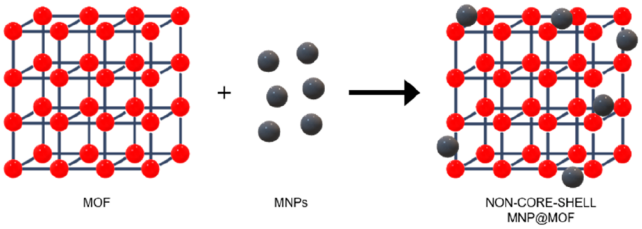

Figure 3. Schematic representation of the mixing strategy.

~ 3000 $m^2 \cdot g^{-1}$) and chemical robustness. Despite the *in vivo* proven biosafe character of MIL-100(Fe),[68] chromium-based materials (even if based on Cr(III)) are considered potentially toxic,[66] ruling out its interest in the biomedical field. However, MIL-101(Cr) is a benchmarked MOF widely proposed as a model in many fields due to its exceptional chemical stability. Indeed, the first synthesis of a magnetic MIL-101(Cr) composite by the mixing approach was reported in 2012, when Huo et al. described the formation of a Fe_3O_4@SiO_2-MIL-101(Cr) composite.[69] For the synthesis, silica-coated iron oxide microparticles (Fe_3O_4@SiO_2, ~ 600 nm with about 30 nm of silica shell) and MIL-101(Cr) submicrometric crystals (~650 nm) were dispersed in an aqueous solution under ultrasonication for 20 min. The negatively charged silica-coated Fe_3O_4 favored the electrostatic interactions with the positively charged MIL-101(Cr), leading to a microsized Fe_3O_4@SiO_2 assembled onto the external surface of the MIL-101(Cr) crystals. The silica coating, with an average thickness of about 30 nm, is required not only for preventing iron oxide corrosion and oxidation but also to favor the static electric interactions with the MOF. The saturation magnetization (M_S) value for Fe_3O_4@SiO_2-MIL-101(Cr) was 21 $emu \cdot g^{-1}$ (vs 76 and 38 $emu \cdot g^{-1}$ for Fe_3O_4 and Fe_3O_4@SiO_2, respectively), keeping the magnetic property for the desired magnetic solid-phase extraction aim. Critically, in this first work, the composite has unsteady characteristics based on too weak interactions between two enormous components attracted to each other in an insufficiently stable structure. In consideration of the pore size and the substantial dimensions of the MNPs, it is evident that these entities are predominantly located on the surface. The concept behind this work was further improved by reducing the size of the MNPs, which will interact more effectively with the MOF surface. Thus, Qian and co-workers[70] promoted the interaction between the here biocompatible iron version of MIL-101(Fe) (~700 nm) and Fe_3O_4 in deionized water by increasing the pH up to 8 with a NaOH solution, which switches the ζ-potential of the MNPs from positive to negative. Even if the Fe_3O_4 nanoparticles presented an average size of ~10−30 nm, through this method, the MNPs were restricted to the outermost layer. The resulting magnetic composite (M_S ~ 26 vs 46 $emu \cdot g^{-1}$ for Fe_3O_4) exhibited a powder X-ray diffraction (PXRD) pattern matching well with the indexed peaks of the Fe_3O_4, and some other peaks consistent with the MIL-101(Fe) structure. However, the majority of the diffraction peaks of the MOF were indistinguishable from the background. This result was attributed to the cover effect of the MNPs, but one could also consider a potential degradation of the Fe carboxylate MOF under basic pH (pK_a carboxylic acids ~3−5 vs pH = 7.4), as previously reported for MIL-100(Fe).[71]

Similarly, magnetic composites γ-Fe_3O_4@MIL-100(Fe) and cit-γ-Fe_3O_4@MIL-100(Fe) with maghemite (γ-Fe_3O_4, ~7−10 nm) and citrate-functionalized maghemite (cit-γ-Fe_3O_4, ~15−20 nm) were synthesized with a mean hydrodynamic diameter of about 160 nm from dynamic light scattering (DLS) analysis.[72] The nanocomposite, showing PXRD peaks of the MIL-100(Fe) and the maghemite, was achieved by mixing the previously microwave (MW)-synthesized MIL-100(Fe) nanoparticles[73] with γ-Fe_3O_4 or cit-γ-Fe_3O_4 at pH 4.2 and 3.5, respectively. The high-resolution transmission electron microscopy (HR-TEM) images revealed MIL-100(Fe) nanoparticles (~130 nm) with a decoration on the outer surface of small aggregates of MNPs. The magnetometry experiments showed a superparamagnetic behavior. Among all the samples the cit-γ-Fe_3O_4@MIL-100(Fe) presented the highest magnetic moment with Brunauer−Emmett−Teller surface areas (S_{BET}) about 1180−1310 $m^2 \cdot g^{-1}$, not significantly reduced compared to S_{BET} ~ 1330 $m^2 \cdot g^{-1}$ of the initial MIL-100(Fe).

In conclusion, the mixing synthetic method is however underdeveloped because, in spite of its simplicity, it has poor control over the final properties of the composite and the association is exclusively based on the formation of weak interactions (mainly electrostatic attraction). Therefore, it results in a lack of preference for MNPs on their directionality within pores or the outer surface of MOFs. Even if the crucial size of the MNPs may be compatible with the pore dimensions of the MOF, then this would be not sufficient to avoid the partial or total presence of the MNPs on the outer surface of the MOF, leading to less stable composites with MNPs' leaching.

2.2. *In Situ* Formation of MNPs in the Presence of the MOF

Another notable pathway to obtain MNP@MOF composites is the "ship in a bottle" strategy, which consists of the *in situ* formation of the MNPs in the presence of the preformed MOF.[74] The magnetic composite is obtained by first incorporating iron ions or precursors of the MNPs in the MOF (mainly via chemical vapor infiltration, solution impregnation, and incipient wetness infiltration[75]) and then, forming the MNPs through a transformation (*e.g.*, phase and/or topotactic transformations, dehydration, reduction)[76] to iron oxide nanoparticles formation (see Figure 4). The MNPs are usually located on the MOF external surface or within the

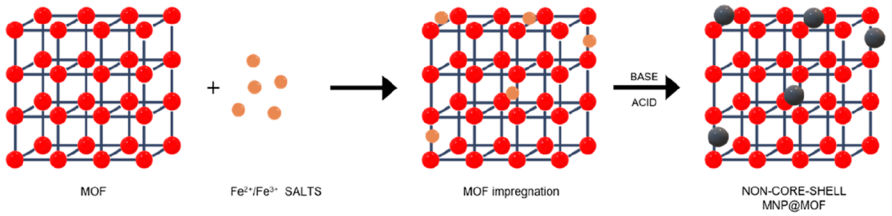

Figure 4. Schematic representation of the *in situ* formation of the MNPs in the presence of presynthesized MOF for non-core−shell MNP@MOF composites.

https://doi.org/10.1021/acsnanoscienceau.3c00041
ACS Nanosci. Au 2024, 4, 85−114

porosity, partially destroying the structure (creating defects) in case of particle size larger than the accessible pore dimension. However, this insertion of defect points in the framework is a hard equilibrium to control, in order to avoid the structure collapse. Otherwise, in the optimiztic and more desired case, the MNPs are well-dispersed inside the MOF,[75] being advantageously protected from degradation or leaching.

In this sense, Wu et al.[77] originally proposed this "ship in a bottle" method to prepare γ-Fe_2O_3@ZIF-8 and γ-Fe_2O_3@MIL-53(Al) composites using rigid microporous zinc(II) 2-methylimidazolate ZIF-8 (ZIF = Zeolite Imidazolate Framework; ~200 nm and S_{BET} ~ 1800 $m^2 \cdot g^{-1}$)[78] and flexible microporous aluminum(III) terephthalate MIL-53(Al) (S_{BET} ~ 1500 $m^2 \cdot g^{-1}$ in the open form structure).[79] The $Fe(acac)_3$ metal precursor was infiltrated in the MOF by the incipient wetness method, and γ-Fe_2O_3 MNPs were formed by pyrolysis (300 °C under N_2 for 1 h). Then, a reduction treatment was performed to form Fe^0 (CO atmosphere at 550 °C for 1 h) and proved the formation of MNPs. The crystallinity of MOFs was retained, as shown by PXRD, and then, the magnetic composites were further investigated for drug encapsulation with the anti-inflammatory and analgesic ibuprofen. Under these conditions, the MNPs conferred a significantly lower M_S than that of pure γ-Fe_2O_3 (33.5 vs 1.8 and 6.1 emu·g^{-1} for γ-Fe_2O_3@ZIF-8 and γ-Fe_2O_3@MIL-53(Al), respectively). The γ-Fe_2O_3 particles were mainly located on the outer surface of the ZIF-8 as large agglomerates; instead, ultrafine MNPs and clusters were observed within the crystalline structure, creating a hollow structure with defects during the pyrolysis process. This fact highlights that the location of the MNPs depends on the method to insert the precursor and its motion under the pyrolysis process, which is challenging to control. In addition, the pyrolysis process could be limited by the MOF thermal stability.

The *in situ* formation of MNPs has also been employed for the preparation of Fe_3O_4@MIL-101(Cr) composite by partial reduction.[80,81] MIL-101(Cr) micrometric crystals were dispersed and sonicated for 30 min at room temperature into a $FeCl_3$ solution to favor the impregnation. The *in situ* formation of MNPs (~10−20 nm) occurred, first, with the addition of Na_2SO_3 solution dropwise. Then, NH_4OH solution was slowly added under an inert atmosphere, leading to the formation of Fe_3O_4 nanoparticles, as supported by PXRD. The final magnetic composite (M_S ~ 15.6 emu g^{-1}), with a particle size of 600−700 nm, was successfully applied in magnetic solid phase extraction (MSPE) combined with ultrahigh performance liquid chromatography-tandem mass spectrometry (UPLC-MS/MS) for the quantitation of eight nonsteroidal anti-inflammatory drugs (NSAIDs) in wastewater and environmental water samples.[80]

As reflected in the examples shown above, the difficulties of this method lay in the homogeneous diffusion of the metal precursors into the MOF and the challenging control of the *in situ* process. Moreover, the MOF stability under the *in situ* conditions is fundamental for the successful formation of the nanocomposite, being this procedure limited to high thermally and chemically robust MOFs.

2.3. *In Situ* Formation of MOF in the Presence of MNPs

One of the main approaches followed for the synthesis of magnetic nanocomposites, known as "bottle around ship", consists of the *in situ* formation of the MOF in the presence of preformed MNPs (Figure 5).[74] The MNPs could be coated

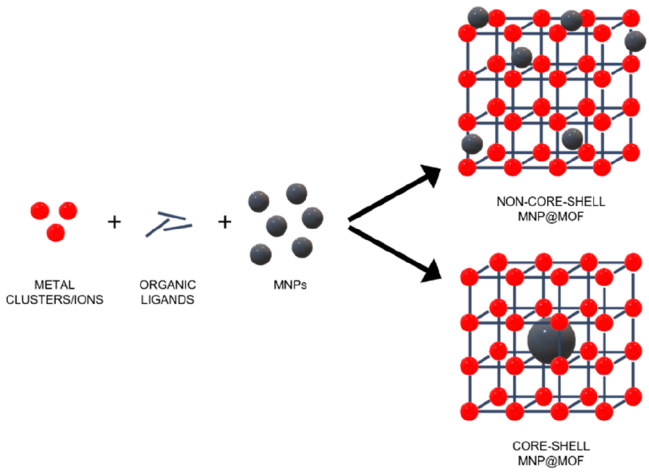

Figure 5. Schematic representation of the in situ formation of the MOF in the presence of presynthesized MNPs for non-core−shell and core−shell MNP@MOF composites.

with different functional groups, polymers, or capping agents.[74] In the following sections, the synthetic methods will be distinguished considering the final architecture (non-core−shell or core−shell) of the composite as well as the MNPs functionalization (uncoated MNP, amine or acidic-coating, etc.).

2.3.1. Non-core−Shell Magnetic Composites.

In the non-core−shell magnetic architecture, the MOF grows in the presence of preformed MNPs, leading to a composite where MNPs are often randomly distributed in/on the MOF.

2.3.1.1. Synthesis of Magnetic Composites with Non-functionalized MNPs. The complex structure of a magnetic nanocomposite can be obtained from the simplest uncoated MNPs, by interacting with the MOF precursors or being incorporated into the porosity that arises as the MOF grows.[82,83]

In this matter, Lohe and collaborators[84] explored the benchmarked microporous copper(II) trimesate HKUST-1 (HKUST = Hong Kong University of Science and Technology; S_{BET} ~ 600−1600 $m^2 \cdot g^{-1}$)[85,86] together with other two MOFs, aluminum(III) 2,6-naphthalenedicarboxylate (DUT-4; DUT = Dresden University of Technolog; S_{BET} ~ 1000−1300 $m^2 \cdot g^{-1}$) and aluminum(III) biphenyl-4,4′-dicarboxylate (DUT-5; S_{BET} ~ 1200−1700 $m^2 \cdot g^{-1}$),[87−89] as an efficient method for magnetically controlled catalyst separation. In this work, the magnetic composites were also studied as model systems for heating-trigger desorption of drug molecules by an external alternating magnetic field (AMF). In the synthesis, MNPs (spherical, ~ 10−20 nm) were added to the organic ligand solution in *N*,*N*-dimethylformamide (DMF). Then, to obtain DUT-4 and DUT-5, an aluminum precursor ($Al(NO_3)_3 \cdot 9H_2O$) was added also in DMF and the mixtures were heated at 180 °C for 24 h in an autoclave. For the preparation of magnetic HKUST-1, $Cu(OAc)_2 \cdot H_2O$ was mixed with the previous MNP/ligand solution and altogether refluxed for 12 h under stirring. The composites exhibited high surface areas within the range of reported values (1394, 1346, and 1248 $m^2 \cdot g^{-1}$ for the HKUST-1, DUT-4, and DUT-5 composites, respectively). Remarkably, all the composites showed magnetic properties, since they were collected through an external magnet. In the case of the magnetic HKUST-1 composite, it was characterized under a magnetic field of 1.7 kA·m^{-1} at a

https://doi.org/10.1021/acsnanoscienceau.3c00041
ACS Nanosci. Au 2024, 4, 85−114

frequency of 183 kHz, presenting a specific absorption rate (SAR) of 11.1 $W \cdot g^{-1}$. Despite the relatively low SAR value, the magnetic HKUST-1 composite showed an accelerated release rate of ibuprofen as the temperature increased under the AMF, representing the first proof of concept of a MOF magnetic nanocomposite demonstrating improved drug release under heating by AMF.

Another example of catalytic application was recently reported by Zamani and colleagues,[90] developing a magnetic porphyrin-loaded MOF. The Fe_3O_4@CoTHPP@UiO-66 composite, based on the robust microporous zirconium(IV) terephthalate UiO-66 (UiO = University of Oslo; CoTHPP-(OAC) = meso-tetrakis(4-hydroxyphenylporphyrinato) cobalt-(II)).[91] The resulting nanocomposite (~400 nm) was prepared by a one-step solvothermal route, first dispersing the MNPs in DMF, then the MOF precursors ($ZrCl_4$ and terephthalic acid) and the desired porphyrin (CoTHPP), for finally carrying out the solvothermal reaction at 120 °C for 24 h in the presence of glacial acetic acid as the modulator. The magnetic nanocomposite formation was confirmed by PXRD and by the magnetization curve (10 $emu \cdot g^{-1}$), presenting a surface area reduced from for the parent UiO-66 (S_{BET} 732 vs 1380 $m^2 \cdot g^{-1}$). The MNPs permitted an easy, low energy and short-time consumption recovery magnetic separation of the composite that improved its reusability as a catalyst, using it for the epoxidation of olefins and allylic alcohols with a yield of the reaction up to 95% and 5 cycles-reusability.

As shown in these examples, the non-core−shell structures based on uncoated MNPs present *a priori* an absence of specific MNPs-MOF interactions, leading to some associated issues. For instance, it could lead to the segregation of the MOF formation, obtaining mixtures of pure components and not composites. Also, the uncoated MNPs usually tend to aggregate in the reaction mixture, leading to the formation of heterogeneous composites. In this sense, solvothermal reactions are usually carried out without stirring, generally preventing a good MNPs dispersion. Finally, the reaction conditions for the preparation of the MOFs should be compatible with the MNPs' stability, limiting the number of suitable MOF structures (generally synthesized under acidic conditions and highly complexant species that could dissolve the MNPs).[92]

2.3.1.2. Synthesis of Magnetic Composites Using with Acid-Functionalized MNPs. An interesting approach to prevent MNPs aggregation and promote specific MNPs-MOF interactions is the MNPs' surface functionalization with acidic or other groups, which can be also regulated in terms of the length of the hydrocarbon chain.

In this sense, Schejn et al.[93] proposed the addition of citrate-capped Fe_3O_4 nanoparticles to form Fe_3O_4@ZIF-8. The citrate-capped Fe_3O_4 nanoparticles and the 2-methyl-1*H*-imidazole ligand (HmIM) were dispersed in water. Then, an aqueous solution of the $Zn(NO_3)_2$ was added, forming the composite at room temperature after only 10 min with a particle size of ~250 nm. The specific surface area and the pore volume (S_{BET} ~ 1856 vs 871 $m^2 \cdot g^{-1}$; 0.71 vs 0.35 $m^3 \cdot g^{-1}$)[78] decreased for the Fe_3O_4@ZIF-8 with respect to ZIF-8, and was justified by the TEM-based location of the MNPs (~10 nm) at the MOF surface, blocking the cavities. The PXRD analysis confirmed the formation of the ZIF-8 and the presence of the Fe_3O_4 nanoparticles. The formation of the composite was favored by the presence of carboxylate groups, which can interact weakly with the MOF precursors (imidazolate and metal ions). Additionally, a more complex composite based on ZIF-8 and ZIF 67 (>450 nm) was synthesized based on citrate-capped Fe_3O_4.[94] The authors introduced the MNPs in the solution of HmIM, adding then the Zn^{2+} solution. After 6 h, HmIM solution was added again. In this way, first, the MOF shell of ZIF-8 was produced, then with $Co(NO_3)_2 \cdot 6H_2O$, HmIM, and folic acid (FA) was obtained a second MOF shell (ZIF-67) functionalized with FA (Fe_3O_4@ZIF-8@ZIF-67/FA). TEM images showed that MNPs (~6 nm) were dispersed in the ZIF-8 structure (~400 nm), and the ZIF-67 shell (~50 nm) maintained the same morphology. In the final composite Fe_3O_4@ZIF-8@ZIF-67/FA, the FA produced agglomerated flower-like structures, desired for the DD purpose. The observed PXRD diffraction peaks for the composites were attributed to the MNPs, ZIF-8, and ZIF-67. However, after the drug encapsulation of a model antitumoral drug (quercetin, Q), the PXRD pattern of Fe_3O_4@ZIF-8@ZIF-67/FA/Q was broadened. The surface areas varied from 42 $m^2 \cdot g^{-1}$ for Fe_3O_4 to 1994, 1203, and 259 $m^2 \cdot g^{-1}$ for Fe_3O_4@ZIF-8, Fe_3O_4@ZIF-8@ZIF-67/FA, and Fe_3O_4@ZIF-8@ZIF-67/FA/Q, respectively, indicating first the MOF porosity contribution, then, the presence of the FA functionalization, and, finally, the drug loading.

Certainly, these examples evidence the challenging control of the MNPs position (e.g., core−shell) in the MOF. Indeed, the functionalization over the MNPs surface may not only establish bonds with the MOF precursors but also the MNPs have to promote the growth of the MOF over them as nucleation seeds.

2.3.1.3. Synthesis of Magnetic Composites Using Polymer-Functionalized MNPs. Another interesting approach to accomplish the composite formation is using surface-engineered MNPs in order to avoid their aggregation, favoring their easy dispersion in solution. The surface functionalization has been mostly based on polymers, such as polyvinylpyrrolidone (PVP) or polystyrenesulfonate (PSS), among others, which could present additional functionalities (*e.g.*, −COOH, poly(dopamine)-PDA) that might help the MOF formation.

On this matter, Fang and colleagues[95] synthesized magnetic MOF nanoparticles based on the ZIF-90 structure, based on zinc and the imidazolate-2-carboxyaldehyde (2-ICA) ligand (S_{BET} ~ 1103−1297 $m^2 \cdot g^{-1}$).[96] The composite was prepared by mixing polyvinylpyrrolidone (PVP)-coated MNPs (Fe_3O_4@PVP, 12 nm) with 2-ICA,= and then immediately pouring the $Zn(NO_3)_2$ into the solution for finally heating at 90 °C for 18 h. The dried MNP@MOF nanocomposite (~64 nm) was attracted by an external magnet, determining a decrease in saturation magnetization from 32 to 7 $emu \cdot g^{-1}$ in the magnetic nanocomposite due to the MOF presence. Interestingly, the nanocomposites indexed ZIF-90 and Fe_3O_4 peaks in the PXRD pattern and presented a kind of core−shell structure, being several MNPs located in the center of the ZIF-90 particles, as evidenced by TEM.

Another non-core−shell structure was also developed using ZIF-90 and (PDA)-coated MNPs (Fe_3O_4@PDA@ZIF-90).[97] Briefly, an ethanolic $Zn(NO_3)_2$ solution was put in contact first with an aqueous solution of Fe_3O_4@PDA nanoparticles, recovering magnetically the MNPs, to then, add the 2-ICA solution. Then, $Zn(NO_3)$, trioctylamine, and 2-ICA solutions were poured in regular intervals until all the precursors' solutions were added and continuously reacted. Trioctylamine, a tertiary amine with large alkyl substituents, can act as both a deprotonating agent and a surfactant, facilitating the nucleation

https://doi.org/10.1021/acsnanoscienceau.3c00041
ACS Nanosci. Au 2024, 4, 85−114

and growth of the MOFs.[96] The product was recovered magnetically, having a saturation magnetization of 9.3 emu·g^{-1} (vs 22.5 and 17.3 emu·g^{-1} for Fe_3O_4 and Fe_3O_4@PDA, respectively). Fe_3O_4@PDA@ZIF-90 exhibited the characteristic peaks of ZIF-90 in PXRD, with however almost no visible peaks corresponding to the MNPs, probably due to the small proportion within the composite. The TEM images clearly showed a non-core−shell structure of about 200 nm, with narrow size distribution and well-dispersion evidenced by DLS, with an agglomeration of the PDA-coated MNPs (∼170 nm) and about 20−30 nm of ZIF-90 growth.

ZIF-8 was also extensively studied here because of its simple and versatile synthesis which allows a fine-tuning of its properties.[78,98] In this regard, Pang and co-workers[99] proposed a Fe_3O_4@ZIF-8 composite (∼150 nm) based on poly(acrylic acid) (PAA) grafted MNPs (Fe_3O_4@PAA, ∼10 nm). The reaction at room temperature involved an aqueous solution of HmIM and Fe_3O_4@PAA nanoparticles, bearing carboxylate groups on their outer surface to prevent aggregation. Then, Zn^{2+} was added, coordinating with these carboxylate groups and subsequently forming the desired MOF composite, with a saturation magnetization in the range of 0.56−4.35 emu·g^{-1}, depending on the Fe_3O_4 content. While the high purity of the resulting magnetite-based nanocomposite was supported by PXRD, the TEM images showed the presence of several MNPs grafted at the surface and also embedded into the MOF.

A noteworthy alternative approach based on ZIF-8 was developed by Zhong et al.,[100] presenting a composite called *Void n*Fe_3O_4@Pd@ZIF-8@ZIF-8, featuring an empty internal cavity. In the multistep synthesis, MNPs were initially combined with polystyrene-*co*-acrylic acid (PS-*co*-AA) nanospheres to produce Fe_3O_4/PS nanospheres. Then, these nanospheres were dispersed in a MeOH solution containing ZIF-8 precursors at room temperature for 3 h. Subsequently, Pd nanoparticles were encapsulated within Fe_3O_4/PS@ZIF-8 using an impregnation method, resulting in Fe_3O_4/PS@Pd@ZIF-8. An additional shell of ZIF-8 was created using a similar procedure. Finally, the PS core was removed from Fe_3O_4/PS@Pd@ZIF-8@ZIF-8 through DMF treatment to create the internal cavity, leading to the final nanocomposite, *Void n*Fe_3O_4@Pd@ZIF-8@ZIF-8. The crystal structure of the composite was confirmed through PXRD. TEM and SEM images revealed a non-core−shell structure with multiple MNPs homogeneously dispersed within the MOF internal surface rather than forming a single core. Notably, the synthesis method facilitated the controlled distribution of MNPs and subsequent Pd nanoparticles. The sizes of Fe_3O_4/PS, Fe_3O_4/PS@Pd, and *Void n*Fe_3O_4@Pd@ZIF-8@ZIF-8 were approximately 410, 450, and 520 nm, respectively. The porous nature of the material exhibited variations in S_{BET}, with values of 192, 62, 306, and 523 m^2·g^{-1} for Fe_3O_4/PS@ZIF-8, Fe_3O_4/PS@Pd@ZIF-8, Fe_3O_4/PS@Pd@ZIF-8@ZIF-8, and *Void n*Fe_3O_4@Pd@ZIF-8@ZIF-8. Indeed, the presence of Pd nanoparticles in the final 30 nm layer affected its porosity, which is partially restored by reducing the solid phase contribution of PS nanospheres. This example represents a novel approach, utilizing a removable template that does not compromise the nanocomposite porosity. The advantage of this template lies in the controlled positioning of MNPs, a feature often absents in other cases, making it an interesting solution.

Another example based on a non-core−shell morphology was reported by Chowdhuri and co-workers,[101,102] developing the Fe_3O_4@IRMOF-3 nanocomposite. The highly porous (S_{BET} = 1568 m^2·g^{-1} and pore volume = 1.07 cm^3·g^{-1})[103] zinc aminoterephthalate IRMOF-3 (Iso Reticular MOF)[104] was solvothermally formed on MNPs. Briefly, Fe_3O_4 nanoparticles (∼10 nm) were well dispersed in a PVP solution (1:1, DMF and absolute ethanol). Then, $Zn(NO_3)_2$ and 2-aminobenzene-1,4-dicarboxylic acid (NH_2−H_2BDC) dissolved in DMF were added to the previous Fe_3O_4 solution, heating at 100 °C for 4 h. Nanoparticles of Fe_3O_4@IRMOF-3 (∼65 nm) were observed through field emission scanning electron microscopy (FESEM), although the average particle size in DLS was around 200 nm, probably associated with slight aggregation in solution.[101] Furthermore, the normalized saturation magnetization values of the synthesized bare Fe_3O_4 and the nanocomposites were observed to be ∼80 and ∼50 emu·g^{-1}, respectively.[101,102] More recently, Taghavi et al.[105] reported a similar non-core−shell Fe_3O_4@IRMOF-3 (∼150 nm with MNPs below 50 nm) with a saturation magnetization of about 60 emu·g^{-1}, making this composite highly promising.

2.3.2. Core−Shell Magnetic Composites. So far, this Review has shown the formation of the MNP@MOF nanocomposites where the particle location is not controlled. However, it is now necessary to explain the great interest in a well-defined core−shell architecture (Figure 2), since locating a single MNP inside (core) a single MOF nanoparticle (shell) is a nice chemical challenge to guarantee the homogeneity of the system, porosity, and intimate interaction between MNPs and MOFs, avoiding the MNPs−MNPs ones.[106] Therefore, it would be ideal for the manipulation of the nanoparticles insertion and the ratio between the MNPs and the MOF precursors content to systematically tune the properties for a precise control over the size, shape, and composition of the nanocomposites.[106] In this section, the more recent examples of core−shell composites will be discussed classifying them as a function of the magnetic core nature (*e.g.*, uncoated, acidic functionalized, amino functionalized, polymer functionalized).

2.3.2.1. Synthesis of Magnetic Composite with Non-functionalized MNPs. Despite the issues related to the uncoated MNPs, their use is still considered for the synthesis of core−shell nanocomposites. The reason is evident in the following examples, where the choice of the uncoated-MNPs is related to their easy fabrication via a simple, and low-cost coprecipitation method. The central objective of the forthcoming analysis centers around the optimization of MOF growth surrounding a magnetic core. To this end, two recent examples have been selected, both adhering to a size criterion of approximately 300 nm because it is significant for biomedical applications.

In this regard, a magnetic nanocomposite based on uncoated-Fe_3O_4 nanoparticles (∼260 nm) and magnesium 2,5-dihydroxyterephthalate Mg-MOF-74 was reported.[107] The nanocomposite was solvothermally (125 °C for 5 h) prepared from a suspension of Fe_3O_4 nanoparticles and $Mg(NO_3)_2$ in a mixture of DMF-ethanol-H_2O (15:1:1), adding then the ligand. The final nanocomposite (∼320 nm) was magnetically collected, identifying both the MOF and the Fe_3O_4 structures by PXRD. However, the BET surface area was much lower than the expected one (265 vs 1250 m^2·g^{-1} for Mg-MOF-74), which could be related to the presence of dense MNPs and the low shell thickness of the MOF.

On the other hand, a more complex structure, Fe_3O_4@UiO-66@UiO-67/CTAB, was achieved with the cationic surfactant hexadecyltrimethylammonium bromide (CTAB) surface mod-

https://doi.org/10.1021/acsnanoscienceau.3c00041
ACS Nanosci. Au 2024, 4, 85−114

ification.[108] In the first step, $ZrCl_4$, 1,4-benzene dicarboxylic acid (H_2BDC), and DMF were mixed with uncoated-Fe_3O_4 nanoparticles, adding then acid modulators (HCl and acetic acid) and heated at 120 °C for 24 h. Second, after the recovery, UiO-67 was formed over the Fe_3O_4@UiO-66 composite following the same procedure but with the biphenyl-4-4′-dicarboxylic acid (H_2BPDC) as the organic linker. Finally, the Fe_3O_4@UiO-66@UiO-67/CTAB composite was obtained by introducing it in a CTAB solution. The final material exhibited an irregular morphology that differs from UiO-66 and UiO-67, presenting a dimension of about 60−130 nm. The magnetization loops indicated a superparamagnetic feature and a high saturation magnetization of about 36 emu·g^{-1} for Fe_3O_4@UiO-66@UiO-67/CTAB, considering the values of saturation magnetization at room temperature of bulk magnetite (92 emu·g^{-1}) and maghemite (76 emu·g^{-1}).[109,110]

As was pointed out in the introduction to this subsection, the limited number of reported works of core−shell nanocomposites emphasizes the difficulties for nanoparticles to be the seed for MOF formation. However, with nanoparticles of suitable size, even if uncoated, a synthesis protocol of a small nanoMOF can lead to a single shell of MOF around a single MNP.

2.3.2.2. Synthesis of Magnetic Composite with Acid- or Amino-Functionalized MNPs. As previously explained, carboxylic groups on the surface of nanoparticles are employed to stabilize them in a well-dispersed solution and to increase the affinity of the MOF in order to grow the crystal on the MNP surface. Another alternative, improving stabilization and preventing agglomeration, is the use of amino groups to increase again the chance of a core−shell architecture. In the following subchapter, some examples are reported with both functionalization over MNPs.

In this matter, Chen et al.[111] prepared magnetic core−shell Fe_3O_4@HKUST-1 (∼50−100 nm) with carboxyl functionalized Fe_3O_4 cores (∼20 nm). The MNPs were dispersed in a mixed solution of DMF/EtOH/H_2O (1:1:1), and PVP was then added as a surface capping agent to promote the core−shell growth together with $Cu(OAc)_2·H_2O$. Finally, with further metal precursor and trimesic acid, the reaction proceeded for 12 h. The BET surface area of the Fe_3O_4 core (S_{BET} ∼ 10 $m^2·g^{-1}$) increased up to 738 $m^2·g^{-1}$ in the Fe_3O_4@HKUST-1 nanostructure, within the range of the MOF itself (S_{BET} = 600−1600 $m^2·g^{-1}$).[86] Furthermore, they achieved a magnetic fluid composite with high particle content (25.0−45.4 wt %) by introducing Fe_3O_4@HKUST-1 core−shell nanoparticles into a carboxymethylcellulose (CMC) solution.[112] According to the literature,[111,112] other Fe_3O_4@HKUST-1 composites were proposed for their good catalytic activities.[113,114] In all the cases, PXRD patterns demonstrated that both phases of Fe_3O_4 and HKUST-1 were present in the composites. The same synthetic protocol, with carboxyl functionalized Fe_3O_4 cores and PVP as a surface capping agent, guaranteed the core−shell Fe_3O_4@HKUST-1 nanocomposite formation, being later further improved with a DMF-free modified version.[113,114]

Notably, for the synthesis of several MNP@ZIF-8 nanocomposites, citric acid (CA) has garnered significant interest. For instance, Hou et al.[115] prepared a core−shell magnetic ZIF-8 via a solvothermal method with glucose oxidase (GOx) embedded into the composite (Fe_3O_4@ZIF-8@GOx). For the synthesis, CA-modified Fe_3O_4 nanoparticles (CA-Fe_3O_4, ∼100 nm) were suspended and sonicated in an EtOH/H_2O (1:1) solution containing $Zn(NO_3)_2$ and HCl. Lastly, an EtOH/H_2O (1:1) solution containing HmIM and PVP was added and stirred. The magnetic Fe_3O_4@ZIF-8 (M_S ∼ 48.2 vs 82.2 emu·g^{-1} for Fe_3O_4) was easily collected with a magnet, exhibiting a core−shell spherical morphology. Additionally, in the PXRD pattern, the diffraction peaks were consistent with the Fe_3O_4 and ZIF-8 patterns.

Slightly different, Lin and colleagues[116] proposed the synthesis of Fe_3O_4@ZIF-8 (∼120 nm) using MNPs (∼6 nm) coated with 3,4-dihydroxyhydrocinnamic acid (DHCA). Prior to the synthesis of the nanocomposite, the MNPs underwent a ligand exchange procedure to substitute oleylamine ligands with DHCA molecules. In this way, their solubility in H_2O was improved, providing also terminal −COOH on the surface of MNPs for coordinating the Zn^{2+} ions. Afterward, in a solution of HmIM, PVP, and Fe_3O_4 nanoparticles, the $Zn(NO_3)_2·6H_2O$ aqueous solution was rapidly poured to afford the final composite. Both FTIR and PXRD determined the presence of Fe_3O_4 and ZIF-8 in the magnetic nanocomposite (M_S ∼ 18.9 vs 44.3 emu·g^{-1} for Fe_3O_4). The hydrothermal method maintains the aforementioned advantages; however, the ligand exchange introduced a slighter modification which permitted the synthesis without ethanol.

Recently, further ZIF-8-based nanocomposites were produced, incorporating Fe_3O_4-nanorods (NRs) as the core material and subsequent decoration with Pt for catalytic purposes (Fe_3O_4-NR@ZIF-8/Pt).[117] During the synthesis process, oleylamine-functionalized Fe_3O_4-NRs were mixed with ZIF-8 precursors in a MeOH solution at room temperature. The resulting nanocomposite was characterized through the analysis of PXRD and FTIR, confirming the successful growth of the MOF and the presence of the Fe_3O_4-NRs. TEM images provided further insights, revealing the length of the Fe_3O_4-NRs to be approximately 700 nm with a width of around 50 nm. Additionally, the synthesis of ZIF-8 led to the formation of a 30 nm MOF shell surrounding the NRs. Instead, Pt content was determined using Energy-dispersive X-ray spectroscopy (EDS), and the surface area as measured by the BET method decreased from 620 (Fe_3O_4-NR@ZIF-8) to 265 $m^2·g^{-1}$ (Fe_3O_4-NR@ZIF-8/Pt), as a consequence of the Pt decoration. Notably, this fascinating material, primarily synthesized for catalytic purposes, also exhibited magnetic characteristics, with M_S of 73.9, 58.9, and 50.2 emu·g^{-1} for Fe_3O_4-NR, Fe_3O_4-NR@ZIF-8, and Fe_3O_4-NR@ZIF-8/Pt, respectively. Thus, this example once again emphasizes the remarkable versatility of ZIF-8 synthesis, even when there are variations in the composition of the magnetic core. Despite the ZIF-8 advantageous synthetic properties (fast, simple, and versatile), its utilization for bioapplications is accompanied by several limitations. Specifically, it demonstrates low to medium stability in aqueous environments. To enhance its long-term performance, stability, and biocompatibility, as well as to improve its targeting capabilities, additional modifications such as functionalization and surface engineering steps (e.g., GOx) become imperative to address these challenges to fully exploit the potential of ZIF-8 for bioapplications. For the simplicity of the synthesis, in the same way, other magnetic core−shell Fe_3O_4@ZIF-8 composites with size ranges from 180 to 400 nm were synthesized with minor modifications but finalized for different applications, such as water treatment,[118] protein separations,[119] bioimaging,[120] drug delivery,[121] and potential theragnostic agents.[122]

https://doi.org/10.1021/acsnanoscienceau.3c00041
ACS Nanosci. Au 2024, 4, 85−114

Similarly, an Au@Pt nanoparticle-decorated magnetic Fe_3O_4@UiO-66 composite[123] (∼100−300 nm) was constructed. PXRD and FTIR of the Fe_3O_4@UiO-66 confirmed the formation of the composite, exhibiting Fe_3O_4 nanoparticles (∼90 nm) interacting with the MOF in the SEM and TEM images. Recently, in a similar manner, the same composites were also synthesized, reaching particle size of the final product about 200 nm,[124] smaller than 100 nm,[125] or even about 16−17 nm.[126] The focus is on achieving a size below 200 nm, targeting suitable sizes for intravenous nanocarriers.[127]

In another study, core−shell Fe_3O_4@MIL-100(Fe) spheres (∼350 nm) were fabricated using citrate-capped Fe_3O_4 magnetic particles.[128] The citrate-functionalized Fe_3O_4 particles (∼250 nm) were dispersed in an ethanol solution, first of $FeCl_3$•$6H_2O$ and then, of H_3BTC at 70 °C for 15 and 30 min, respectively. This mixture acted as a precursor of Fe_3O_4@MIL-100(Fe), which was dispersed into a solution of $FeCl_3$•$6H_2O$ and H_3BTC under stirring and heated at 70 °C for 24 h for the MOF growing. The magnetic composite exhibited a size of 350 nm, with PXRD and FTIR analyses establishing the presence of both Fe_3O_4 and MIL-100(Fe) phases. In a reduced particle size range, Tregubov et al.[129] prepared as well Fe_3O_4@MIL-100(Fe) nanocomposite (∼100 nm) just increasing the temperature to 95 °C and keeping it for 12 h. In these cases, the solvothermal synthesis was anticipated with a short step, which created a precursor for the next step. The precursor acted as a seed for the MOF growth, and the MNPs (∼80 nm) were in contact with the metal ions and the organic linkers for 30 min to create the first interactions for the further shell framework growth in the solvothermal procedure. The reasoning behind this is to facilitate the interaction of the MNPs with the precursors of the MOF under stirring, enhancing the dispersion of the Fe_3O_4 nanoparticles. Therefore, MNPs in the static condition of the solvothermal reaction were less encouraged to aggregate.

Instead, Li and co-workers[130] used Fe_3O_4-NH_2 nanoparticles (∼158 nm) to MW-assisted synthesize Fe_3O_4-NH_2@MIL-101(Fe)-NH_2 core−shell nanocomposites (∼268 nm) since the amino group of MNPs could improve the interaction with the carboxylic groups of the organic linker. The obtained magnetic MOFs were recovered by a magnet (M_S ∼ 20−21 emu·g^{-1} vs Twenty-seven emu·g^{-1} for Fe_3O_4-NH_2). The efficient MW heating gave rise to a highly homogeneous Fe_3O_4-NH_2@MIL-101(Fe)-NH_2 nanocomposite. Actually, this strategy has been employed in MOFs synthesis in the past decade not only for the short reaction times but also because the high yield and the properties (tuning crystal size) are affected by the specific and almost instantaneous and homogeneous heating.[131] The microwave-assisted method is almost unexplored for the synthesis of MNP@MOF nanocomposites; however, in the near future, we expect an improvement in this method. One of the issues around this approach is the temperature, and consequently, the pressure, in the microwave vessels, because generally fast reactions are correlated to higher temperature with respect to the solvothermal synthesis. Currently, there is a dearth of evidence concerning the influence of radiation on MNPs. Nevertheless, it is worth noting that certain studies have reported evidence of a decrystallization effect in powder magnetite when exposed to microwave radiation for a brief duration of only 5 min near its Curie temperature.[132] Although this finding does not provide insights into the behavior of MNPs under specific conditions, it could suggest potential limitations for the synthesis of nanocomposites involving MOFs.

2.3.2.3. Synthesis of Magnetic Composite with Polymer-Functionalized MNPs. As previously stated, the core−shell architecture does certainly offer superior control over the shape, morphology, and size of the nanocomposites.[133] However, it depends on the addition of a mediator between the magnetic core and the shell growth.[133] Examples of these capping agents are once again polymers, facilitating the MOF overgrowth[134] and also affecting the magnetic properties of the final magnetic nanocomposite.

Based on PVP-coated iron oxide particles, Zhuang et al.[135] synthesized a 70 nm core−shell composite with a PVP-Fe_3O_4 core (∼50 nm) and a ZIF-8 shell with encapsulated fluorescein. Zhang et al.[136] also prepared Fe_3O_4@ZIF-8 magnetic core−shell composites, but as microspheres (∼800 nm, M_S = 54.6 vs 63.2 emu·g^{-1} of Fe_3O_4) starting from poly(styrenesulfonate, sodium salt) (PSS) functionalized Fe_3O_4 microspheres (∼600 nm) mixed with methanol, $Zn(NO_3)_2$·$6H_2O$, and HmIM. Upon heating (50 °C/3h), the resulting composite showed diffraction peaks corresponding to both components, and the core−shell structure was clearly evidenced by microscopy. The aforementioned examples depict two opposing extremities regarding their dimensions. The former exemplifies dimensions that hold greater relevance to biomedical applications, albeit the study fails to thoroughly investigate the material's magnetic properties and its potential application in biomedical contexts. Conversely, the latter serves as an illustration of a scenario wherein the magnetic core is employed merely as a means of material retrieval in catalytic applications. In addition, the variability in the selection of polymer to facilitate the growth of MOF shell is noteworthy. Specifically, in the former instance, the commonly employed amphiphilic and nonionic PVP was utilized and, in the latter case, the anionic PSS was opted for due to its established efficacy in reducing the surface charge to increasingly negative values (up to −26.9 mV from an initial value of −7.56 mV for unmodified MNPs). This reduction might promote interaction between the metal cation for deposition and subsequent MOF nucleation.

An alternative approach for forming polymer coatings over the MNPs is the use of PDA. For instance, the $CoFe_2O_4$@PDA@ZIF-8 nanocomposite[137] evidenced the chelating effect of the PDA. Moreover, a different $CoFe_2O_4$magnetic core (∼70 nm) was employed, which exhibited a mesoporous structure. The magnetic nanocomposite (36.4 vs 68.5 and 50.3 emu·g^{-1} for $CoFe_2O_4$ and $CoFe_2O_4$@PDA, respectively) was obtained at room temperature after 30 min, starting from $CoFe_2O_4$@PDA (∼100 nm) dispersed in a $Zn(NO_3)_2$ methanol solution and, subsequently, with the continuous dripping of HmIM solution. In the PXRD patterns, the characteristic peaks of the cubic spinel phase of $CoFe_2O_4$ and the crystalline ZIF-8 could be found. Furthermore, the porosity of the magnetic core increased with respect to the MNPs from S_{BET} ∼164 to 349.6 m^2·g^{-1} due to the presence of the MOF. Finally, the architecture and morphology of the composite in TEM revealed a core−shell structure of around 150 nm. The PDA presence was proved to be essential for the formation of the ZIF-8 because, in the absence of the polymer, the interactions between the MNPs and the ZIF-8 do not form a core−shell architecture. Moreover, the negatively charged magnetic core advantageously presents hydrophilic open voids, which has extended the encapsulation capability of the

https://doi.org/10.1021/acsnanoscienceau.3c00041
ACS Nanosci. Au 2024, 4, 85−114

hydrophobic ZIF-8 positively charged shell presented in the other nanocomposites.

A further example is the production of spheres consisting of Fe_3O_4@PDA@Cu_3 (BTC)$_2$ (~300−500 nm; S_{BET} ~ 161 $m^2 \cdot g^{-1}$).[138] Specifically, Fe_3O_4@PDA (~280 nm) were dispersed in an ethanol solution of $Cu(OAc)_2 \cdot H_2O$ and trimesic acid and altogether was heated at 70 °C. The composite formation was proved by PXRD. In this interesting work, the interface between the magnetic core and the MOF overgrowth was evidenced by TEM. The PDA was a homogeneous coating over the Fe_3O_4 surface, which stimulate the crystallization of the Cu_3 (BTC)$_2$ because the metal ions could be coordinated by the phenolic hydroxyl and amino groups of the PDA.[138] From polydopamine-modified Fe_3O_4 particles, also Deng and colleagues[139] described a solvothermal method for synthesizing a magnetic MIL-101(Fe) composite. A solution of $FeCl_3 \cdot 6H_2O$ and H_2BDC in DMF was added to the magnetic Fe_3O_4@PDA particles (~270 nm), then, and heated at 110 °C for 24 h. The TEM images clearly exhibited a core−shell structure with about 30 nm-thick shell of MIL-101(Fe) on the Fe_3O_4@PDA core. The thin coating of PDA once again acted as an interface between the MNPs and the framework structure.

Similarly, this strategy has been exploited also for Zr-MOF composites.[140,141] In a solvothermal synthesis, Fe_3O_4@PDA particles (~250−300 nm) were dissolved in a DMF solution containing $ZrCl_4$ and the different dicarboxylate organic linkers (H_2BDC,[140,141] H_2BPDC,[141] and [2,2′-bipyridine]-5,5′-dicarboxylic acid (H_2BPYDC)[141]). The functional groups (−OH, $-NH_2$) of PDA can chelate to Zr^{4+}, enabling MOF growth onto the MNP surface.[141] In the H_2BDC case,[140] upon heating at 140 °C for 20 min, a porous core−shell nanocomposite (~400 nm and S_{BET} ~ 216.14 $m^2 \cdot g^{-1}$) with an increase in the thickness of the PDA shell from 40 nm on the MNPs to an additional 47 nm of MOF was observed. The nanocomposite exhibited diffraction peaks consistent with the MOF growth and the MNPs presence. In the other study,[141] the mixture solution of Fe_3O_4@PDA and Zr-MOF precursors was heated to 140 °C under stirring for 8 h. The PXRD patterns of all the nanocomposites exhibited peaks for Fe_3O_4 and the MOF's crystalline structure, confirming the synthesis of Fe_3O_4@UiO-66, Fe_3O_4@UiO-66-PYDC, Fe_3O_4@UiO-67 and Fe_3O_4@UiO-67-BPYDC. The TEM images of all magnetic nanocomposites showed a core−shell composite with a shell thickness of the MOF of about 40−75 nm, and an average size of about 280−300 nm for the nanoparticles.[141]

As shown in the described studies, PDA coating of MNPs has provided functional groups (−OH, $-NH_2$) as anchoring points for Cu-, Fe-, and Zr-MOFs. However, the polymer coating also affects the Fe_3O_4 core's magnetic properties together with the MOF shell. Indeed, in general, the bare MNPs have a saturation magnetization which decreases with the surface coating and, even more, with the MOF shell. Nevertheless, the magnetic properties are tunable with an optimized synthesis. In fact, the *in situ* core−shell method relies on control of the size, as well as the shape and morphology control. Therefore, a control of the thickness of the MOF shell as well as the starting magnetic nanocore can tune the nanocomposites' properties.

In recent years, other researchers proposed the synthesis of Fe_3O_4@UiO-66 or Fe_3O_4@UiO-66-NH_2 nanocomposites employing PAA. Zhao and colleagues[142] directly dispersed Fe_3O_4 nanoparticles (treated with PAA and urea, with a diameter size of ~150 nm) into a DMF solution of the synthetic precursors of UiO-66 ($ZrCl_4$, NH_2-H_2BDC). The core−shell Fe_3O_4@UiO-66 showed a UiO-66 shell of about 25 nm thickness, while the composite size was about 240 nm.[142] The M_S of both Fe_3O_4@UiO-67-BPYDC[141] and Fe_3O_4@UiO-66[142] exhibited similar values within the range of approximately ~50 emu·g^{-1} (vs ~70−75 emu·g^{-1} for Fe_3O_4). However, it was noteworthy that only the latter has undergone adequate dimension to facilitate its investigation as a theragnostic system, as elaborated on subsequently (see section 3.3: Theragnostics).

2.3.2.4. Synthesis of Magnetic Composite with Carbon- or SiO_2-Functionalized MNPs. In addition to the aforementioned methods, there are two other possibilities. In the first case, MNP@MOFs can be synthesized employing Fe_3O_4@carbon (Fe_3O_4@C) nanoparticles. Besides the role in the stabilization of the magnetic core in the reaction mixture, the porous carbon shell can improve the imaging properties of the nanocomposites due to the carbon dots fluorescence. On this matter, He and co-workers[143] synthesized ZIF-8 nanocomposites using Fe_3O_4@C nanospheres as the core. The nanocomposite (~220 nm) was simply synthesized at 60 °C for 1 h by adding Fe_3O_4@C nanospheres (~190 nm) in a methanol solution containing $Zn(NO_3)_2 \cdot 6H_2O$ and HmIM.

In the second strategy, silica-capped MNPs (Fe_3O_4@SiO_2) are employed, with the SiO_2 capping conferring lower cytotoxicity to the MNPs.[144] Moreover, the thickness of the silica surface over the Fe_3O_4 core can be easily tuned,[145] and then, the magnetic responsivity varied as well as the porosity properties related to the mesoporous silica.[144] Additionally, through different silanization agents, different functionalities can be included to promote the interactions with the MOF precursors. In the field of MNP@MOF nanocomposites, core−shell structures of Fe_3O_4@SiO_2@MIL-100(Fe) were fabricated[146−148] by the reaction mixture of Fe_3O_4@SiO_2 (~360,[146] 50,[147] 20[148] nm) with the MIL-100(Fe) precursors under reflux at 100 °C for 8 h. In all these composites (~440,[146] 50,[147] 50[148] nm), the PXRD patterns confirmed the MIL-100(Fe) structure and the Fe_3O_4 phase.[146] In this case, the detection of the magnetic component into MIL-100(Fe) could be recognized. It was observed a magnetic saturation decrease from 82.5 emu·g^{-1} for the MNPs to 30 emu·g^{-1} in the nanocomposite due to the SiO_2 and MIL-100(Fe) shells, permitting an easy magnetic separation. However, the identification of the iron content by EDS did not allow to discriminate between the Fe_3O_4 and the MIL-100(Fe), distinguishing the Fe_3O_4 core from the MOF shell only by TEM.[146]

Instead, Jia et al.[149] presented a thermoresponsive polymer, poly(*N*-isopropylacrylamide) (PNIPAM), tethered to Fe_3O_4@SiO_2@MOF core−shell magnetic nanospheres. The magnetic composite Fe_3O_4@SiO_2@UiO-66-NH_2 was fabricated from Fe_3O_4@SiO_2 nanospheres (~200−300 nm) obtained by carboxylate-terminated reaction with succinic anhydride and (3-aminopropyl)triethoxysilane (APTES). The magnetic nanosphere were ultrasonically mixed with a DMF solution containing the UiO-66-NH_2 precursors ($ZrCl_4$, NH_2-H_2BDC and acetic acid). Fe_3O_4@SiO_2@UiO-66-NH_2 (MOF shell ~ 30−50 nm) was obtained at 130 °C for 4 h under stirring, and after drying, the composite underwent to a subsequent reaction in chloroform using PNIPAM-NHS at 60 °C for 24 h. The Fe_3O_4@SiO_2@UiO-66-NH_2−PNIPAM nanospheres reached dimensions around 350−450 nm, presenting magnetic properties (M_S ~ 45.60 emu·g^{-1}) with S_{BET} ~ 262 $m^2 \cdot g^{-1}$ and

https://doi.org/10.1021/acsnanoscienceau.3c00041
ACS Nanosci. Au 2024, 4, 85−114

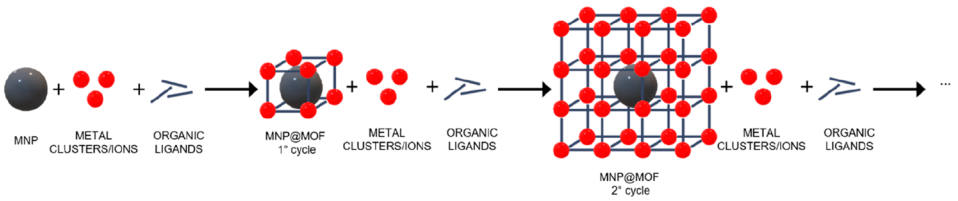

Figure 6. Schematic representation of the layer-by-layer (LbL) strategy.

indexing the PXRD pattern to UiO-66-NH_2 and Fe_3O_4. In the same manner, Yang et al.[150] fabricated Fe_3O_4@SiO_2@UiO-67 by dispersing Fe_3O_4@SiO_2 in a $ZrCl_4$ solution for the complexation of Zr^{4+} and adding then H_2BDC and glacial acetic acid (heating at 120 °C for 24 h). The resulting Fe_3O_4@SiO_2@UiO-67 nanocomposites (224−258 nm; MOF shell thickness ∼ 20 nm) were characterized by SEM and TEM, and compared with Fe_3O_4 (∼170 nm) and Fe_3O_4@SiO_2 (∼208−232 nm). The composite exhibited a saturated magnetization lower than that of Fe_3O_4 (61.0 emu·g^{-1}) and Fe_3O_4@SiO_2 (47.3 emu·g^{-1}), specifically 20.9 emu·g^{-1}. Although, as expected, the shell reduced the magnetic properties, the MOF presence was there to influence its positive features, such as the porosity and biocompatibility.

The most evident "bottle around ship" strategy was reported by Huang and colleagues,[151] Fe_3O_4@SiO_2@$Cu(OH)_2$, where the self-template shell of $Cu(OH)_2$ over Fe_3O_4@SiO_2 nanoparticles (∼15 nm) promoted the conversion of $Cu(OH)_2$ into HKUST-1. Briefly, Fe_3O_4@SiO_2@$Cu(OH)_2$ in a water−ethanol solution of the organic linker (H_3BTC) gave rise to core−shell nanostructures (MOF shell ∼ 5−10 nm) of Fe_3O_4@SiO_2@HKUST-1 at room temperature after stirring for 12 h. This method was not so different from what was previously reported, the Cu ions being able to interact with the magnetic core before the MOF growth. The Fe_3O_4@SiO_2@$Cu(OH)_2$ precursor acted as a seed for the crystallization of the MOF, favoring a core−shell architecture.

2.4. Layer-by-Layer Strategy

The layer-by-layer (LbL) strategy has the purpose to control the crystal growth of the MOF over the MNPs. The synthetic strategy is a step-by-step sequential repeated cycle of immersion in solutions of the metal precursor and solutions of organic ligand[152] or MOF precursors solutions, first proposed in 2007 for HKUST-1.[65] The protocol proposed by Shekhah was et al. extended to different MOF structures.[153] Herein, we will present the extension of this strategy for the synthesis of magnetic composites, where the first layer of the MOF is over a MNP and the thickness of the MOF shell is controlled by the number of repeating cycles performed, as represented in Figure 6.

2.4.1. Synthesis of Magnetic Composites with Acid- Or Thiol-Functionalized MNPs. As was pointed out earlier, MNP functionalization has been employed for several advantages. In the LbL method, Ke and co-workers[154] proposed magnetic core−shell spheres of Fe_3O_4@HKUST-1 or Fe_3O_4@MIL-100(Fe), subsequently, numerous works[155−169] followed the same synthetic protocol with mainly a carboxylic functionalization over the magnetic core or thiol groups. In general, COOH-functionalized Fe_3O_4 MNPs ranging from 20 to 500 nm were dispersed in solutions of $Cu(CH_3COO)_2{\cdot}H_2O$ or $FeCl_3{\cdot}6H_2O$ precursors, respectively for Fe_3O_4@HKUST-1 or Fe_3O_4@MIL-100(Fe) composites. After 15−30 min and a magnetic recovery of the Fe_3O_4 nanoparticles, the organic linker solution (H_3BTC) was mixed with the MNPs for 30 min at 25, 40, or 70 °C. These two steps formed a cycle to coat Fe_3O_4 with a layer of MOFs and each cycle was subsequently repeated several times. Generally, the diffraction peaks for the samples Fe_3O_4@HKUST-1 in the PXRD pattern matched well with those of both Fe_3O_4 and crystalline HKUST-1.[154−156,162] In the case of SEM and TEM investigation for Fe_3O_4@HKUST-1, the images showed a spherical-shaped morphology with a core−shell structure with narrow size distribution and uniform dispersion (ranging from 210 nm to 1.5 μm depending on the number of assembling layers).[154−156,162] The magnetic Fe_3O_4@HKUST-1 composites exhibited BET surface area variable depending on the number of cycles employed, with values from 57 to 668 $m^2{\cdot}g^{-1}$; as expected the surface area increases with a larger number of MOF layers.[154−156,162] Moreover, the magnetic properties and separability were also tested. For instance, the core−shell microspheres desired in the selective removal of Hg^{2+} and Pb^{2+} were separated in a few seconds in an aqueous solution by placing a permanent magnet near the glass bottle.[162] The saturation magnetization varied from ∼14 to 43 emu·g^{-1} and all core−shell MNPs exhibited superparamagnetic behavior at room temperature, which also depicted the strong magnetic response to an AMF.

In the case of Fe_3O_4@MIL-100(Fe),[154,157−161,163−169] the diffraction peaks for the samples were consistent with the crystalline phases of Fe_3O_4 and MIL-100(Fe). However, the intensities of MIL-100(Fe) patterns in some diffractograms were very weak, which was correlated to the low thickness of the MOF shell.[158,161,166] By SEM and TEM, the magnetic composites reported a core−shell structure, with an average size dependent on the diameter of the MNP core and also on the number of layers, varying from 150 nm up to 1 μm.[154,157−161,163−169] The BET surface areas of Fe_3O_4@MIL-100(Fe) increased with increasing assembly cycles, ranging from ∼36 to 899 $m^2{\cdot}g^{-1}$ in the different composites reported.[154,158−161,164−169] This general trend was due to the decreasing contribution of nonporous Fe_3O_4 MNPs to the total mass of the magnetic core−shell nanoparticles.[158] Furthermore, the majority of these Fe_3O_4@MIL-100(Fe) presented magnetization saturation values in the range of ∼20−56 emu·g^{-1}.[154,158,160,163−169] It was observed either the presence of a magnetic hysteresis loop or no obvious remanence or coercivity at 25 °C. Therefore, the magnetic composites possessed ferromagnetic or superparamagnetic features and, for the majority of them, it was observed a simple magnetic separation in the solution media through a magnet in a few seconds. The great number of studies on MIL-100(Fe) based composite was related to the versatility of MIL-100(Fe), which had good *in vitro* and *in vivo* biocompatibility as well as important drug loadings for biomedical applications, and, moreover, a potential application for separations through strong coordination with guest molecules.[160]

https://doi.org/10.1021/acsnanoscienceau.3c00041
ACS Nanosci. Au 2024, 4, 85−114

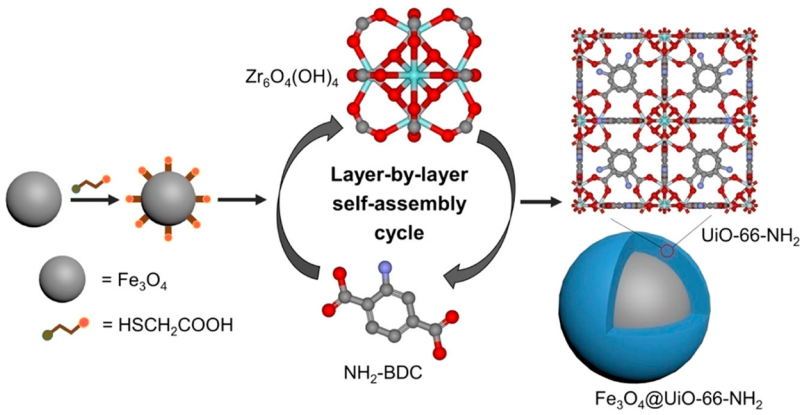

Figure 7. Schematic illustration for the layer-by-layer fabrication of core−shell Fe_3O_4@UiO-66-NH_2. Reproduced from ref 173. Copyright 2019 American Chemical Society.

Furthermore, the LbL strategy has also been proposed for other composites. For instance, Zheng et al.[170] developed a Fe_3O_4@ZIF-8 core−shell structure (~530 nm). The synthetic protocol consisted of citrate-Fe_3O_4 (~390 nm) solution mixed with $Zn(NO_3)_2{\cdot}6H_2O$ and HmIM, heating later at 70 °C for 20 min and, separating the product with a magnet. The thickness of the ZIF-8 shell was increased by repeating the above process several times. Likewise, also Liu et al.[171] reported the fabrication of core−shell Fe_3O_4@ZIF-8. Both studies confirmed the Fe_3O_4@ZIF-8 formation by PXRD, indexing the diffraction peaks of Fe_3O_4 and crystalline ZIF-8. The specific surface areas were about 1075 $m^2{\cdot}g^{-1}$, lower than that of the isolated ZIF-8 (S_{BET} ~ 1709 $m^2{\cdot}g^{-1}$)[171] as an effect of the Fe_3O_4 core on the formation of ordered microporous. On the other hand, the effect of the shell on the magnetic core was translated into a saturation magnetization value of 14.38 $emu{\cdot}g^{-1}$.[170] A similar procedure was followed also for the complex multifunctional system, Fe_3O_4@PAA/AuNCs/ZIF-8 (~130 nm).[172] In this case, oleic acid (OA)-capped MNPs (~20 nm) underwent, first, a polymer coating process with PAA, and then the gold nanoclusters (AuNCs) were integrated into the synthetic step for the MOF growth to obtain a theragnostic agent that combines multiple capabilities for cancer treatment.

Another MOF widely used for this strategy was UiO-66-NH_2. In this sense, Chen and co-workers[173] reported a core−shell Fe_3O_4@UiO-66-NH_2. During the synthesis, Fe_3O_4 nanoparticles (~200−300 nm) functionalized with carboxylic moieties were immersed, first, in the metal node $[Zr_6O_4(OH)_4]^{12+}$ precursor solution, and then, in the organic linkers (NH_2−H_2BDC) solution, respectively for 15 and 20 min (Figure 7). Before each subsequent immersion step, MNPs were recovered with a magnet and washed. After 20 cycles, the MOF shell was only around 13 nm, leading to a composite size of about 300−350 nm. The surface area increased for the magnetic Fe_3O_4 core with the MOF shell (S_{BET} ~ 11 vs 76 $m^2{\cdot}g^{-1}$, respectively), far from the high value of the isolated UiO-66-NH_2 (S_{BET} ~ 735 $m^2{\cdot}g^{-1}$). The crystal growth was however not uniform throughout the magnetic iron oxide core. Therefore, the final morphology and structure may not justify the enormous effort and highly time-consuming of the method.

Thus, the synthesis of materials using the LbL technique offers significant advantages in terms of adaptability in the final structure and consequent properties; therefore, in the optimization of the nanocomposite performance in diverse fields, offering a highly customizable approach to achieve desired applications. This versatility arises from the control of the number of synthetic cycles, directly correlated to the thickness of the resulting MOF, enabling adjustments to the porosity and magnetization characteristics. However, in contrast to the core−shell *in situ* formation of the MOF in the presence of MNPs, the LbL method is a more time-consuming procedure, with complex scalability.

2.4.2. Synthesis of Magnetic Composites with Polymer-Functionalized MNPs. In the LbL approach, for instance, Li et al.[174] presented a core−shell Fe_3O_4@IRMOF-3, through the growth promotion of the MOF modifying the surface of the MNPs with PVP. In brief, the synthesis included the mixture of a dissolution of $Zn(NO_3)_2$ and NH_2−H_2BDC in DMF, with PVP in DMF:EtOH (3:2) and Fe_3O_4 nanoparticles, heating then at 100 °C for 4 h under vigorous stirring. All the previous steps were repeated several times. The PXRD patterns possessed diffraction peaks assigned to both Fe_3O_4 and the MOF. Also, it was demonstrated that a certain dosage of the polymer not only stabilized the MNP but also favored the crystalline growth of the MOF. In TEM images, after three cycles, the spherically shaped Fe_3O_4 nanoparticles (~200−500 nm) were embedded in micrometric IRMOF-3 crystals, with a BET surface area and pore volume of 238 $m^2{\cdot}g^{-1}$ and 0.31 $cm^3{\cdot}g^{-1}$. The saturation magnetization values of Fe_3O_4 decreased from 78.5 to 13.5 $emu{\cdot}g^{-1}$, in the case of the composite formation due to the presence of the MOF layer. In this example, the synthesis involved uncoated-MNPs, where the presence of a polymer was necessary to favor the dispersion of the magnetic core and the consequent MOF growth.

Instead, Miao and colleagues[175] synthesized a core−shell magnetic Fe_3O_4@P4VP(poly(4-vinylpyridine))@MIL-100(Fe) composite. In this example, the PAA-functionalized Fe_3O_4 where involved in a polymer-shell formation, Fe_3O_4@P4VP, to favor the interactions between pyridine and Fe^{3+}. Then, Fe_3O_4@P4VP nanospheres (magnetic core ~200 nm and polymer shell ~38 nm) were dispersed in an ethanol solution, first, of $FeCl_3{\cdot}6H_2O$ for 15 min and collected with a magnet; subsequently, they were dispersed in an H_3BTC ethanolic solution and stirred at 70 °C for 30 min. These steps were repeated, giving a composite confirmed in the PXRD pattern. In the HR-TEM, the images clearly showed a 200 nm-diameter magnetic core with a shell thickness of the polymer of 38 nm and the outer MIL-100(Fe) thickness ranging between 15 and 90 nm, depending on the number of assembling cycles

https://doi.org/10.1021/acsnanoscienceau.3c00041
ACS Nanosci. Au 2024, 4, 85−114

(from 5 to 20 cycles). The magnetization saturation values decreased from 73.90 emu·g^{-1} for Fe_3O_4-(PAA) to 47.35 and 28.21 emu·g^{-1}, respectively for Fe_3O_4@P4VP and Fe_3O_4@P4VP@MIL-100(Fe). These results indicated that the materials exhibited a strong magnetic response.

2.4.3. Synthesis of Magnetic Composites with SiO_2-Functionalized MNPs. The versatility of the SiO_2-functionalized MNPs to obtain a core−shell structure via the LbL method was only proposed in the work conducted by Jiang et al.[176] A sophisticated nanocomposite consisting of two distinct 3D MOF structures based on the same ligand, namely, SiO_2@Fe_3O_4@Yb-MOF@Nd-MOF, was proposed, involving the SiO_2@Fe_3O_4 as a core template for the successive synthesis of multiple MOF layers. In the first synthetic step, the SiO_2-functionalized MNPs were added to a solution containing ytterbium(III) acetate at 80 °C for 5 min in a DMF/H_2O mixture. Subsequently, the resulting mixture was centrifuged to separate the precipitate from the supernatant. In the second step, the separated precipitate was once again suspended in a solution containing terphenyl-3,4″,5-tricarboxylic acid (H_3L) ligand. This step followed a similar procedure to that of the first step. Moving on to the third step, a solution of neodymium(III) trichloride was employed, following the same sequence as in step 1. Finally, in the fourth step, the process from step 2 was repeated. All these complex steps were then cyclically repeated 14 times. Based on TEM images, the MNPs' core could be identified, enveloped by a silica layer with a thickness < 6.5 nm. Additionally, sequential layering of MOFs ranging from 9.86 to 21.63 nm was observed, resulting in a total nanocomposite size of approximately 150−200 nm. This innovative example introduces in the LbL method the alternating arrangement of two MOFs that share the same ligand. The resulting structure appears to be relatively complex and warrants further investigation, particularly concerning the magnetic properties of the core and the surface area characteristics, as well as the variability of the properties increasing the cycle number.

3. APPLICATIONS OF MAGNETIC METAL−ORGANIC FRAMEWORK COMPOSITES IN THE BIOMEDICAL FIELD

As mentioned in the Introduction, combining MOFs as promising nanocarriers and MNPs to provide potential imaging, targeted release, and hyperthermia, makes the MNP@MOF nanocomposites particularly interesting in diagnosis, therapy, and theragnostics. The most recent developments will be covered in this section, categorized in therapy, MRI, and theragnostics, comprising nanocomposites with sizes below 500 nm, and analyzing the potential of these systems for their real application.

3.1. Therapy

The administration of therapeutic agents by nanocarriers has been developed to minimize toxicity and side effects, increase the efficacy avoiding early clearance, and ensuring a progressive and located drug release within the active sites.[177,178] Since 2006 and 2010, when micrometric[8] and nanoscaled[6] MOFs were originally proposed as DDSs, great advances have been achieved in this exciting topic.[179,180] In particular, this section will describe in detail the use of MNP@MOF nanocomposites as DDS, providing representative examples. Finally, as far as we know, the only work describing magnetic nanocomposite as magnetic hyperthermia (MHT) agents will be presented, as a nice combination of MHT and DDS to further improve the therapeutic efficacy.

Based on one of the most used families of MOFs for bio applications, as a proof of concept, the anti-inflammatory drug ibuprofen (IBU) was successfully encapsulated in a γ-Fe_2O_3@MIL-53(Al) nanocomposite, reaching a drug loading of 110 mg·g^{-1} with a long progressive release in PBS at 37 °C (7 days).[77] Considering the potential toxicity of this Al-based MOF, the IBU was successively loaded in a magnetic LbL composite (M_S ∼ 50.69 and 20.42 emu·g^{-1}, after 40 and 20 cycles, respectively) based on the biocompatible MIL-100(Fe) (Fe_3O_4@MIL-100(Fe)),[158] achieving higher IBU loadings (310 mg·g^{-1}) associated with a greater porosity. In this exploratory research, the IBU release under simulated physiological conditions (PBS, pH 7.4) took place for about 35% in the first 2 h, then it slowed down and was completed in 70 h. These works evidenced the possibility to encapsulate drugs into magnetic nanocomposites. However, these preliminary studies only tested the drug encapsulation and the release without further practical considerations (*e.g.* biocompatibility, *in vitro* and *in vivo* therapies).

In recent times, significant effort has been predominantly placed on the encapsulation of more challenging antitumoral drugs. As far as cancer therapy is concerned, a large number of studies have reported the use of the convenient fluorescent antitumoral drug doxorubicin (DOX), widely used in clinics to treat a variety of human diseases, including Hodgkin's lymphoma, leukemia, multiple myeloma, breast cancer, osteosarcoma, ovarian cancer, and lung cancer.[181] This chemotherapeutic product was granted FDA approval as the first nanodrug in 1995 and, at present, is known under the brand name Doxil, a liposomal formulation.[182] Even if the DOX hydrochloride salt formulations on the market have a high therapeutic index and high efficacy against a variety of solid tumors, they are also associated with significant side effects including heart damage, typhlitis, cardiac arrhythmias, nausea, and vomiting.[181] Thus, DOX delivery through nanocarriers has garnered considerable interest. Within the magnetic MOF-based nanocomposites, DOX was encapsulated in Fe_3O_4-NH_2@MIL-101(Fe)-NH_2 (∼140−330 nm; M_S ∼ 20.47−21.32 emu·g^{-1} vs 27.67 emu·g^{-1} for Fe_3O_4-NH_2).[130] Its DOX loading capacity was optimized by using different MNP:MOF ratios, reaching the highest loading (360 mg·g^{-1}) at 1:1 molar ratio due to the improved porosity (S_{BET} = 96 m^2·g^{-1} vs 12−88 m^2·g^{-1}). The relative amount of dense MNPs in comparison to the pure MOF elucidates the significantly diminished porosity of the nanocomposite (pure MOF reaching 1800 m^2·g^{-1}).[183] The drug release, dependent on pH, was faster under acidic media due to MOF degradation, simplifying targeted DOX release in acidic cancer cells. Nevertheless, 37−61% of DOX release from the composite in simulated body fluid (SBF) at pH 7.4 occurred in 48 h, more gradually than pristine MIL-101(Fe)-NH_2. Furthermore, cytotoxicity tests pointed out the biocompatibility of the nanocomposite and the applicability of the DOX-loaded composite as a DDS. In this sense, the biocompatibility and controlled DOX release in an acidic environment were further guaranteed by coating a Fe_3O_4@Fe-MOF composite with hydroxyapatite (HAp),[184] although HAp is present in the body at the hard tissue level. In this case, the DOX capacity was 53 and 75 mg·g^{-1} in Fe_3O_4@Fe-MOF and Fe_3O_4@Fe-MOF@HAp, respectively. Indeed, the HAp-coating not only increased the drug cargo but also contributed to a more gradual release

https://doi.org/10.1021/acsnanoscienceau.3c00041
ACS Nanosci. Au 2024, 4, 85−114

Table 1. Comparative Overview of Magnetic Nanocomposites for Therapy[a]

MNP@MOF	OL	MP for MOF	MNP@MOF size [MNPs] (nm)	M_S (emu·g^{-1})	drug	DL (mg·g^{-1})	LE (%)	TCL	ref
γ-Fe_2O_3@MIL-53(Al)	H_2BDC	Al^{3+}	not reported (NR)	6.1	IBU	110	NR	–	77
Fe_3O_4@MIL-100(Fe)	H_3BTC	Fe^{3+}	90–150 [20]	50.7 (20 layers) and 20.4 (40 layers)		310	NR	–	158
Fe_3O_4-NH_2@MIL-101(Fe)-NH_2	NH_2-H_2BDC	Fe^{3+}	140—330 [140]	20.5–21.3	DOX	360	NR	HeLa	130
Fe_3O_4@Fe-MOF@HAp	H_3BTC	Fe^{3+}	400 [300]	34		75	NR	HeLa	184
Fe_3O_4@ZIF −8	HmIM	Zn^{2+}	70–100 [9]	–		120	12	MHCC97H	185
Fe_3O_4@ZIF-8	HmIM	Zn^{2+}	180 [120]	18.6–48.1		330	77	HeLa	121
Fe_3O_4@UiO-66-NH_2/GDY	NH_2-H_2BDC	Zr^{2+}	250 [<150]	21.6		438	NR	HeLa	189
Fe_3O_4@PDA@ZIF-90	2-ICA	Zn^{2+}	200 [140–160]	9.2		160	80	HeLa	97

[a]OL = organic linker, MP = metal precursor, DL = drug loading, LE = loading efficiency, TCL = targeted cell line.

(at pH 7.4, 25 vs 46% after around 11.7 h from the HAp-coated and noncoated systems, respectively). Finally, cytotoxic assays confirmed the biocompatibility of both composites and the selective DOX effect on HeLa cells.

Another nanocomposite that was employed for DOX release was based on ZIF-8. In this study, DOX was encapsulated in the Fe_3O_4@ZIF-8 nanocomposite (~70–100 nm) with a content of about 120 mg·g^{-1} and a loading efficiency of 12%.[185] The release was proven to be controlled over time without a burst effect, and its *in vitro* biosafety was demonstrated on the hepatocarcinoma cell line (MHCC97H). Similarly, in the biocompatible Fe_3O_4@ZIF-8 nanocomposite (~180 nm, M_S ~ 18.6–37.2 vs 48.1 emu·g^{-1} for Fe_3O_4), developed by Chen and co-workers,[121] the DOX encapsulation was enhanced (330 mg·g^{-1}, 76.6% of loading efficiency). In this latest example, an elevated concentration of DOX during encapsulation may have increased loading efficiency. Plausibly, it is due to a surplus of DOX adsorbed in the outer surface due to the electrostatic interaction between the negatively charged carboxylate groups and positively charged DOX molecules.[186] Additionally, the strong coordinative affinity of the C–O and C═O groups may contribute to the formation of coordination bonding of Zn^{2+}-DOX in aqueous solutions.[187] The drug release in PBS after 48 h was higher at pH 5.5 (63%) than at pH 7.4 (33%), showing again a pH dependence that was in line with the acidic environment in the cancer cell. Moreover, the resulting Fe_3O_4@ZIF-8 nanocomposite evidenced photothermal effects under laser irradiation (808 nm), showing a selective cancer cell death for the Fe_3O_4@ZIF-8-enriched area. This study investigated the magnet-targeted photothermal effect of the composites in a preliminary manner. Prior studies indicated that Fe_3O_4 nanoparticles exhibit an outstanding photothermal effect,[188] hence, this work showed that the formation of composites does not impede cancer treatment under these laser conditions. Furthermore, the possibility of evaluating promising combined antitumoral therapies, considering DOX-encapsulated Fe_3O_4@ZIF-8, warrants further investigation.

Likewise, a magnetic composite based on the UiO-66-NH_2 material was studied as DDS for the anticancer DOX, proposing Fe_3O_4@UiO-66-NH_2 (~150 nm) with hybridization over a layered 2D material, the graphdiyne (GDY).[189] In the resulting complex nanocomposite (~250 nm; Fe_3O_4@UiO-66-NH_2/GDY), the macroporous structure of the GDY offered an ulterior surface for drug uptake, resulting in a high DOX loading content of 438 mg·g^{-1}. Once more, the composite demonstrated a pH-dependent DOX release (after 36 h, 49 vs 34% released at pH 5 and pH 7.4, respectively), negligible cytotoxicity, and efficient endocytosis-mediated drug carrier uptake in HeLa cells. Notably, the antitumor activity of the DOX-loaded Fe_3O_4@UiO-66-NH_2/GDY nanocomposite was evaluated *in vivo* in BALB/c-nu mice, displaying no obvious toxicity with promising tumor-targeting and -inhibition when compared with the free DOX (77.8 vs 27.7%).

As anticipated in the introduction of this section, magnetic nanocomposites present also a strong potential in the development of MHT oncological therapy. MHT consists of increasing the temperature (42–46 °C) in a target tumoral tissue by using nanoheating probes (i.e., MNPs) under an AMF in the kHz radiofrequency range.[190,191] In clinical use, for patient safety, a frequency of 100 kHz and a magnetic field amplitude of 15 kA·m^{-1} is generally employed.[190,191] In this regard, the only reported example so far was Fe_3O_4@PDA@ZIF-90 with an average particle size of about 200 nm, originally reported for combined MHT and chemotherapy.[97] This magnetic nanocomposite (M_S ~ 9.2 vs 22.5 and 17.3 emu·g^{-1} for Fe_3O_4 and Fe_3O_4@PDA, respectively) exhibited a good increase of temperature from 30 to 45.6 °C under an AMF at 409 kHz and 14.3 kA·m^{-1} for 20 min. In this experiment, the frequency of the AMF is 4-fold greater than the value for clinical use. For comparison, under the same conditions, Fe_3O_4 and Fe_3O_4@PDA controls led to a temperature increase up to 77.5 and 49.4 °C, not adapted to safe physiological values. Furthermore, the DOX-loaded Fe_3O_4@PDA@ZIF-90 composite (160 mg·g^{-1}, with a loading efficiency of 80%) demonstrated a faster release as the acidity increases (PBS pH 7.4, 6.0, and 4.5). This fact, together with the magnetic heating, could favor the DOX release at the tumor level, combining chemotherapy and MHT. In fact, for DOX-loaded Fe_3O_4@PDA@ZIF-90, cell death was enhanced under an AMF, demonstrating a hyperthermia therapy in combination with chemotherapy for only the drug-loaded nanocomposites (i.e., cell viability without AMF, with AMF once and twice, respectively, for the composite = 110, 60 and 40% and DOX-loaded composite = 80, 30 and 10%).

Table 1 summarizes all the examples developed in this section. Note here that DOX has been mainly selected as the active ingredient, mostly as a proof of concept due to (i) its dimensions (around 15.4 Å), compatible with the pore size of various MOFs;[192] (ii) its fluorescence, facilitating its quantification and intracellular tracking (confocal microscopy); and (iii) its high efficacy against several tumors, despite severe drawbacks (*e.g.* cardiotoxicity,[193,194] self-association tendency in aqueous solution,[195,196] drug resistance[197]). High

https://doi.org/10.1021/acsnanoscienceau.3c00041
ACS Nanosci. Au 2024, 4, 85–114

Table 2. Comparative Review of Magnetic Nanocomposites for MRI[a]

MNP@MOF	OL	MP for MOF	MNP@MOF size (nm)	M_S (emu·g^{-1})	B (T)	r_1 (mM^{-1}·s^{-1})	r_2 (mM^{-1}·s^{-1})	r_2/r_1	TCL	ref
Fe_3O_4@ZIF-8	HmIM	Zn^{2+}	120	18.9	0.5	15.1*[b]	372.0**[c]	24.6***[d]	HUVEC, 4T1	116
Fe_3O_4@MIL-100(Fe)@CDM	H_3BTC	Fe^{3+}	250		0.23	NR	157	NR		129

[a]OL = organic linker, MP = metal precursor, B = magnetic field, TCL = targeted cell line. [b]For pH 7.4, 28.4 (pH 6.2 and 4 mM of GSH), and 30 (pH 5 and 4 mM of GSH). [c]For pH 7.4, 238.9 (pH 6.2 and 4 mM of GSH), and 176.3 (pH 5 and 4 mM of GSH). [d]For pH 7.4, 8.4 (pH 6.2 and 4 mM of GSH), and 5.7 (pH 5 and 4 mM of GSH).

drug loading ranging from 75 to 438 mg·g^{-1} (loading efficiency 12−96%) was obtained with a pH-dependent release, emphasizing its promoted delivery under an acidic microenvironment favored in tumor cells, lysosomes, or endosomes (pH ∼ 4.5−7.8) as opposed to the pH of normal cells or blood (pH ∼ 7.4).[30] The stimuli-responsive drug delivery as an acidic response has been correlated to the degradation of the framework, where pH-sensitive bonds (amine, imide, or carboxylates) may lead to the release of the cargo.[179,198]

Furthermore, the mean values of the M_S are disclosed in Table 1, encompassing a range from 6.1 to 51 emu·g^{-1}. The M_S plays a crucial role in the context of MHT, as the heating efficiency, affected by the specific loss power (SLP), is directly proportional to its square,[199] requiring high M_S values to achieve elevated SLP.[199] In this sense, M_S is influenced by factors such as the size and shape of the MNP.[199] Although also depending on experimental conditions (*e.g.* strength and frequency of applied AMF), few theoretical[200] and experimental[201] studies determined an optimal size of MNPs for a maximum heating efficiency of around 15−20 nm. The presented examples have predominantly larger MNPs size than the ideal range for MHT. The most favorable outcome is observed in the nanocomposite with MNP size of approximately 20 nm,[158] yet a considerable number of them still exhibits a commendable MS value. Indeed, the value of MNPs generally tends to reach the bulk value and the typical range of 30−50 emu·g^{-1} can be regarded as a favorable outcome.[202] Notably, MHT was solely validated in one single case, indirectly determining the nanocomposites effect on the cell viability.[97] Even further, this nanocomposite reported a low M_S (9.12 emu·g^{-1}), indicating that this parameter is not sufficient to evaluate the MHT efficacy. As a matter of fact, it is crucial to acknowledge that determining the optimal conditions for MHT implementation can be a complex endeavor, necessitating intricate instruments (*e.g.*, superconducting quantum interference device (SQUID), alternating current (AC) magnetometer, and magnetic nanoheating device) and methodologies (*e.g.*, combined magnetic and *in vitro* techniques). It is worth noting that most of the referenced papers are confined to *in vitro* investigations, with merely one study presenting *in vivo* assessments, raising pertinent inquiries concerning the clinical feasibility and applicability of these magnetic nanocomposites.

3.2. MRI

This section will present the principal findings of the current investigation on magnetic MOF nanocomposites as contrast agents for MRI, as an interesting noninvasive diagnostic technique in soft tissues, characterized by unlimited signal penetration depth, lack of ionizing radiation, and wide clinical applicability.[203,204] The contrast agents improve the image contrast because they decrease the longitudinal or transverse proton relaxation times (T_1 and T_2, respectively) of the hydrogen nuclei of the water molecules present in our tissues.[203,204] In the last years, it has been proposed to replace the traditionally used T_1-weighted MRI contrast agent gadolinium (Gd^{3+}) chelates with other inorganic nanoparticles with enhanced contrast, sensitivity, and MRI detection capability.[203] One of those with remarkable performances is the magnetic iron oxide, also reported as T_1-weighted MRI contrast agents when they are small and isolated, depending on its magnetic effect on its composition, size, shape, and assembly.[205] The preparation of MNP@MOF composites can be seen as an efficient method to ensure the dispersion of the MNPs, improve their contrast agent properties, and provide additional relevant properties associated with the MOF (*e.g.*, porosity, versatile composition, drug loading, inherent therapeutic effect, targeting; see section 3. Theragnostic). Even more, although not reported so far, MOFs could provide intrinsic additional imaging properties by using MRI-active MOFs based on Gd(III), Mn(II), and Fe(III).[206,207] Thus, to date, only two reports have described the MRI-activity of MOF composites, by integrating MNPs (Table 2).

The first work was reported by Tregubov et al.,[129] preparing Fe_3O_4@MIL-100(Fe) with a coating of carboxymethyl dextran sodium salt (CMD), resulting in Fe_3O_4@MIL-100(Fe)@CMD with a hydrodynamic diameter in PBS of about 250 nm. The Fe_3O_4@MIL-100(Fe) and Fe_3O_4@MIL-100(Fe)@CMD nanocomposites possessed a transverse relaxivity of about 140 and 157 mM^{-1}·s^{-1}, respectively, considered interesting values close to the highest value reported between the commercialized contrast agent, in particular, the Feridex/Endorem, with a transverse relaxivity of about 152 mM^{-1}·s^{-1}.[208] In further *in vivo* MRI investigations, a darkening effect was concentrated mainly in the spleen and liver, reticuloendothelial organs in charge of removing foreign compounds. This outcome serves however as a clear demonstration of the nanocomposite's potential suitability for imaging applications. Further surface functionalization of the composites could facilitate evasion of the reticuloendothelial system or specific targeting.[209]

The second example, proposed by Lin and colleagues,[116] took advantage of the magnetic properties of a Fe_3O_4@ZIF-8 nanocomposite (∼120 nm, M_S ∼ 18.9 vs 44.3 emu·g^{-1} for Fe_3O_4) as a responsive T_2−T_1 switching contrast agent. The PBS-colloidally stable nanocomposite was however disassembled at acidic pH (6.2 and 5), and also in the presence of glutathione (GSH) at pH 7.4, 6.2, and 5, concluding that acidic conditions and GSH are degrading the system. However, further qualitative (i.e., PXRD) and quantitative characterization (i.e., inductively coupled plasma (ICP), high performance liquid chromatography (HPLC)) could better support the chemical and structural stability of this composite.

https://doi.org/10.1021/acsnanoscienceau.3c00041
ACS Nanosci. Au 2024, 4, 85−114

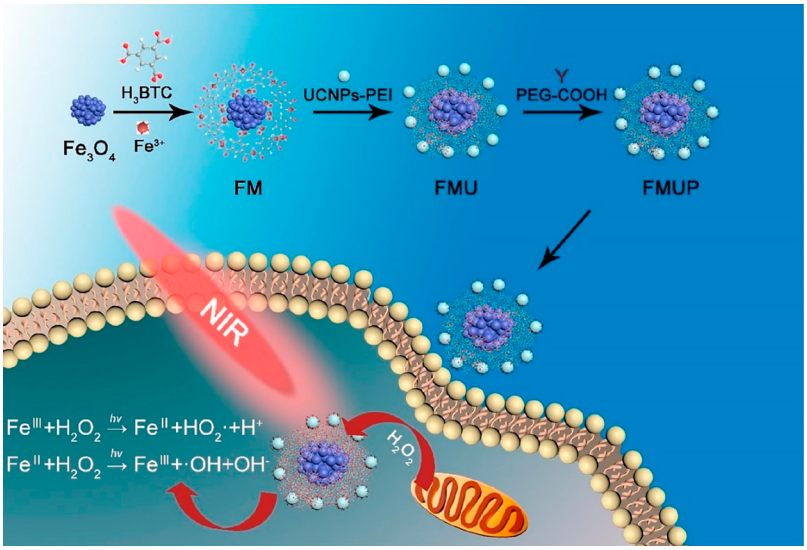

Figure 8. Schematic illustration of the synthesis process of Fe_3O_4@MIL-100(Fe)-UCNPs-PEG (FMUP), and the intracellular photon-Fenton reaction of FMUP with intracellular H_2O_2 under the irradiation of 980 nm. Reproduced from ref 161 with permission from Copyright 2018 Elsevier B.V.

Remarkably, the pH- and GHS-dependent degradation can be advantageously used in the acidic and GSH-overexpressed environment of cancer cells, exhibiting an inverse contrast behavior when the pH decreases and/or the GSH concentration increases. Indeed, under neutral conditions (pH = 7.4), Fe_3O_4@ZIF-8 was a T_2-contrast agent with a ratio of transverse and longitudinal relaxation rates (r_2/r_1) of 24.6, while by the composite disassembling at low pH and GSH, the system switched to a T_1-contrast agent with a r_2/r_1 ratio of 8.4 and 5.7 in case of 4 mM of GSH with pH 6.2 and pH 5, respectively. The r_2/r_1 ratios are higher than the range value (1.03−5.63) of the majority of the commercialized T_2 contrast agents such as Resovist (4.17) and Feridex/Endorem (5.63), at 0.47 T in water at 37 °C.[208] After demonstrating good biocompatibility in human umbilical vein endothelial cells (HUVECs) and a mouse breast cancer cell line (4T1), the *in vivo* MRI detection in mice bearing a 4T1 breast tumor revealed a T_2-darkening effect in the liver and a trigger T_2−T_1 switching to brightening contrast in the tumor. This high proved the potential of these composites as MRI contrast agents.

3.3. Theragnostics

MOFs have garnered significant attention in the biomedical field also as theragnostic systems, with reports of several comprehensive reviews highlighting guest inclusions into MOFs to achieve combined therapeutic and diagnostic capabilities.[20,48,210−216] Herein, we present a range of recent examples showcasing the use of MNP@MOFs for theragnostic purposes. These examples are organized according to our established criteria, progressing from the simplest to the most intricate nanocomposite configurations among each MOF's family.

One of the first examples presented two composites based on the biocompatible MIL-100(Fe) MOF with maghemite (γ-Fe_3O_4) and citrate-functionalized maghemite (cit-γ-Fe_3O_4).[72] These materials were prepared by a simple mixing method that easily provides composites although not very homogeneous. By varying the maghemite content (1 or 10 wt %), the transverse relaxivity for the cit-γ-Fe_3O_4@MIL-100(Fe)-1% and cit-γ-Fe_3O_4@MIL-100(Fe)-10% composites were about 93 and 21 $mM^{-1}{\cdot}s^{-1}$, respectively, being lower than the pure cit-γ-Fe_3O_4 (∼180 $mM^{-1}{\cdot}s^{-1}$). The best performing cit-γ-Fe_3O_4@MIL-100(Fe)-10% nanocomposite encapsulating DOX (14 wt %) was investigated both *in vitro* and *in vivo*, disclosing good biocompatibility and higher anticancer effect than the free DOX on prostatic cancer cells (PC3). Also, they demonstrated *in vivo* a good contrast for T_2-weighted images as well as T_1 contrast agent in a specific ultrashort echo time (UTE) sequence.

Subsequently, Wang et al.[160] also studied the MIL-100(Fe) by the *in situ* growth of the MOF over a carbon shell with carbon dots embedded and the iron oxide core (Fe_3O_4@C), proposing the resulting Fe_3O_4@C@MIL-100(Fe) composite for bioimaging and DDS of the anticancer dihydroartemisinin (DHA). The high DHA cargo (805 $mg{\cdot}g^{-1}$; efficiency of 80.5%) was released in PBS (pH 6.2 and 5.0), being favored under an acidic environment. Concomitantly to the drug release, the MIL-100(Fe) structure collapsed and released Fe^{3+} to the medium, which could be reduced to Fe^{2+} by reductive molecules of the cells (*e.g.*, ferric reductase) and the acidity of tumor cells. The Fe_3O_4@C@MIL-100(Fe) composite exhibited good *in vitro* biocompatibility; however, with an increased cytotoxicity of the DHA-loaded Fe_3O_4@C@MIL-100(Fe) by the generated reactive oxygen species (ROS) as a consequence of both the produced Fe^{2+} and the released DHA. Remarkably, promising *in vivo* anticancer therapy was evidenced, with low side effects and a higher tumor inhibition for DHA-loaded composites (M_S ∼ 21.2 vs 44.4 $emu{\cdot}g^{-1}$ for Fe_3O_4@C), in particular, when an external magnetic field was applied. Additionally, the carbon-shell MNPs contributed with a double bioimaging effect, combining fluorescence optical imaging and MRI (r_2 ∼ 352.45 $mM^{-1}{\cdot}s^{-1}$ at 3 T and 25 °C).

Both of the presented composites are based on the biocompatible MIL-100(Fe), although they differ primarily in the phase of the MNPs employed, specifically maghemite and magnetite in the former and latter cases, respectively. Unlike the first example, the second report extends beyond *in vivo* MRI studies, showcasing a significant antitumor effect in an *in*

https://doi.org/10.1021/acsnanoscienceau.3c00041
ACS Nanosci. Au 2024, 4, 85−114

vivo animal model and attesting to the remarkable potential for engaging in future clinical experiments of great interest.

Additionally, another complex system based on MNP@MIL-100(Fe) was prepared based on upconversion nanoparticles (UPNPs) for PCT and PDT assisted by computed tomography (CT) and upconversion luminescence (UCL) imaging.[161] Through the LbL method, the MOF was synthesized as a shell over the MNPs core and later UPNPs were added. The surface of the resulting composite (~300 nm, Figure 8) was coated with carboxylate-terminal polyethylene glycol (PEG-COOH; Fe_3O_4@MIL-100(Fe)-UCNPs-PEG; FMUP), keeping a BET surface area of about 106 $m^2 \cdot g^{-1}$, with this low surface being associated with the low MOF content (approximately 6%). Indeed, the much higher mass concentrations of Fe_3O_4 and UCNPs were estimated to be approximately 30 and 53%, respectively. Interestingly, this complex system was formed by a N−P heterojunction, where the Fe_3O_4 nanoparticle was an n-type semiconductor and MIL-100(Fe) was a p-type semiconductor. For the first time, this nanocomposite was observed from this perspective, noticing that Fe_3O_4@MIL-100(Fe) (FU) absorbs below 500 nm, with a band energy of about 2.16 eV in the UV−vis diffuse reflectance spectroscopy (DRS). Therefore, the UCNPs acted as a photosensitizer that absorb the near-infrared (NIR) excitation light and convert it to UV−vis light. The combination of them in this heterojunction system was able to produce hydroxyl radicals ($^{\bullet}OH$), one of the toxic ROS, exhibiting a PDT activity. A higher ROS generation capability and, therefore, the highest cell death in HeLa cells, was observed for the Fe_3O_4@MIL-100(Fe)-UCNPs-PEG upon NIR excitation (980 nm laser) with clear detection of the cell death through the confocal laser scanning microscopy (CLSM). Moreover, the Fe_3O_4@MIL-100(Fe)-UCNPs with tested hemocompatibility and low toxicity were further studied for tumor inhibition in mice upon a subcutaneous injection of the carcinoma cells of the uterine cervix of U14, demonstrating a high antitumoral effect. Indeed, for the mice treated with Fe_3O_4@MIL-100(Fe)-UCNPs under the 980 nm NIR laser for 15 min (0.9 W/cm^2, 5 min break after 8 min excitation) at the tumor site, it was observed a slight decrease of the relative tumor volume with respect to the enormous relative volume increase of the control systems. In comparison to its predecessors, this nanocomposite undoubtedly embodies a more intricate system, encompassing the incorporation of UCNPs to enhance therapy efficiency and PEG functionalization to improve MOF stability and biocompatibility. Furthermore, the presence of UCNPs was exploited for *in vitro* and *in vivo* CT and UCL imaging, demonstrating good signals and, therefore, good results for a promising theragnostic agent. Nevertheless, further investigation can be conducted to explore the potential contributions of MNPs, such as MRI imaging or MHT. Undoubtedly, the nanocomposite possesses an untapped potential that warrants further exploration.

Apart from the MIL-100(Fe), there are also several reports based on the extensively studied ZIF-8. For instance, an amino-terminal polyethylene glycol (PEG-NH_2) coated Fe_3O_4@ZIF-8 nanocomposite (~97 nm) with magnetic properties (M_S ~ 6.6 vs 42.6 $emu \cdot g^{-1}$ for Fe_3O_4) was investigated.[122] The drug loading of the antitumoral arsenic trioxide (ATO, $As(OH)_3$) was performed before the polymer coating in an aqueous solution, encapsulating a relatively low amount (53 $mg \cdot g^{-1}$). Note here that the PEG-NH_2 coating could promote a partial release of the drug cargo, with a decrease, indeed, in the determined As content by ICP from 14.35 ± 0.02 to 13.95 ± 0.03 wt %. Subsequently, the drug release in PBS at pH 6.0 or 7.4 revealed 27 or 17% of ATO released after 1 h, 80 or 44% after 1 day, and a maximum of 80% or 53% after 7 days, respectively. The difference in both pH values was related to the partial (pH 7.4) and total (pH 6.0) degradation of the ZIF-8 shell of the composite due to the low hydrolytic stability of this MOF. Furthermore, negligible cytotoxicity was detected in fibroblasts for both drug-loaded and drug-free composites, whereas in malignant atypical teratoid rhabdoid tumor cell lines (BT12 and BT16) the drug-loaded composite presented cytotoxicity. Besides, all the systems provided a good T_2-weighted contrast agent in MRI at 1.5 T in 0.1% agar solution at the temperature of 37 °C, resulting in r_2/r_1 ratios of 48.51, 10.67, and 12.39 for Fe_3O_4 nanoclusters, the drug-free, and the drug-loaded Fe_3O_4@ZIF-8@PEG-NH_2 nanocomposites, respectively. These results highlight the potential of this system because the r_2/r_1 ratio is higher than one of the highest reported between the commercialized T_2 contrast agent, such as Resovist (7.0) and Feridex/Endorem (8.7), at 1.5 T in water at 37 °C.[208] We should however consider that the conditions (agar solution) are far from biological environments, in which the composite could exhibit a completely different chemical and colloidal stability.

Another example of the ZIF-8 nanocomposite was synthesized by He et al.[143] by growing the MOF on carbon shell magnetic cores (Fe_3O_4@C@ZIF-8; ~ 190 nm) and encapsulating a very high content of DOX (730 $mg \cdot g^{-1}$). As shown in previous cases, the drug release was favored under acidic conditions (after 200 h, 95 vs 38% under pH 5.5 and 7.4, respectively). The *in vitro* biocompatibility of Fe_3O_4@C@ZIF-8 and the higher toxicity of DOX-loaded Fe_3O_4@C@ZIF-8 rather than the free-DOX were evidenced on A549 cells. The magnetic nanocomposite (M_S ~ 12 vs 28 $emu \cdot g^{-1}$ for Fe_3O_4@C) reported a promising value of r_2 of about 331.8 $mM^{-1} \cdot s^{-1}$ at 3.0 T in water solution at 25 °C. This specific relaxivity is more than double the value reported for the commercialized T_2 contrast agent Resovist, which is 160 $mM^{-1} \cdot s^{-1}$ at 3.0 T in water at 37 °C.[208] In the previous system, Fe_3O_4@ZIF-8@PEG-NH_2,[122] the cytotoxicity tests were conducted only *in vitro* (fibroblasts and cancer cell lines), suggesting a target cell death for the cancer cells through the cargo release of the DOX-loaded nanocomposites. Instead, in the case of Fe_3O_4@C@ZIF-8, the study was extended to *in vivo* therapeutic efficacy studies upon intravenous administration in mice bearing established A549 cells (lung cancer model), exhibiting an accumulation in the tumor site due to the EPR effect and a clearance mechanism mainly directed to the liver through the T_2*-weighted MR images. Subsequent evaluation of the therapeutic effect demonstrated an average tumor suppression efficacy of the DOX-encapsulated nanocomposite of about 64.5% (vs 16.1% and 12.8% of the free DOX and the not-encapsulated Fe_3O_4@C@ZIF-8, respectively). However, in the first approach, the selection of the PEG-coating suggests that there are some concerns about stability and shelf life of a product based on ZIF-8, which is not considered in the second example. The second example impressively presents *in vivo* efficacy for the therapeutic aspect, coupled with promising MRI detection capabilities.

In an upgrading attempt, Bian et al.[172] fabricated a multifunctional nanocomposite based on Fe_3O_4@ZIF-8 implemented by gold nanoclusters (AuNCs). The MNPs

https://doi.org/10.1021/acsnanoscienceau.3c00041
ACS Nanosci. Au 2024, 4, 85−114

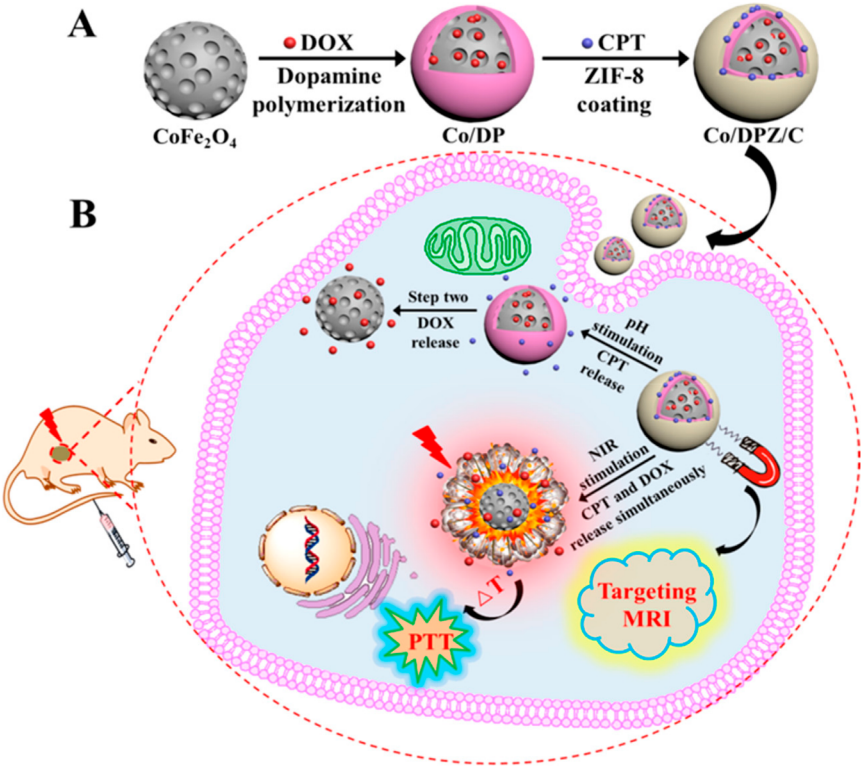

Figure 9. (A) Synthesis of CPT- and DOX-loaded $CoFe_2O_4$@PDA@ZIF-8 nanocarrier and (B) theragnostic strategy of CPT- and DOX-loaded $CoFe_2O_4$@PDA@ZIF-8 nanocarrier for magnetically guided multidrug chemotherapy and photothermal synergistic therapy with pH and NIR-stimulation release. Reproduced from ref 137. Copyright 2017 American Chemical Society.

were initially PAA-coated (~90 nm), adding then GSH capped AuNCs and finally, growing the ZIF-8 over the Fe_3O_4@PAA/AuNCs to obtain the Fe_3O_4@PAA/AuNCs/ZIF-8 nanocomposite (~130 nm) with a moderate magnetic effect (M_S ~ 8.2 vs 44.4 emu·g^{-1} for Fe_3O_4). By associating the DOX with exceptional loadings (1540 mg·g^{-1}; therapy), this theragnostic agent combines a trimodal imaging by (i) MRI (Fe_3O_4 nanoparticles), with a r_2 value of about 53.8 mg^{-1}·mL·s^{-1} at 1.2 T, revealing a r_2 value between the commercialized T_2 contrast agents Resovist (61 mM^{-1}·s^{-1}) and Feridex/Endorem (41 mM^{-1}·s^{-1}) at 1.5 T in water at 37 °C;[208] (ii) computed X-ray tomography (Au), exhibiting the nanocomposite a CT imaging contrast behavior, with increasing intensity of CT signals with the nanocomposite concentration, and (iii) fluorescence optical imaging (FOI), evidencing a more emitting intensity at 609.6 nm of Fe_3O_4@PAA/AuNCs/ZIF-8 than discrete AuNCs at same concentration due to aggregation-enhanced fluorescence (AEF) effect. In comparison to the previous example, the drug loading value in this case demonstrates a remarkable increase (730 vs 1540 mg·g^{-1}) possibly attributed to adsorption on the outer surface of MOF. However, drug release studies in PBS pH 5.3 at 37 °C only showed an initial DOX release of 12.2% within the first 15 min, ruling out the weak association of a large drug amount to the composite. Subsequently, a sustained release was reached, *a priori* associated with a prolonged therapeutic effect. Additionally, *in vitro* studies in human liver cancer cells HepG-2 of this trimodal cancer imaging composite revealed the desired intensity signals of CT and MR (T_2) dependence on the composite concentration and the cell uptake (λ_{em} ~ 609.6 nm) via endocytosis. For the therapeutic effect, the magnetic DOX-loaded composite was suitable for promising magnetically targeted drug delivery, displaying a recovery with a magnet in solution, and pH-sensitive drug release (PBS, pH 7.4 vs 5.3), consistent with the desired preferential release in the acidic cancer cells. The biocompatibility of the Fe_3O_4@PAA/AuNCs/ZIF-8 composite was supported *in vitro* and *in vivo*. Additionally, its intravenous administration for the *in vivo* tumor inhibition in hepatocarcinoma of a H-22 xenograft demonstrated a higher average inhibition rate (70%) in the DOX-loaded Fe_3O_4@PAA/AuNCs/ZIF-8, rather than DOX-free (39%). Respect to the Fe_3O_4@C@ZIF-8, the Fe_3O_4@PAA/AuNCs/ZIF-8 system exhibited a r_2 of about 53.8 mM^{-1}·s^{-1} at 1.2 T, which is compatible with the commercialized T_2 systems at 1.5 T in water at 37 °C (i.e., Resovist and Feridex/Endorem with 41 and 61 mM^{-1}·s^{-1}, respectively).[208] This system has demonstrated trimodal imaging capabilities *in vitro*, which, combined with the *in vivo* tumor suppression efficacy, holds promising potential for synergistic diagnosis and therapy.

Instead, the complex system Fe_3O_4@ZIF-8@ZIF-67/FA/Q[94] (quercetin, Q) exhibits a secondary shell composed of a distinct MOF (ZIF-67), in conjunction with a FA modification that distinguishes it from preceding examples. In the present intricate system, the antitumoral drug (Q) encapsulation and release reported the highest value of efficiency (~93%) at pH 5 with a release of ~79 and 90% of Q after 1 and 9 h in PBS solution at pH 5, respectively. Certainly, the distinct characteristics and attributes of the magnetic core are subject to modification due to the presence and interactions of these dissimilar and overlapping shells. Indeed, the phantom images confirmed the contrast enhancement, therefore, the increase in relaxivity with increasing Fe_3O_4 concentration and the value of r_2 relaxivity were 429.6, 112.0, 85.9 mM^{-1} s^{-1} for Fe_3O_4, Fe_3O_4@ZIF-8, and Fe_3O_4@ZIF-8@ZIF-67/FA nanoparticles

https://doi.org/10.1021/acsnanoscienceau.3c00041
ACS Nanosci. Au 2024, 4, 85−114

at 3 T and 22.5 °C, respectively. The values suggested the possibility to use the nanocomposite as an efficient (T_2) MRI contrast agent. Indeed, the values of r_2 for Fe_3O_4@ZIF-8@ZIF-67/FA are within the range of the commercialized contrast agents measured in water at 37 °C at the same magnetic field.[208] Therefore, the strong MRI signal and drug loading make promising this nanocomposite for theragnostic purposes. In fact, the viability of MCF-7 (FA receptor negative cell line) and MDA-MB-231 (FA receptor positive cell line) cells and the flow cytometric analysis showed a specific uptake by MDA-MB-231 due to the FA targeting, with a toxicity of ∼40, 60, and 80% in MDA-MB-231 cells for higher Fe_3O_4@ZIF-8@ZIF-67/FA/Q concentrations (27, 40.25, and 54 $\mu g \cdot mL^{-1}$, respectively). The noteworthy aspect pertains to the safety associated with the chosen MOFs. The resolution of this inquiry can only be attained through additional *in vivo* testing.

Up to this point, we have seen a magnetic core based on Fe_3O_4. As an alternative, Yang et al.[137] developed a smart pH/NIR dual-stimulus-responsive $CoFe_2O_4$@PDA@ZIF-8 nanocomposite (∼150 nm, Figure 9) based on a mesoporous magnetic $CoFe_2O_4$ containing DOX. Briefly, a PDA layer was first incorporated into the DOX-loaded $CoFe_2O_4$ and, subsequently, a ZIF-8 shell. The latter favored a second encapsulation of the anticancer camptothecin (CPT), which was introduced during the MOF synthesis. The novelty of this DDS lies in both its unconventional magnetic core and its porosity, which translates into a dual loading capacity. Indeed, this system had a loading efficiency of about 98% for DOX and 46% for CPT (the loading value for DOX could be estimated around 98% with respect to the magnetic core, instead, it was not possible to extract in case of CPT due to lack in experimental details related to nanocomposites amount). The cargo release was consistent with the desired pH-response, with the release content of 61% for CPT and 37% for DOX at pH 5.0. Moreover, it had two-stage acidic-mediated processes associated with the degradation of ZIF-8 and PDA, favoring first CPT release in 12 h and, then, DOX in 40 h. The nanocomposite exhibited also a NIR-stimulation release profile, which evidenced a burst release of the two drugs under an 808 nm laser because the magnetic core had a thermal expansion, disintegrating both the PDA and ZIF-8. Furthermore, $CoFe_2O_4$@PDA@ZIF-8 exhibited good viability in HepG2 cells. In contrast, the nanocomposite showed significant cytotoxicity in the case of all the drug combinations (DOX, CPT, DOX+CPT) with/without NIR-stimulation, with the highest cell death for the CPT-loaded $CoFe_2O_4$@PDA@ZIF-8 with NIR, proving the *in vitro* efficacy of the system. In addition, the magnetic $CoFe_2O_4$@PDA@ZIF-8 (M_S ∼ 36.4 vs 68.5 $emu \cdot g^{-1}$ for $CoFe_2O_4$) demonstrated a T_2-weighted imaging capacity at 1.2 T (r_2 = 38.3 vs 53.3 $mM^{-1} \cdot s^{-1}$ $CoFe_2O_4$@PDA), in the range of the highest value for the commercialized T_2 contrast agent (at 1.5 T in water at 37 °C[208]). Interestingly, a significant darkening *in vivo* effect (HepG2 tumor-bearing mice) was observed in the liver upon 1 h postinjection of the drugs-loaded composite and, after 9 h, in the tumor region. Subsequently, considering the *in vitro* photothermal effect of CPT- and DOX-loaded $CoFe_2O_4$@PDA@ZIF-8 (T > 65 °C), the *in vivo* performance was studied in a HepG2 xenograft tumor-bearing mice model. After 9 h-injection, according to the highest MRI darkening signal at the tumor site, the light−heat conversion under NIR laser was tested, resulting in an increase from 32 to 50 °C in the cancer area after only 10 min exposure. In conclusion, the *in vivo* PTT and simultaneous CPT and DOX therapy showed a promising synergistic effect on tumor size inhibition (from relative tumor volume 5.5 ± 1.2 (PBS) to 0.6 ± 0.2 for nanosystems under NIR), with histologic coagulative tumor necrosis of 90%. In addition, upon the location of a magnet located in the proximity of the tumor site (magnetic guided therapy) without NIR, the relative tumor volume was about 0.9 ± 0.4 with a tumor necrosis of 80% (vs 1.2 ± 0.6 and 75% in the case of nonmagnetically guided CPT and DOX therapy). The dual drug therapy combined with the implementation of magnetically guided administration and NIR laser reached a relative tumor volume of 0.3 ± 0.1 (magnet + NIR), with histologic coagulative tumor necrosis of 97%. These results, associated with the absence of appreciable damages or inflammatory lesions on normal tissues after treatment, demonstrated safe and potential applications. This example serves as a notable demonstration of the potential to leverage the "tissue transparent window", emphasizing the already-established significance of MOFs in PTT.[217] Further, this advanced research highlights an unconventional approach wherein the noninvasive placement of a magnet in proximity to the tumor site in mice contributes to enhance the formulation efficacy. This groundbreaking approach, first pioneered by Falcaro and collaborators, involved spatial control pertaining to MNPs@MOF within microfluidic circuits.[83] The potential implications of this concept are far-reaching, as it paved the way to extend and position control techniques in therapeutics within organisms, thereby enabling sophisticated control over drug delivery systems. Nonetheless, further studies dealing with the biodistribution and safety of both ZIF-8 and $CoFe_2O_4$ would complete this really nice piece of work.

Apart from the guided-therapy using the magnetic properties of MNPs, its therapeutic effect can be also explored under an external AMF. In discussing therapy involving MNPs, the primary focus is often on utilizing a high-frequency alternating magnetic field (HF-AMF, 50−400 kHz) to induce localized temperature elevation (or magnetic hyperthermia; MHT).[218] However, in the forthcoming example, the recent advancements in various magnetic nanocomposites have led to the exploration of an alternative approach utilizing extremely low-frequency alternating magnetic fields (ELF-AMF, 0.01−10 kHz).[218] Indeed, in several magnetic nanocomposites (e.g., magnetoliposomes),[218−223] extensive investigations have been conducted to examine drug release promotion under lower magnetic field strength. In the case of MNP@MOF, Fang et al.[95] proposed a magnetic Fe_3O_4@ZIF-90 nanocomposite (∼65 nm) conjugated with rat serum albumin (RSA; M_S ∼ 7 vs 49 $emu \cdot g^{-1}$ for Fe_3O_4) as an AMF-triggered DDS, under potential MRI observation. Indeed, MRI studies reported a good transverse relaxivity (r_2) of about ∼133.7 $mM^{-1} \cdot s^{-1}$ under 7 T and a T_2-weighted darkening effect in images. Further studies with different magnetic fields will permit to better compare it with commercial products, even if some recent studies are investigating also this magnetic field for human brain disorders.[224] Additionally, Fe_3O_4@ZIF-90 was able to encapsulate the antitumoral drug 5-FU with a progressive release in PBS (50% released in 7 h), which could be accelerated by applying an ELF-AMF (50% released upon 1.5 h under ELF-AMF with a frequency of 20 Hz applied for 20 min every 1 h). An ELF-AMF applied for even 3 h did not provoke any MHT effect, which was detected only under an HF-AMF using 488 kHz for 10 min, with an increase of temperature of about 15 °C. Therefore, this study presents the

https://doi.org/10.1021/acsnanoscienceau.3c00041
ACS Nanosci. Au 2024, 4, 85−114

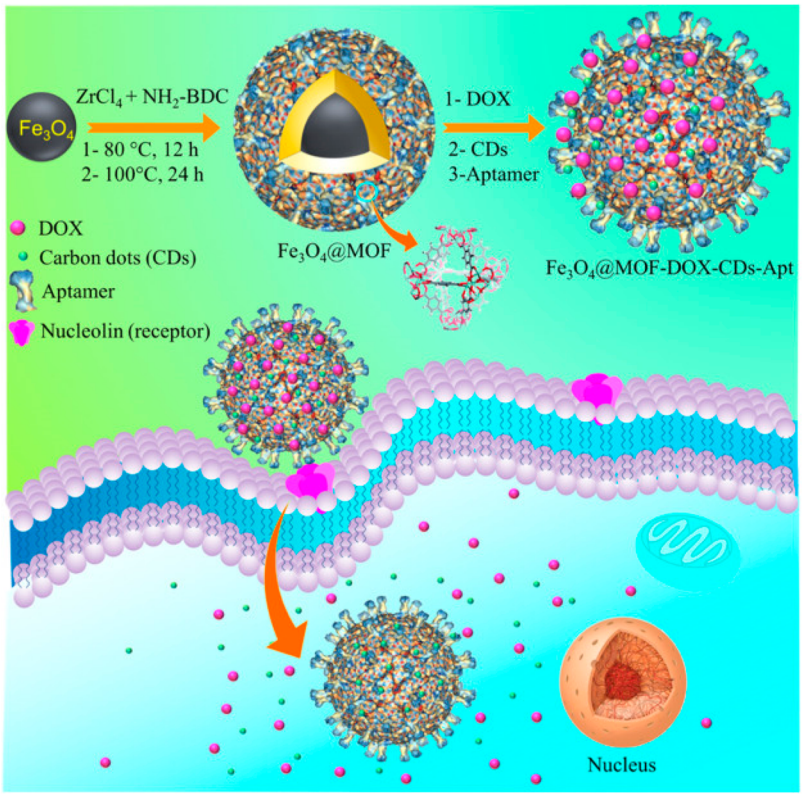

Figure 10. Schematic illustration of the synthesis of UiO-66-NH_2 on the as-synthesized magnetic Fe_3O_4 nanoparticles, and postmodification of the nanostructure with DOX, carbon dots, and nucleolin-binding aptamer conjugation. Subsequently, a schematic illustration of the cell internalization of the Fe_3O_4@MOF-DOX-CDs-Apt via a nucleolin-mediated interaction and pH-triggered DOX release in lysosome or endosome of the cancer cells. Reproduced from ref 126 with permission from Copyright 2020 Elsevier Inc.

initial instance of employing ELF-AMF in a magnetic nanocomposite based on MOFs. Undoubtedly, this system represents a potential alternative pathway for exploration in the coming years, extending this approach to *in vitro* and subsequently *in vivo* investigations.

In the family of UiO, three interesting works are reported. First, Zhao et al.[142] proposed a biocompatible Fe_3O_4@UiO-66 nanocomposite (~240 nm; M_S ~ 51.6 vs 69.7 emu·g^{-1} for Fe_3O_4) with an extremely high DOX loading capacity (2000 mg·g^{-1} and efficiency of 66.3% wt). The authors attributed the substantial drug capacity to the extensive surface area of the shell and the UiO-66/DOX interactions; notably, the stable coordination bonding between the deprotonated hydroxyls in DOX and the numerous Zr^{4+}, as confirmed by UV−vis spectroscopy and X-ray photoelectron spectroscopy (XPS)[142] as well as other interactions ($\pi-\pi$ stacking between the aromatic anthracycline and the aromatic ligand, hydrogen bonding, etc.). However, this extreme loading could be also related to surface adsorption or to the presence of a large number of defects in the UiO-66 structure, promoting the interactions and a larger porosity. Afterward, the drug was gradually delivered as a function of the pH in PBS, with a sustained release of DOX in 41 days of 36, 22, 17, and 14% at pH 4.0, 5.0, 6.0, and 7.4, respectively. As already stated, the release of drugs in buffer solutions under acidic pH is influenced by various factors. The stability of the MOF can be impacted by the phosphate groups, able to coordinate Zr replacing the interactions with both DOX and the organic linker. Additionally, the protonation of the amino group in DOX leads to a positively charged DOX molecule, thus weakening its interactions with the MOF, which presented a less negative surface zeta potential under acidic conditions. Even at a low dose (20 mg·L^{-1}), DOX-loaded Fe_3O_4@UiO-66 composites manifest 60% of cell death in HeLa cells, comparable with free DOX. The antitumor activity of DOX-loaded Fe_3O_4@UiO-66 increased either with the DOX loading or with longer incubation times, supporting a progressive release under these conditions. Furthermore, *in vivo* safety and biodistribution studies demonstrated the low toxicity of the magnetic composite with accumulations mainly in the spleen and liver, as expected for nonfunctionalized nanoparticles.[209] In addition, Fe_3O_4@UiO-66 had a T_2 contrast agent behavior with an important r_2 ~ 255.9 $mM^{-1}·s^{-1}$, revealing the *in vitro* MR images with a concentration-dependent darkening effect. Experimental conditions used a slightly higher magnetic field, closer to one of the generally applied ones (0.55 vs 0.47 T), and a low temperature (32 vs 37 °C). The determined r_2 is higher than the majority of the commercialized T_2 contrast agents, with maximum value for Resovist at 0.47 T in plasma at 37 °C.[208] *In vivo* studies in HeLa tumor-bearing mice intravenously injected with the nanocomposites showed good T_2-weighted MR signals in the tumor after 1 h postinjection with a maximum of darkness after 9 h, verifying a tumor growth inhibition after 21 days postinjection.

In another work dealing with a DOX-containing Fe_3O_4@UiO-66-NH_2 nanocomposite (drug loading content 62 wt %), Alijani and co-workers[126] proposed a tiny DOX-loaded core−shell nanostructure (~16 nm) with the conjugation of highly fluorescent carbon dots (CDs) and a nucleolin-binding aptamer (Apt), AS1411. This system, denoted as Fe_3O_4@

https://doi.org/10.1021/acsnanoscienceau.3c00041
ACS Nanosci. Au 2024, 4, 85−114

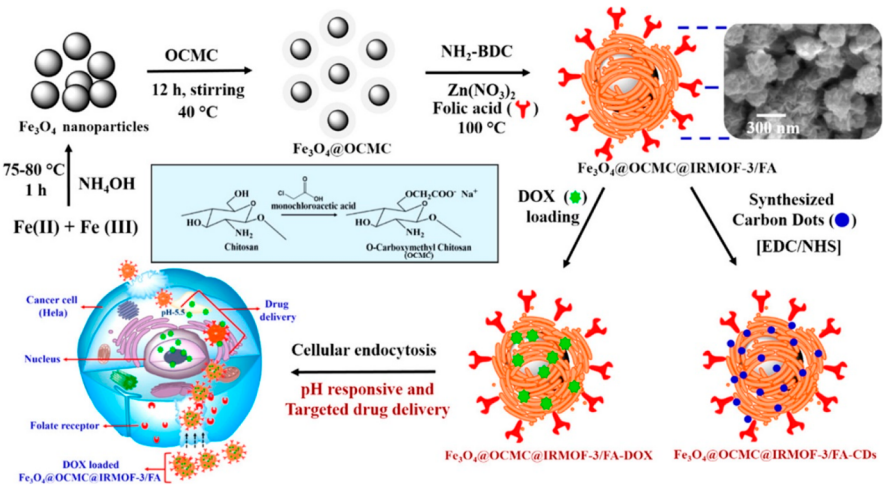

Figure 11. Schematic representation of the synthetic procedure for the FA encapsulated magnetic nanoscaled MOFs as targeted DOX carriers. Reproduced from ref 102. Copyright 2016 American Chemical Society.

UiO-66-NH_2-DOX-CDs-Apt (Figure 10), was investigated as a stimuli-responsive antitumoral drug carrier and cellular bioimaging. Additionally, the cytotoxicity on normal HUVEC and human epithelial breast cancer cells (MDA-MB-231), characterized by nucleolin overexpression, was evaluated for Fe_3O_4@MOF, Fe_3O_4@MOF-DOX, Fe_3O_4@MOF-DOX-CDs, and Fe_3O_4@MOF-DOX-CDs-Apt. In the HUVEC cells, it was observed good cell viability (>90%) for all the composites. Meanwhile, in the MDA-MB-231, it was reported a concentration-dependent toxicity in the two DOX-loaded systems. At the same concentration, the highest toxicity was obtained with Fe_3O_4@MOF-DOX-CDs-Apt, with a 77% of cancer cells death by mainly apoptosis induction. Henceforth, a selective therapeutic effect was proven. Subsequently, cell internalization mediated by aptamer-nucleolin recognition was confirmed in the MDA-MB-231 cancer cell line. Regarding the *in vitro* drug release, Fe_3O_4@MOF-DOX-CDs-Apt at pH 5.5 and 7.4 exhibited a progressive release over time without burst effect and, after 4 days, of about 29.1% and 47.3% at pH 7.4 and pH 5.5, respectively.

Finally, based also on Fe_3O_4@UiO-66-NH_2, Wu et al.[225] developed a theragnostic nanocomposite (~40−60 nm) loaded with the 5-FU (efficiency 11%, the loading value was not possible to extract due to lack in experimental details related to 5-FU content) and a water-soluble carboxylatopillar[6]arene (WP6) coating, known as Fe_3O_4@UiO-66-NH_2@WP6. The drug loading proceeded before the WP6 functionalization, to ensure high drug loading and furthermore promote the release in cancer cells, although postfunctionalization could promote delivery of the active cargo. Indeed, the drug release was facilitated by acidic pH (7 vs 5), temperature, and divalent metal ions in the body (*e.g.* Ca^{2+} and Zn^{2+}), weakening the interaction of the WP6 due to its carboxylate groups chelated by them. The 5-FU-loaded Fe_3O_4@UiO-66-NH_2@WP6 (M_S ~ 46.8 vs 89.3 emu·g^{-1} for Fe_3O_4) could be separated by an external magnetic field and, furthermore, the Fe_3O_4 in the nanoplatform imparted superparamagnetism. Also, 5-FU-loaded Fe_3O_4@UiO-66-NH_2@WP6 demonstrated good *in vitro* biocompatibility on normal HUVEC and an antitumoral activity in HeLa cells. Finally, the nanocomposite behaved as a T_2-weighted MRI contrast agent with an evident darkening effect of MRI signals in HeLa cells and a r_2 of about 72.2 $mM^{-1}·s^{-1}$ under a 7 T magnetic field. In contrast with commercial contrasts, generally employed at 1.5 T for clinical instruments and at 0.47 T for relaxation measurements,[208] here the darkening effect is investigated at a high magnetic field strength of 7 T. Emerging research trends currently to explore higher magnetic fields, aiming to provide a rationale for its implementation since, as opposed to lower magnetic fields, their superior signal-to-noise and contrast-to-noise ratios. These enhanced ratios facilitate high-resolution imaging and improved contrast, thereby enabling easier identification of lesions and structural alterations associated with brain disorders.[224] In the case of Fe_3O_4@UiO-66 and Fe_3O_4@UiO-66-NH_2@WP6, the obtained r_2 values are particularly compelling for a simpler nanocomposite. Conversely, despite the proven targeting in Fe_3O_4@UiO-66-NH_2-DOX-CDs-Apt and the bright green emission of CDs under UV light, further investigations are required to explore the potential of this system as fluorescence imaging or MRI agent.

Nanocomposites based on other MOF structures were also prepared. For instance, a magnetic core−shell Fe_3O_4@IRMOF-3 nanocomposite conjugated with FA (200 nm; M_S ~ 48.9 vs 80.46 emu·g^{-1} for Fe_3O_4) was proposed for theragnostic,[101] associating the antitumoral paclitaxel (PTX; 123.2 mg·g^{-1} and efficiency of 82%). The cytotoxicity assays in HeLa and murine fibroblast (NIH3T3) revealed a selective and concentration-dependent toxic effect only for PTX-loaded Fe_3O_4@IRMOF-3/FA, with a cell death higher for cancerous cells. Additionally, the fluorescence microscopy confirmed an endocytosis cell uptake of Fe_3O_4@IRMOF-3/FA and the MRI study in a clinical scanner (1.5 T) reported a darkening signal in HeLa cells. Even if the M_S presented a promising value, the system was not further investigated for MHT. Lastly, the PTX-loaded Fe_3O_4@IRMOF-3/FA system exhibited a controlled drug release over time in a simulated physiological media at pH 7.4, underlining its potentiality as a DDS and T_2-weighted MRI contrast agent. As an alternative, Chowdhuri and co-workers[102] reported an interesting more complex IRMOF-3 composite (Figure 11) based on O-carboxymethyl chitosan (OCMC) functionalized MNPs (Fe_3O_4@OCMC) and fluorescence CDs, evaluating its optical imaging. The MOF growth occurred on the Fe_3O_4@OCMC nanoparticles in the presence of FA, showing a flower-like morphology (~200 nm), and

https://doi.org/10.1021/acsnanoscienceau.3c00041
ACS Nanosci. Au 2024, 4, 85−114

Table 3. Comparative Review of Magnetic Nanocomposites for Theragnostics[a]

MNP@MOF	MNP	OL	MP for MOFs	MNP@ MOF size (nm)	M_S ($emu \cdot g^{-1}$)	D	B (T)	r_1 ($mM^{-1} \cdot s^{-1}$)	r_2 ($mM^{-1} \cdot s^{-1}$)	r_2/r_1	T	drug	DL ($mg \cdot g^{-1}$)	LE (%)	TCL	ref
γ-Fe_3O_4@MIL-100(Fe) and cit-γ-Fe_3O_4@MIL-100(Fe)	Fe_3O_4	NH_2-H_2BDC	Fe^{3+}	150−170	35−62	MRI	7	NR	93*[b]	NR	DDS	DOX	140	NR	PC3	72
Fe_3O_4@C@MIL-100(Fe)	Fe_3O_4	NH_2-H_2BDC	Fe^{3+}	190	21.2	FOI and MRI	3	NR	352.45	NR	DDS	DHA	804.9	80.5	HeLa and A549	160
Fe_3O_4@MIL-100(Fe)-UCNPs-PEG	Fe_3O_4	NH_2-H_2BDC	Fe^{3+}	300	NR	CT and UCL	NR	NR	NR	NR	PCT and PDT	NR	NR	NR	L929 and HeLa	161
Fe_3O_4@ZIF-8@PEG-NH_2	Fe_3O_4	HmIM	Zn^{2+}	97	6.6	MRI	3	2.37	25.25	10.67	DDS	ATO	70	NR	fibroblast, BT12, and BT16	122
Fe_3O_4@C@ZIF-8	Fe_3O_4	HmIM	Zn^{2+}	190	12	MRI	3	NR	331.79	NR	DDS	DOX	730	NR	A549	143
Fe_3O_4@PAA/AuNCs/ZIF-8	Fe_3O_4	HmIM	Zn^{2+}	130	8.2	MRI, CT, and FOI	1.2	NR	53.79	NR	DDS	DOX	1540	81.1	HepG-2	172
Fe_3O_4@ZIF-8@ZIF-67/FA	Fe_3O_4	HmIM	Zn^{2+}, Co^{2+}	>450		MRI	3	2.042	85.86	NR	DDS	Q	NR	93	MCF-7 and MDA-MB-231	94
$CoFe_2O_4$@PDA@ZIF-8	$CoFe_2O_4$	HmIM	Zn^{2+}	150	36.4	MRI	1.2	NR	38.3	NR	DDS	DOX and CPT	NR	98 (DOX) and 46 (CPT)	HepG2	137
Fe_3O_4@ZIF-90	Fe_3O_4	2-ICA	Zn^{2+}	65	7	MRI	7	NR	133.7	NR	DDS under ELF-AMF	5-FU	NR	NR		95
Fe_3O_4@IRMOF-3/FA	Fe_3O_4	NH_2-H_2BDC	Zn^{2+}	200	48.9	MRI	1.5	NR	NR	NR	DDS	PTX	123.2	82.04	HeLa and NIH3T3	101
Fe_3O_4@OCMC@IRMOF-3/FA	Fe_3O_4	NH_2-H_2BDC	Zn^{2+}	250	51	FOI					DDS	DOX	163	96	L929 and HeLa	102
Fe_3O_4@UiO-66	Fe_3O_4	NH_2-H_2BDC	Zr^{4+}	240	51.6	MRI	0.5	NR	255.87	NR	DDS	DOX	2000	NR	3T3 and HeLa	142
Fe_3O_4@UiO-66-NH_2-DOX-CDs-Apt	Fe_3O_4	NH_2-H_2BDC	Zr^{2+}	16**[c]		FOI					DDS	DOX	62	NR	HUVEC and MDA-MB-231	126
Fe_3O_4@UiO-66-NH_2@WP6	Fe_3O_4	NH_2-H_2BDC	Zr^{4+}	40−60	46.8	MRI	7	NR	72.23***[d]	NR	DDS	5-FU	NR	10.9	HUVEC and HeLa	225
Fe_3O_4@C@P-MOF	Fe_3O_4	TCPP****[e]	Fe^{3+}	95	24.5	FOI and MRI	1.2	1.23	72.6	59.0	PTT and PDT	NR	NR	NR	MCF-7 cells	226

[a]OL = organic linker, MP = metal precursor, D = diagnosis, B = magnetic field, *T* = therapy, DL = drug loading, LE = loading efficiency, TCL = targeted cell line. [b]cit-γ-Fe_3O_4@MIL-100(Fe)-10% (with a 10 wt % of maghemite content) [c]Value for just Fe_3O_4@UiO-66-NH_2 [d]Drug-loaded nanoplatform [e]TCPP: [5, 10, 15, 20-Tetrakis (4-carboxyl)-21*H*, 23*H*-porphine]

https://doi.org/10.1021/acsnanoscienceau.3c00041
ACS Nanosci. Au 2024, 4, 85−114

promoting targeted drug delivery toward the overexpression of folate receptor in various tumors. Finally, highly fluorescent CDs (~10 nm) were conjugated to the FA-nanocomposite for optical imaging. Actually, the UV−vis absorbance spectrum of Fe_3O_4@OCMC@IRMOF-3/FA showed two bands, at 280 nm characteristic of n−π^* transitions of FA and ~345 nm due to IRMOF-3 (330 nm) and the $\pi-\pi^*$ transitions of FA (360 nm). In point of fact, the magnetic nanocomposite (M_S ~ 51 vs 78 and 66.5 emu·g^{-1} for Fe_3O_4 and Fe_3O_4@OCMC, respectively) exhibited also a fluorescent band, with intensities tuned by the excitation wavelength. Therefore, the CDs presence permitted the monitoring of the intracellular uptake into the folate-overexpressed HeLa cells, demonstrating an endocytosis process favored by FA recognition. Besides, the Fe_3O_4@OCMC@IRMOF-3/FA nanocomposite underwent a physical DOX encapsulation (163 mg·g^{-1}; efficiency 96%), where the loading efficiency may be correlated with the surface adsorption of the drug onto the complex nanocomposite.[186] In addition, the *in vitro* toxicity of the unloaded nanocomposite showed biocompatibility while the DOX-loaded nanocomposite reported a selective toxic effect toward cancer cells via apoptosis due to the FA-conjugation. Lastly, Fe_3O_4@OCMC@IRMOF-3/FA exhibited good stability under physiological media at pH 7.4, with a higher drug release at lower pH (48 and 55% of DOX released with respect to 22 and 27% at pH 5.5 and 7.4 after 12 and 24 h, respectively). In both IRMOF-3-based examinations, FA-conjugation was exploited to achieve selective endocytosis. Despite the promising MRI capabilities of these systems, even demonstrating fluorescence imaging when associated with CDs, it would be worthwhile to pursue *in vivo* studies investigating their biodistribution, elimination, safety, and efficacy.

Another nanocomposite, Fe_3O_4@C@P-MOF (~95 nm, M_S ~ 24.5 emu·g^{-1}) based on a Fe_3O_4@C core (M_S ~ 39.8 emu·g^{-1}) and a porphyrin-MOF (PMOF) was prepared,[226] proposing a dual-imaging and dual-therapy. An imaging-guided therapy was possible for this system, which presented a MRI darkening effect at 1.2 T with a r_2 ~ 72.6 $mM^{-1}\cdot s^{-1}$ and r_2/r_1 of about 59.0 (note here that the experimental temperature was set at 30 °C). Indeed, the r_2/r_1 ratio is higher than the best reported for commercialized T_2 contrast agents (Resovist 7.01 and Feridex/Endorem 8.72), with also a higher r_2 value (Resovist 61 and Feridex/Endorem 41) at 1.5 T in water at 37 °C.[208] Moreover, the optical properties highlighted potential not only for FOI but also for PTT and PDT, with a strong absorption band at 416 nm and four peaks over an extended broad absorption band that covered all the spectrum until the NIR region. The emission capacity (λ_{em} ~ 688 nm with λ_{ex} ~ 553 nm) and the significant Stocks shifts extended the nanocomposite also as a fluorescent imaging system. Related to the therapy, the photothermal tests revealed a significant rise in temperature (>50 °C) under 808 nm NIR irradiation. This is a value maybe too high for safety, although more real tests will be required. Furthermore, the PTT efficiency was independent of the PDT one, which reported a $^1O_2$ generation under 655 nm irradiation with a $^1O_2$ quantum yield of ~44%. From a solution to *in vitro* test, further interesting results showed, first, the nanocomposite biocompatibility in breast cancer MCF-7 cells. Then, upon irradiation for 10 min under 665 nm (PDT) or 808 nm (PTT), an increase in toxicity was reported by increasing the nanocomposite concentration and by cotreating with both PDT and PTT. Fixing a dose of 20 mg·kg^{-1}, then the biocompatibility was further confirmed in female BALB/c-nu mice, without evident side effects. The *in vivo* dual-imaging efficiency for intravenously injected Fe_3O_4@C@P-MOF was verified in healthy nude mice and MCF-7 tumor-bearing nude mice, qualitatively reporting after 22 h in both MR and fluorescence imaging an accumulation in the liver, with a clearance within 8 days through feces and urine. In the presence of a tumor, it was observed intense fluorescent and MRI signals in the cancer region after 26 h, assigned to an EPR effect. The high tumor uptake was *in vivo* studied for PTT, PDT, and PTT-PDT co-therapy, reporting the highest tumor growth inhibition in the synergistic dual-therapy compared to single PTT, single PDT, just composites and control. Additionally, *ex vivo* tests reported an efficient uptake of the nanocomposites in the tumor tissue, analyzing all the major organs dissected and imaged with both MRI and FOI. From our perspective, this particular example is undeniably highly biologically relevant, although may lack some MOF chemical information (structural, textural, etc.). The amalgamation of MRI properties offered by the MNPs, coupled with the diagnostic and therapeutic attributes contributed by the MOF, holds great promise within the nanocomposite.

Overall, Table 3 comprehensively presents the data pertaining to the selected theragnostic examples, evidencing once again that benchmarked MOF families are prevalent (MIL-100(Fe), UiO-66, ZIF-8), although here two new MOF structures are also introduced with interesting performances (*e.g.* IRMOF-3 and PMOF). Most of them with a particle size from 50 to 250 nm, compatible with an intravenous administration of course, dependent also on their biological chemical and colloidal stability, which will significantly influence their biodistribution, elimination, safety and efficacy. In terms of magnetic properties, M_S values range from 6.6 to 62 emu·g^{-1}. Although mostly with relatively low M_S values, few composites demonstrate higher values such as 51,[102] 52,[142] and 62,[72] many of these systems combine magnetic properties with the incorporation of other types of nanoparticles to enhance their imaging and therapy capabilities. Some of these complex nanocomposites present noteworthy competitive MRI results, comparable with commercially available contrast agents. Nonetheless, it is evident that there remains limited exploration of the magnetic properties specifically for therapeutic aspects, especially within the realm of MHT.

4. CHALLENGES AND PERSPECTIVES

Studies over the last 15 years have achieved great development of MOFs and MNPs, as well as their composites, in the biomedical field, including drug delivery, bioimaging, and theragnostics. The main idea behind the development of this type of composites materials is to enhance and exploit the properties of the two components in an additive and/or synergistic manner, combining high biocompatibility (even an intrinsic therapeutic MOF activity) and efficient chemotherapy with complementary magnetic hyperthermia therapies, magnetically guided targeting and/or MRI, among others.

The current synthetic strategies based on magnetic MOF composites have been categorized into: mixing, *in situ* formation of MNPs in the presence of MOFs, *in situ* formation of MOFs in the presence of MNPs, and layer-by-layer (LbL) protocols. One of the main challenges is to favor the interaction between the MNP and the MOF. In this sense, strong interactions are required to promote (a) the encapsulation of MNPs within the framework (mixing), (b) the incorporation of MNP's precursor (MNPs *in situ*

https://doi.org/10.1021/acsnanoscienceau.3c00041
ACS Nanosci. Au 2024, 4, 85−114

formation), and (c) the growth of a MOF shell around the MNP (*in situ* MOF growth and LbL). Furthermore, the interactions should lead to a stable composite with the desired properties.

Another key factor is controlling the ratio of MNPs per MOF as well as the MNPs location in the final composite, leading to a lack of reproducibility and homogeneity in the composite synthesis. To date, there is no evidence in the literature on how to control the distribution of the MNPs within a porous matrix by mixing or *in situ* MNP growth method, promoting their formation exclusively onto the surface or, even, leading to the formation of outer aggregates (close to a physical mixture of MNPs and MOFs) that are difficult or impossible to be lately removed. This is the reason why *in situ* MOF formation methods with presynthesized MNPs and LbL strategies are much more developed in order to finely tune the morphology, although here the chemical and colloidal stability of the MNPs under the synthetic conditions of the MOF should be considered. In this sense, it remains still unclear the exact conditions necessary to obtain core−shell over non-core−shell structures. Undoubtedly, a more comprehensive understanding of the interactions that favor core−shell versus non-core−shell structures will potentially raise the interest in this topic.

At present, such a knowledge gap impedes its development, reproducibility, and subsequent scale-up. Thus, the current scientific literature is still far from achieving a marketable product suitable for biomedical purposes. To optimize synthetic procedures for such systems, various critical aspects need to be addressed, including: (i) the selection of precursors that are amenable to large-scale production, with particular attention given to their solubility; (ii) the use of water as the reaction media for environmentally friendly conditions, maintaining mild synthetic conditions (temperatures and pressures), compatible with MNPs' stability; and (iii) the development of convenient washing processes for the large-scale implementation, allowing the nanocomposite recovery and avoiding aggregation phenomena.

As for their application, when employing them as DDSs, the main challenge lies in achieving adequate magnetic properties that can facilitate potential drug release under a magnetic field, such as in the case of MHT. The ultimate goal is to create a nanocomposite that enhances drug transport capabilities beyond what the individual components can achieve alone. While the current work holds great promise, it is important to note that it primarily focuses on a more or less model drug (DOX; with already commercialized nanoformulations) as the main encapsulated active ingredient. The size of the pores within the MOF nanocarrier may limit the range of drugs that can be investigated. One of the challenges toward new drugs for these nanocarriers is understanding the interactions that facilitate and promote drug encapsulation within the porous matrix, and the subsequent manipulation of these interactions to achieve controlled and potentially targeted drug release through the properties of magnetic nanoparticles. Furthermore, it is essential to conduct *in vivo* studies, not only to demonstrate controlled and targeted drug release but also to evaluate the potential advantages of these nanocomposites over existing drugs in terms of increasing their efficacy while minimizing their adverse effects. Multitude of challenges must be addressed for their widespread clinical use for theragnostic. Nevertheless, the benefits of magnetic nanocomposites for this application could be significant, including the ability to diagnose and treat diseases with greater precision and efficiency, leading to improved patient outcomes.. In this sense, the strategies to address the current limitations and challenges in the development of MNP@MOF composites in the biomedical field include: (1) investigating intrinsic activity of both MNPs and MOFs to promote the formation of highly effective and safe nanocomposites and evaluating the MNP-MOF interactions through advanced characterization techniques (*e.g.*, NMR, HR-TEM, 3D tomography reconstruction); (2) extending synthesis optimization with standard operating procedures, prioritizing biocompatible and available precursors and solvents for a step forward large-scale production; (3) developing nanocomposites that enhance drug transport capabilities beyond what the individual components (MOF or MNPs) can achieve alone, with a focus on understanding the interactions that facilitate and promote drug encapsulation/release by using spectroscopic analysis or computational studies; (4) conducting comprehensive *in vitro* and *in vivo* studies to ensure the safety and efficacy of the nanocomposites, as well as to demonstrate controlled and targeted drug release, potentially leading to improved patient outcomes. These strategies aim to overcome the challenges and limitations associated with MNP@MOF composites, ultimately paving the way for their widespread clinical use in theragnostic applications.

In conclusion, the key point is to study the factors that promote the formation of MNP@MOF nanocomposites, subsequently, by investigating the stability, porosity, biocompatibility, and intrinsic activity of both MNPs and MOFs. In this sense, researchers can develop nanocomposites that are highly effective and safe for their use in nanomedicine. After synthesis optimization, such procedures must be extended for reproducible large-scale production while maintaining the desirable properties of the nanocomposites. Finally, both the safety and efficacy of the nanocomposites must be ensured through comprehensive *in vitro* and *in vivo* studies to propose them in the future for the biomedical market.

AUTHOR INFORMATION

Corresponding Author

Patricia Horcajada − *Advanced Porous Materials Unit, IMDEA Energy Institute, 28935 Madrid, Spain;* orcid.org/0000-0002-6544-5911; Email: patricia.horcajada@imdea.org

Authors

Darina Francesca Picchi − *Advanced Porous Materials Unit, IMDEA Energy Institute, 28935 Madrid, Spain;* orcid.org/0009-0008-7941-3671

Catalina Biglione − *Advanced Porous Materials Unit, IMDEA Energy Institute, 28935 Madrid, Spain;* orcid.org/0000-0001-7361-7093

Complete contact information is available at: https://pubs.acs.org/10.1021/acsnanoscienceau.3c00041

Author Contributions

CRediT: Conceptualization by P.H., D.F.P wrote the review, C.B. and P.H. reviewed it and support the writing. All the authors have accepted responsibility for the entire content of this submitted manuscript and approved submission. CRediT: **Darina Francesca Picchi** investigation, writing-original draft, writing-review & editing; **Catalina Biglione** investigation,

https://doi.org/10.1021/acsnanoscienceau.3c00041
ACS Nanosci. Au 2024, 4, 85−114

supervision, writing-review & editing; **Patricia Horcajada** conceptualization, funding acquisition, project administration, resources, supervision, writing-review & editing.

Notes

The authors declare no competing financial interest.

■ ACKNOWLEDGMENTS

This work was supported by the Marie Skłodowska-Curie Actions, HeatNMof ITN under Grant ID: 860942. C.B. thanks the European Union's Horizon Europe Research and Innovation Programme for the Marie Sklodowska-Curie grant agreement No 101061833 (BioPolyMOF).

■ REFERENCES

(1) Horcajada, P.; Gref, R.; Baati, T.; Allan, P. K.; Maurin, G.; Couvreur, P.; et al. Metal-Organic Frameworks in Biomedicine. *Chem. Rev.* **2012**, *112*, 1232−1268.
(2) Lu, K.; Aung, T.; Guo, N.; Weichselbaum, R.; Lin, W. Nanoscale Metal-Organic Frameworks for Therapeutic, Imaging, and Sensing Applications. *Adv. Mater.* **2018**, *30* (37), 1707634.
(3) Demir Duman, F.; Forgan, R. S. Applications of Nanoscale Metal-Organic Frameworks as Imaging Agents in Biology and Medicine. *J. Mater. Chem. B* **2021**, *9* (16), 3423−3449.
(4) Ma, X.; Lepoitevin, M.; Serre, C. Metal-Organic Frameworks towards Bio-Medical Applications. *Mater. Chem. Front.* **2021**, *5* (15), 5573−5594.
(5) Yang, J.; Yang, Y. W. Metal-Organic Frameworks for Biomedical Applications. *Small* **2020**, *16* (10), 1906846.
(6) Horcajada, P.; Chalati, T.; Serre, C.; Gillet, B.; Sebrie, C.; Baati, T.; Eubank, J. F.; Heurtaux, D.; Clayette, P.; Kreuz, C.; Chang, J. S.; Hwang, Y. K.; Marsaud, V.; Bories, P. N.; Cynober, L.; Gil, S.; Férey, G.; Couvreur, P.; Gref, R. Porous Metal-Organic-Framework Nanoscale Carriers as a Potential Platform for Drug Deliveryand Imaging. *Nat. Mater.* **2010**, *9* (2), 172−178.
(7) Rieter, W. J.; Taylor, K. M. L.; An, H.; Lin, W.; Lin, W. Nanoscale Metal-Organic Frameworks as Potential Multimodal Contrast Enhancing Agents. *J. Am. Chem. Soc.* **2006**, *128* (28), 9024−9025.
(8) Horcajada, P.; Serre, C.; Vallet-Regí, M.; Sebban, M.; Taulelle, F.; Férey, G. Metal-Organic Frameworks as Efficient Materials for Drug Delivery. *Angew. Chemie - Int. Ed.* **2006**, *45* (36), 5974−5978.
(9) Zhou, H.-C.; Long, J. R.; Yaghi, O. M. Introduction to Metal-Organic Frameworks. *Chem. Rev.* **2012**, *112* (2), 673−674.
(10) Zhou, H. C. J.; Kitagawa, S. Metal-Organic Frameworks (MOFs). *Chem. Soc. Rev.* **2014**, *43* (16), 5415−5418.
(11) Velásquez-Hernández, M. de J.; Linares-Moreau, M.; Astria, E.; Carraro, F.; Alyami, M. Z.; Khashab, N. M.; Sumby, C. J.; Doonan, C. J.; Falcaro, P. Towards Applications of Bioentities@MOFs in Biomedicine. *Coord. Chem. Rev.* **2021**, *429*, 213651.
(12) Giménez-Marqués, M.; Hidalgo, T.; Serre, C.; Horcajada, P. Nanostructured Metal-Organic Frameworks and Their Bio-Related Applications. *Coord. Chem. Rev.* **2016**, *307*, 342−360.
(13) Cai, W.; Wang, J.; Chu, C.; Chen, W.; Wu, C.; Liu, G. Metal - Organic Framework-Based Stimuli-Responsive Systems for Drug Delivery. *Adv. Sci.* **2019**, *6* (1), 1801526.
(14) Xu, Q. Y.; Tan, Z.; Liao, X. W.; Wang, C. Recent Advances in Nanoscale Metal-Organic Frameworks Biosensors for Detection of Biomarkers. *Chin. Chem. Lett.* **2022**, *33* (1), 22−32.
(15) Wang, H. S. Metal-Organic Frameworks for Biosensing and Bioimaging Applications. *Coord. Chem. Rev.* **2017**, *349*, 139−155.
(16) Wyszogrodzka, G.; Marszałek, B.; Gil, B.; Dorozyński, P. Metal-Organic Frameworks: Mechanisms of Antibacterial Action and Potential Applications. *Drug Discovery Today* **2016**, *21* (6), 1009−1018.
(17) Shen, M.; Forghani, F.; Kong, X.; Liu, D.; Ye, X.; Chen, S.; Ding, T. Antibacterial Applications of Metal-Organic Frameworks and Their Composites. *Compr. Rev. Food Sci. Food Saf.* **2020**, *19* (4), 1397−1419.
(18) Lan, G.; Ni, K.; Lin, W. Nanoscale Metal-Organic Frameworks for Phototherapy of Cancer. *Coord. Chem. Rev.* **2019**, *379*, 65−81.
(19) Guo, C.; Ma, X.; Wang, B. Metal-Organic Frameworks-Based Composites and Their Photothermal Applications. *Acta Chim. Sin.* **2021**, *79* (8), 967.
(20) Rojas, S.; Arenas-Vivo, A.; Horcajada, P. Metal-Organic Frameworks: A Novel Platform for Combined Advanced Therapies. *Coord. Chem. Rev.* **2019**, *388*, 202−226.
(21) Kelkar, S. S.; Reineke, T. M. Theranostics: Combining Imaging and Therapy. *Bioconjugate Chem.* **2011**, *22* (10), 1879−1903.
(22) Qiu, Y.; Tan, G.; Fang, Y.; Liu, S.; Zhou, Y.; Kumar, A.; Trivedi, M.; Liu, D.; Liu, J. Biomedical Applications of Metal-Organic Framework (MOF)-Based Nano-Enzymes. *New J. Chem.* **2021**, *45* (45), 20987−21000.
(23) Singh, N.; Qutub, S.; Khashab, N. M. Biocompatibility and Biodegradability of Metal Organic Frameworks for Biomedical Applications. *J. Mater. Chem. B* **2021**, *9* (30), 5925−5934.
(24) Ettlinger, R.; Lächelt, U.; Gref, R.; Horcajada, P.; Lammers, T.; Serre, C.; Couvreur, P.; Morris, R. E.; Wuttke, S. Toxicity of Metal-Organic Framework Nanoparticles: From Essential Analyses to Potential Applications. *Chem. Soc. Rev.* **2022**, *51* (2), 464−484.
(25) Linnane, E.; Haddad, S.; Melle, F.; Mei, Z.; Fairen-Jimenez, D. The Uptake of Metal-Organic Frameworks: A Journey into the Cell. *Chem. Soc. Rev.* **2022**, *51* (14), 6065−6086.
(26) Zhao, D.; Zhang, W.; Yu, S.; Xia, S. L.; Liu, Y. N.; Yang, G. J. Application of MOF-Based Nanotherapeutics in Light-Mediated Cancer Diagnosis and Therapy. *J. Nanobiotechnology* **2022**, *20* (1), 1−28.
(27) Sajid, M. Toxicity of Nanoscale Metal Organic Frameworks: A Perspective. *Environ. Sci. Pollut. Res.* **2016**, *23* (15), 14805−14807.
(28) Wuttke, S.; Zimpel, A.; Bein, T.; Braig, S.; Stoiber, K.; Vollmar, A.; Müller, D.; Haastert-Talini, K.; Schaeske, J.; Stiesch, M.; Zahn, G.; Mohmeyer, A.; Behrens, P.; Eickelberg, O.; Bölükbas, D. A.; Meiners, S. Validating Metal-Organic Framework Nanoparticles for Their Nanosafety in Diverse Biomedical Applications. *Adv. Healthc. Mater.* **2017**, *6* (2), 1600818.
(29) Simon-Yarza, T.; Mielcarek, A.; Couvreur, P.; Serre, C. Nanoparticles of Metal-Organic Frameworks: On the Road to In Vivo Efficacy in Biomedicine. *Adv. Mater.* **2018**, *30* (37), 1707365.
(30) Cedrún-Morales, M.; Ceballos, M.; Polo, E.; del Pino, P.; Pelaz, B. Nanosized Metal-Organic Frameworks as Unique Platforms for Bioapplications. *Chem. Commun.* **2023**, *59*, 2869.
(31) Giliopoulos, D.; Zamboulis, A.; Giannakoudakis, D.; Bikiaris, D.; Triantafyllidis, K. Polymer/Metal Organic Framework (MOF) Nanocomposites for Biomedical Applications. *Mol. 2020, Vol. 25, Page 185* **2020**, *25* (1), 185.
(32) Kitao, T.; Zhang, Y.; Kitagawa, S.; Wang, B.; Uemura, T. Hybridization of MOFs and Polymers. *Chem. Soc. Rev.* **2017**, *46* (11), 3108−3133.
(33) Dechnik, J.; Gascon, J.; Doonan, C. J.; Janiak, C.; Sumby, C. J. Mixed-Matrix Membranes. *Angew. Chemie Int. Ed.* **2017**, *56* (32), 9292−9310.
(34) Lian, X.; Fang, Y.; Joseph, E.; Wang, Q.; Li, J.; Banerjee, S.; Lollar, C.; Wang, X.; Zhou, H. C. Enzyme-MOF (Metal-Organic Framework) Composites. *Chem. Soc. Rev.* **2017**, *46* (11), 3386−3401.
(35) Liang, W.; Wied, P.; Carraro, F.; Sumby, C. J.; Nidetzky, B.; Tsung, C. K.; Falcaro, P.; Doonan, C. J. Metal-Organic Framework-Based Enzyme Biocomposites. *Chem. Rev.* **2021**, *121* (3), 1077−1129.
(36) Falcaro, P.; Ricco, R.; Yazdi, A.; Imaz, I.; Furukawa, S.; Maspoch, D.; Ameloot, R.; Evans, J. D.; Doonan, C. J. Application of Metal and Metal Oxide Nanoparticles@MOFs. *Coord. Chem. Rev.* **2016**, *307*, 237−254.
(37) Zheng, G.; Pastoriza-Santos, I.; Pérez-Juste, J.; Liz-Marzán, L. M.; biomaGUNE, C.; Pastoriza-antos, I. Plasmonic Metal-Organic Frameworks. *SmartMat* **2021**, *2* (4), 446−465.

(38) Yuan, N.; Zhang, X.; Wang, L. The Marriage of Metal-Organic Frameworks and Silica Materials for Advanced Applications. *Coord. Chem. Rev.* **2020**, *421*, 213442.
(39) Liu, J.; Huang, M.; Hua, Z.; Dong, Y.; Feng, Z.; Sun, T.; Chen, C. Polyoxometalate-Based Metal Organic Frameworks: Recent Advances and Challenges. *ChemistrySelect* **2022**, *7* (18), No. e202200546.
(40) Buso, D.; Jasieniak, J.; Lay, M. D. H.; Schiavuta, P.; Scopece, P.; Laird, J.; Amenitsch, H.; Hill, A. J.; Falcaro, P. Highly Luminescent Metal-Organic Frameworks Through Quantum Dot Doping. *Small* **2012**, *8* (1), 80−88.
(41) Aguilera-Sigalat, J.; Bradshaw, D. Synthesis and Applications of Metal-Organic Framework-Quantum Dot (QD@MOF) Composites. *Coord. Chem. Rev.* **2016**, *307*, 267−291.
(42) Liu, X. W.; Sun, T. J.; Hu, J. L.; Wang, S. D. Composites of Metal-Organic Frameworks and Carbon-Based Materials: Preparations, Functionalities and Applications. *J. Mater. Chem. A* **2016**, *4* (10), 3584−3616.
(43) Chronopoulos, D. D.; Saini, H.; Tantis, I.; Zbořil, R.; Jayaramulu, K.; Otyepka, M. Carbon Nanotube Based Metal-Organic Framework Hybrids From Fundamentals Toward Applications. *Small* **2022**, *18* (4), 2104628.
(44) Zhu, Q. L.; Xu, Q. Metal-Organic Framework Composites. *Chem. Soc. Rev.* **2014**, *43* (16), 5468−5512.
(45) Lelouche, S. N. K.; Biglione, C.; Horcajada, P. Advances in Plasmonic-Based MOF Composites, Their Bio-Applications, and Perspectives in This Field. *Expert Opin. Drug Delivery* **2022**, *19* (11), 1417−1434.
(46) Aghayi-Anaraki, M.; Safarifard, V. Fe3O4@MOF Magnetic Nanocomposites: Synthesis and Applications. *Eur. J. Inorg. Chem.* **2020**, *2020* (20), 1916−1937.
(47) Zhao, G.; Qin, N.; Pan, A.; Wu, X.; Peng, C.; Ke, F.; Iqbal, M.; Ramachandraiah, K.; Zhu, J. Magnetic Nanoparticles@Metal-Organic Framework Composites as Sustainable Environment Adsorbents. *J. Nanomater.* **2019**, *2019*, 1.
(48) Zhao, H.; Serre, C.; Dumas, E.; Steunou, N. *Functional MOFs as Theranostics*; Elsevier Inc., 2020.
(49) Persano, S.; Das, P.; Pellegrino, T. Magnetic Nanostructures as Emerging Therapeutic Tools to Boost Anti-tumour Immunity. *Cancers (Basel).* **2021**, *13* (11), 2735.
(50) Mody, V. V.; Cox, A.; Shah, S.; Singh, A.; Bevins, W.; Parihar, H. Magnetic Nanoparticle Drug Delivery Systems for Targeting Tumor. *Appl. Nanosci.* **2014**, *4* (4), 385−392.
(51) Estelrich, J.; Escribano, E.; Queralt, J.; Busquets, M. A. Iron Oxide Nanoparticles for Magnetically-Guided and Magnetically-Responsive Drug Delivery. *IJMS* **2015**, *16* (12), 8070−8101.
(52) McBain, S. C.; Yiu, H. H. P.; Dobson, J. Magnetic Nanoparticles for Gene and Drug Delivery. *Int. J. Nanomedicine* **2008**, 3 (2), 169−180.
(53) Kolosnjaj-Tabi, J.; Di Corato, R.; Lartigue, L.; Marangon, I.; Guardia, P.; Silva, A. K. A.; Luciani, N.; Clément, O.; Flaud, P.; Singh, J. V.; Decuzzi, P.; Pellegrino, T.; Wilhelm, C.; Gazeau, F. Heat-Generating Iron Oxide Nanocubes: Subtle "Destructurators" of the Tumoral Microenvironment. *ACS Nano* **2014**, *8* (5), 4268−4283.
(54) lian, Y.; Wang, L.; Cao, J.; Liu, T.; Xu, Z.; Yang, B.; Huang, T.; Jiang, X.; Wu, N. Recent Advances on the Magnetic Nanoparticle-Based Nanocomposites for Magnetic Induction Hyperthermia of Tumor: A Short Review. *Adv. Compos. Hybrid Mater.* **2021**, *4* (4), 925−937.
(55) Felton, C.; Karmakar, A.; Gartia, Y.; Ramidi, P.; Biris, A. S.; Ghosh, A. Magnetic Nanoparticles as Contrast Agents in Biomedical Imaging: Recent Advances in Iron- and Manganese-Based Magnetic Nanoparticles. *Drug Metabolism Reviews*; Taylor & Francis, 2014; pp 142−154.
(56) Israel, L. L.; Galstyan, A.; Holler, E.; Ljubimova, J. Y. Magnetic Iron Oxide Nanoparticles for Imaging, Targeting and Treatment of Primary and Metastatic Tumors of the Brain. *J. Controlled Release* **2020**, *320*, 45−62.
(57) Jeon, M.; Halbert, M. V.; Stephen, Z. R.; Zhang, M. Iron Oxide Nanoparticles as T1 Contrast Agents for Magnetic Resonance Imaging: Fundamentals, Challenges, Applications, and Prospectives. *Adv. Mater.* **2021**, *33* (23), 1906539.
(58) Yu, E. Y.; Bishop, M.; Zheng, B.; Ferguson, R. M.; Khandhar, A. P.; Kemp, S. J.; Krishnan, K. M.; Goodwill, P. W.; Conolly, S. M. Magnetic Particle Imaging: A Novel in Vivo Imaging Platform for Cancer Detection. *Nano Lett.* **2017**, *17* (3), 1648−1654.
(59) Reddy, L. H.; Arias, J. L.; Nicolas, J.; Couvreur, P. Magnetic Nanoparticles: Design and Characterization, Toxicity and Biocompatibility, Pharmaceutical and Biomedical Applications. *Chem. Rev.* **2012**, *112* (11), 5818−5878.
(60) Mahmoudi, M.; Sant, S.; Wang, B.; Laurent, S.; Sen, T. Superparamagnetic Iron Oxide Nanoparticles (SPIONs): Development, Surface Modification and Applications in Chemotherapy. *Adv. Drug Delivery Rev.* **2011**, *63* (1−2), 24−46.
(61) Etemadi, H.; Buchanan, J. K.; Kandile, N. G.; Plieger, P. G. Iron Oxide Nanoparticles: Physicochemical Characteristics and Historical Developments to Commercialization for Potential Technological Applications. *ACS Biomater. Sci. Eng.* **2021**, *7* (12), 5432−5450.
(62) Li, X.; Li, W.; Wang, M.; Liao, Z. Magnetic Nanoparticles for Cancer Theranostics: Advances and Prospects. *J. Controlled Release* **2021**, *335* (June), 437−448.
(63) Martins, P. M.; Lima, A. C.; Ribeiro, S.; Lanceros-Mendez, S.; Martins, P. Magnetic Nanoparticles for Biomedical Applications: From the Soul of the Earth to the Deep History of Ourselves. *ACS Appl. Bio Mater.* **2021**, *4* (8), 5839−5870.
(64) Ricco, R.; Malfatti, L.; Takahashi, M.; Hill, A. J.; Falcaro, P. Applications of Magnetic Metal-Organic Framework Composites. *J. Mater. Chem. A* **2013**, *1* (42), 13033−13045.
(65) Shekhah, O.; Wang, H.; Kowarik, S.; Schreiber, F.; Paulus, M.; Tolan, M.; Sternemann, C.; Evers, F.; Zacher, D.; Fischer, R.; Woll, C. Step-by-Step Route for the Synthesis of Metal-Organic Frameworks. *J. Am. Chem. Soc.* **2007**, *129* (49), 15118−15119.
(66) Levina, A.; Lay, P. A. Chemical Properties and Toxicity of Chromium(III) Nutritional Supplements. *Chem. Res. Toxicol.* **2008**, *21* (3), 563−571.
(67) Férey, C.; Mellot-Draznieks, C.; Serre, C.; Millange, F.; Dutour, J.; Surblé, S.; Margiolaki, I. Chemistry: A Chromium Terephthalate-Based Solid with Unusually Large Pore Volumes and Surface Area. *Science (80-.).* **2005**, *309* (5743), 2040−2042.
(68) Baati, T.; Njim, L.; Neffati, F.; Kerkeni, A.; Bouttemi, M.; Gref, R.; Najjar, M. F.; Zakhama, A.; Couvreur, P.; Serre, C.; Horcajada, P. In Depth Analysis of the in Vivo Toxicity of Nanoparticles of Porous Iron(Iii) Metal-Organic Frameworks. *Chem. Sci.* **2013**, *4* (4), 1597−1607.
(69) Huo, S. H.; Yan, X. P. Facile Magnetization of Metal-Organic Framework MIL-101 for Magnetic Solid-Phase Extraction of Polycyclic Aromatic Hydrocarbons in Environmental Water Samples. *Analyst* **2012**, *137* (15), 3445−3451.
(70) Qian, X.; Zhang, Y.; Jiang, Z.; Wang, D.; Huang, C.; Li, Y. Fe3O4 and Metal-Organic Framework MIL-101(Fe) Composites Catalyze Luminol Chemiluminescence for Sensitively Sensing Hydrogen Peroxide and Glucose. *Talanta* **2018**, *179*, 43−50.
(71) Bellido, E.; Guillevic, M.; Hidalgo, T.; Santander-Ortega, M. J.; Serre, C.; Horcajada, P. Understanding the Colloidal Stability of the Mesoporous MIL-100(Fe) Nanoparticles in Physiological Media. *Langmuir* **2014**, *30* (20), 5911−5920.
(72) Sene, S.; Marcos-Almaraz, M. T.; Menguy, N.; Scola, J.; Volatron, J.; Rouland, R.; Grenèche, J. M.; Miraux, S.; Menet, C.; Guillou, N.; Gazeau, F.; Serre, C.; Horcajada, P.; Steunou, N. Maghemite-NanoMIL-100(Fe) Bimodal Nanovector as a Platform for Image-Guided Therapy. *Chem.* **2017**, *3* (2), 303−322.
(73) Horcajada, P.; Surblé, S.; Serre, C.; Hong, D. Y.; Seo, Y. K.; Chang, J. S.; Grenèche, J. M.; Margiolaki, I.; Férey, G. Synthesis and Catalytic Properties of MIL-100(Fe), an Iron(III) Carboxylate with Large Pores. *Chem. Commun.* **2007**, No. 27, 2820−2822.

https://doi.org/10.1021/acsnanoscienceau.3c00041
ACS Nanosci. Au 2024, 4, 85−114

(74) Xiang, W.; Zhang, Y.; Lin, H.; Liu, C. J. Nanoparticle/Metal-Organic Framework Composites for Catalytic Applications: Current Status and Perspective. *Molecules* **2017**, *22* (12), 2103.
(75) Zhang, Y.; Zhou, Y.; Zhao, Y.; Liu, C. J. Recent Progresses in the Size and Structure Control of MOF Supported Noble Metal Catalysts. *Catal. Today* **2016**, *263*, 61−68.
(76) Ahn, T.; Kim, J. H.; Yang, H. M.; Lee, J. W.; Kim, J. D. Formation Pathways of Magnetite Nanoparticles by Coprecipitation Method. *J. Phys. Chem. C* **2012**, *116* (10), 6069−6076.
(77) Wu, Y. N.; Zhou, M.; Li, S.; Li, Z.; Li, J.; Wu, B.; Li, G.; Li, F.; Guan, X. Magnetic Metal-Organic Frameworks: γ-Fe2O3@MOFs via Confined in Situ Pyrolysis Method for Drug Delivery. *Small* **2014**, *10* (14), 2927−2936.
(78) Park, K. S.; Ni, Z.; Côté, A. P.; Choi, J. Y.; Huang, R.; Uribe-Romo, F. J.; Chae, H. K.; O'Keeffe, M.; Yaghi, O. M. Exceptional Chemical and Thermal Stability of Zeolitic Imidazolate Frameworks. *Proc. Natl. Acad. Sci. U. S. A.* **2006**, *103* (27), 10186−10191.
(79) Loiseau, T.; Serre, C.; Huguenard, C.; Fink, G.; Taulelle, F.; Henry, M.; Bataille, T.; Férey, G. A Rationale for the Large Breathing of the Porous Aluminum Terephthalate (MIL-53) Upon Hydration. *Chem. - A Eur. J.* **2004**, *10* (6), 1373−1382.
(80) Wang, T.; Zhao, P.; Lu, N.; Chen, H.; Zhang, C.; Hou, X. Facile Fabrication of Fe3O4/MIL-101 (Cr) for Effective Removal of Acid Red 1 and Orange G from Aqueous Solution. *Chem. Eng. J.* **2016**, *295*, 403−413.
(81) Wang, T.; Liu, S.; Gao, G.; Zhao, P.; Lu, N.; Lun, X. Magnetic Solid Phase Extraction of Non-Steroidal Anti-Inflammatory Drugs from Water Samples Using a Metal Organic Framework of Type Fe3O4/MIL-101 (Cr), and Their Quantitation by UPLC-MS/MS. *Microchim Acta* **2017**, *184*, 2981−2990.
(82) Doherty, C. M.; Knystautas, E.; Buso, D.; Villanova, L.; Konstas, K.; Hill, A. J.; et al. Magnetic Framework Composites for Polycyclic Aromatic Hydrocarbon Sequestration. *J. Mater. Chem.* **2012**, *22*, 11470−11474.
(83) Falcaro, P.; Lapierre, F.; Marmiroli, B.; Styles, M.; Zhu, Y.; Takahashi, M.; Hill, A. J.; Doherty, C. M. Positioning an Individual Metal-Organic Framework Particle Using a Magnetic Field. *J. Mater. Chem. C* **2013**, *1* (1), 42−45.
(84) Lohe, M. R.; Gedrich, K.; Freudenberg, T.; Kockrick, E.; et al. Heating and Separation Using Nanomagnet-Functionalized Metal-Organic Frameworks. *Chem. Commun.* **2011**, *47*, 3075−3077.
(85) Chui, S. S. Y.; Lo, S. M. F.; Charmant, J. P. H.; Orpen, A. G.; Williams, I. D. A Chemically Functionalizable Nanoporous Material [Cu3(TMA)2 (H2O)3](N). *Science (80-.).* **1999**, *283* (5405), 1148−1150.
(86) Bouson, S.; Krittayavathananon, A.; Phattharasupakun, N.; Siwayaprahm, P.; Sawangphruk, M. Antifungal Activity of Water - Stable Copper - Containing Metal - Organic Frameworks. *R. Soc. Open Sci.* **2017**, *4*, 170654.
(87) Senkovska, I.; Hoffmann, F.; Fröba, M.; Getzschmann, J.; Böhlmann, W.; Kaskel, S. New Highly Porous Aluminium Based Metal-Organic Frameworks: Al(OH)(Ndc) (Ndc = 2,6-Naphthalene Dicarboxylate) and Al(OH)(Bpdc) (Bpdc = 4,40-Biphenyl Dicarboxylate). *Microporous Mesoporous Mater.* **2009**, *122* (1−3), 93−98.
(88) Vinu, M.; Lin, W. C.; Raja, D. S.; Han, J. L.; Lin, C. H. Microwave-Assisted Synthesis of Nanoporous Aluminum-Based Coordination Polymers as Catalysts for Selective Sulfoxidation Reaction. *Polymers (Basel).* **2017**, *9* (10), 498.
(89) Kurisingal, J. F.; Li, Y.; Sagynbayeva, Y.; Chitumalla, R. K.; Vuppala, S.; Rachuri, Y.; Gu, Y.; Jang, J.; Park, D. W. Porous Aluminum-Based DUT Metal-Organic Frameworks for the Transformation of CO2 into Cyclic Carbonates: A Computationally Supported Study. *Catal. Today* **2020**, *352*, 227−236.
(90) Zamani, S.; Abbasi, A.; Masteri-Farahani, M.; Rayati, S. One-Pot, Facile Synthesis and Fast Separation of a UiO-66 Composite by a Metalloporphyrin Using Nanomagnetic Materials for Oxidation of Olefins and Allylic Alcohols. *New J. Chem.* **2022**, *46* (2), 654−662.
(91) Cavka, J. H.; Jakobsen, S.; Olsbye, U.; Guillou, N.; Lamberti, C.; Bordiga, S.; Lillerud, K. P. A New Zirconium Inorganic Building Brick Forming Metal Organic Frameworks with Exceptional Stability. *J. Am. Chem. Soc.* **2008**, *130* (42), 13850−13851.
(92) Stock, N.; Biswas, S. Synthesis of Metal-Organic Frameworks (MOFs): Routes to Various MOF Topologies, Morphologies, and Composites. *Chem. Rev.* **2012**, *112* (2), 933−969.
(93) Schejn, A.; Mazet, T.; Falk, V.; Balan, L.; Aranda, L.; Medjahdi, G.; Schneider, R. Fe3O4@ZIF-8: Magnetically Recoverable Catalysts by Loading Fe3O4 Nanoparticles inside a Zinc Imidazolate Framework. *Dalt. Trans.* **2015**, *44* (22), 10136−10140.
(94) Pandit, P.; Bhagat, S.; Rananaware, P.; Mohanta, Z.; Kumar, M.; Tiwari, V.; Singh, S.; Brahmkhatri, V. P. Iron Oxide Nanoparticle Encapsulated; Folic Acid Tethered Dual Metal Organic Framework-Based Nanocomposite for MRI and Selective Targeting of Folate Receptor Expressing Breast Cancer Cells. *Microporous Mesoporous Mater.* **2022**, *340* (May), 112008.
(95) Fang, J.; Yang, Y.; Xiao, W.; Zheng, B.; Lv, Y.; Liu, X.; Ding, J. Extremely Low Frequency Alternating Magnetic Field-Triggered and MRI-Traced Drug Delivery by Optimized Magnetic Zeolitic Imidazolate Framework-90 Nanoparticles. *Nanoscale* **2016**, *8*, 3259−3263.
(96) Jones, C. G.; Stavila, V.; Conroy, M. A.; Feng, P.; Slaughter, B. V.; Ashley, C. E.; Allendorf, M. D. Versatile Synthesis and Fluorescent Labeling of ZIF-90 Nanoparticles for Biomedical Applications. *ACS Appl. Mater. Interfaces* **2016**, *8*, 7623−7630.
(97) Chen, J.; Liu, J.; Hu, Y.; Tian, Z.; Zhu, Y. Metal-Organic Framework-Coated Magnetite Nanoparticles for Synergistic Magnetic Hyperthermia and Chemotherapy with PH-Triggered Drug Release. *Sci. Technol. Adv. Mater.* **2019**, *20* (1), 1043−1054.
(98) Yaghi, O. M.; Kalmutzki, M. J.; Diercks, C. S. *Introduction to Reticular Chemistry*; Wiley Blackwell, 2019.
(99) Pang, F.; He, M.; Ge, J. Controlled Synthesis of Fe3O4/ZIF-8 Nanoparticles for Magnetically Separable Nanocatalysts. *Chem. - A Eur. J.* **2015**, *21* (18), 6879−6887.
(100) Zhong, Y.; Mao, Y.; Shi, S.; Wan, M.; Ma, C.; Wang, S.; Chen, C.; Zhao, D.; Zhang, N. Fabrication of Magnetic Pd/MOF Hollow Nanospheres with Double-Shell Structure: Toward Highly Efficient and Recyclable Nanocatalysts for Hydrogenation Reaction. *ACS Appl. Mater. Interfaces* **2019**, *11* (35), 32251−32260.
(101) Chowdhuri, A. R.; Bhattacharya, D.; Sahu, S. K. Magnetic Nanoscale Metal Organic Frameworks for Potential Targeted Anticancer Drug Delivery, Imaging and as an MRI Contrast Agent. *Dalt. Trans.* **2016**, *45* (7), 2963−2973.
(102) Chowdhuri, A. R.; Singh, T.; Ghosh, S. K.; Sahu, S. K. Carbon Dots Embedded Magnetic Nanoparticles @Chitosan @Metal Organic Framework as a Nanoprobe for PH Sensitive Targeted Anticancer Drug Delivery. *ACS Appl. Mater. Interfaces* **2016**, *8*, 16573−16583.
(103) Britt, D.; Tranchemontagne, D.; Yaghi, O. M. Metal-Organic Frameworks with High Capacity and Selectivity for Harmful Gases. *Proc. Natl. Acad. Sci. U. S. A.* **2008**, *105* (33), 11623−11627.
(104) Eddaoudi, M.; Kim, J.; Rosi, N.; Vodak, D.; Wachter, J.; O'Keeffe, M.; Yaghi, O. M. Systematic Design of Pore Size and Functionality in Isoreticular MOFs and Their Application in Methane Storage. *Science (80-.).* **2002**, *295* (5554), 469−472.
(105) Taghavi, F.; Khojastehnezhad, A.; Khalifeh, R.; Rajabzadeh, M.; Rezaei, F.; et al. Design and Synthesis of a New Magnetic Metal Organic Framework as a Versatile Platform for Immobilization of Acidic Catalysts and CO2 Fixation Reaction. *New J. Chem.* **2021**, *45*, 15405.
(106) Lu, G.; Li, S.; Guo, Z.; Farha, O. K.; Hauser, B. G.; Qi, X.; Wang, Y.; Wang, X.; Han, S.; Liu, X.; Duchene, J. S.; Zhang, H.; Zhang, Q.; Chen, X.; Ma, J.; Loo, S. C. J.; Wei, W. D.; Yang, Y.; Hupp, J. T.; Huo, F.; Chye, S.; Loo, J.; Wei, W. D.; Yang, Y.; Hupp, J. T. Imparting Functionality to a Metal-Organic Framework Material by Controlled Nanoparticle Encapsulation. *Nat. Chem.* **2012**, *4*, 310−316.
(107) Li, J.; Wang, J.; Ling, Y.; Chen, Z.; Gao, M.; Zhang, X.; Zhou, Y. Unprecedented Highly Efficient Capture of Glycopeptides by Fe3O4@Mg-MOF-74 Core-Shell Nanoparticles. *Chem. Commun.* **2017**, *53* (28), 4018−4021.

(108) Li, L.; Xu, Y.; Zhong, D.; Zhong, N. CTAB-Surface-Functionalized Magnetic MOF@MOF Composite Adsorbent for Cr(VI) Efficient Removal from Aqueous Solution. *Colloids Surfaces A Physicochem. Eng. Asp.* **2020**, *586* (Vi), 124255.
(109) Cullity, B. D.; Graham, C. D. *Introduction to Magnetic Materials*; John Wiley & Sons, Inc., 2008.
(110) Fock, J.; Bogart, L. K.; González-Alonso, D.; Espeso, J. I.; Hansen, M. F.; Varón, M.; Frandsen, C.; Pankhurst, Q. A. On the "centre of Gravity" Method for Measuring the Composition of Magnetite/ Maghemite Mixtures, or the Stoichiometry of Magnetite-Maghemite Solid Solutions, via 57 Fe Mössbauer Spectroscopy. *J. Phys. D Appl. Phys. J. Phys. D Appl. Phys.* **2017**, *50* (16pp), 265005.
(111) Chen, Y.; Huang, X.; Feng, X.; Li, J.; Huang, Y.; et al. Facile Fabrication of Magnetically Recyclable Metal-Organic Framework Nanocomposites for Highly Efficient and Selective Catalytic Oxidation of Benzylic C-H Bonds. *Chem. Commun.* **2014**, *50*, 8374−8377.
(112) Chen, Y.; Huang, X.; Zhang, S.; Li, S.; Cao, S.; Pei, X.; Zhou, J.; Feng, X.; Wang, B. Shaping of Metal-Organic Frameworks: From Fluid to Shaped Bodies and Robust Foams. *J. Am. Chem. Soc.* **2016**, *138*, 10810−10813.
(113) Yang, S.; Zhang, Z.-H.; Chen, Q.; He, M.-Y.; Wang, L. Magnetically Recyclable Metal-Organic Framework@Fe3O4 Composite-Catalyzed Facile Reduction of Nitroarene Compounds in Aqueous Medium. *Appl. Organomet. Chem.* **2018**, *32* (3), 1−6.
(114) Wang, L.; Yang, S.; Chen, L.; Yuan, S.; Chen, Q.; He, M.-Y.; Zhang, Z.-H. Magnetically Recyclable Cu-BTC@Fe3O4 Composite-Catalyzed C(Aryl)-S-P Bond Formation Using Aniline, P(O) H Compounds and Sulfur Powder. *Catal. Sci. Technol.* **2017**, *7*, 2356−2361.
(115) Hou, C.; Wang, Y.; Ding, Q.; Jiang, L.; Li, M.; Zhu, W.; Pan, D.; Zhu, H.; Liu, M. Facile Synthesis of Enzyme-Embedded Magnetic Metal-Organic Frameworks as a Reusable Mimic Multi-Enzyme System: Mimetic Peroxidase Properties and Colorimetric Sensor. *Nanoscale* **2015**, *7*, 18770−18779.
(116) Lin, J.; Xin, P.; An, L.; Xu, Y.; Tao, C.; Tian, Q.; Zhou, Z.; Hu, B.; Yang, S. Fe3O4-ZIF-8 Assemblies as PH and Glutathione Responsive: T2- T1 Switching Magnetic Resonance Imaging Contrast Agent for Sensitive Tumor Imaging in Vivo. *Chem. Commun.* **2019**, *55* (4), 478−481.
(117) Yu, Y.; Zhong, Y.; Xie, D.; Luo, G.; Mao, Y.; Yuan, M.; Xiao, W.; Wang, S.; Chen, C. Fe3O4 Nanorods Coated with ZIF-8 and Decorated with Pt Nanoparticles as Magnetically Actuated Nanoscale Stirring Bars for Catalytic Dye Degradation, H2Production, and Hydrogenation of Olefins. *ACS Appl. Nano Mater.* **2021**, *4* (10), 10999−11006.
(118) Huo, J.; Xu, L.; Yang, J. E.; Cui, H.; Yuan, B.; Fu, M. Magnetic Responsive Fe3O4-ZIF-8 Core-Shell Composites for Efficient Removal of As(III) from Water. *Colloids Surfaces A* **2018**, *539*, 59−68.
(119) Zheng, J.; Lin, Z.; Lin, G.; Yang, H.; Zhang, L. Preparation of Magnetic Metal-Organic Framework Nanocomposites for Highly Specific Separation of Histidine-Rich Proteins. *J. Mater. Chem. B* **2015**, *3*, 2185−2191.
(120) Li, Y.; Tang, J.; He, L.; Liu, Y.; Liu, Y.; Chen, C.; Tang, Z. Core-Shell Upconversion Nanoparticle@Metal-Organic Framework Nanoprobes for Luminescent/Magnetic Dual-Mode Targeted Imaging. *Adv. Mater.* **2015**, *27* (27), 4075−4080.
(121) Chen, G.; Yu, B.; Lu, C.; Zhang, H.; Shen, Y.; Cong, H. Controlled Synthesis of Fe3O4@ZIF-8 Nanoparticles for Drug Delivery. *CrystEngComm* **2018**, *20* (46), 7486−7491.
(122) Ettlinger, R.; Moreno, N.; Ziółkowska, N.; Ullrich, A.; Krug von Nidda, H. A.; Jirák, D.; Kerl, K.; Bunzen, H. In Vitro Studies of Fe3O4-ZIF-8 Core-Shell Nanoparticles Designed as Potential Theragnostics. *Part. Part. Syst. Charact.* **2020**, *37* (12), 1−9.
(123) Luo, Z.; Sun, D.; et al. DNA Nanotetrahedron Linked Dual-Aptamer Based Voltammetric Aptasensor for Cardiac Troponin I Using a Magnetic Metal-Organic Framework as a Label. *Microchim Acta* **2019**, *186* (374), 1−10.
(124) Ahmadijokani, F.; Tajahmadi, S.; Heidarian, M.; Bahi, A.; Rezakazemi, M.; Molavi, H.; Ko, F.; Arjmand, M. Fe3O4@PAA@UiO-66-NH2Magnetic Nanocomposite for Selective Adsorption of Quercetin. *Chemosphere* **2021**, *275*, 130087.
(125) Ahmadipouya, S.; Heidarian, M.; Ahmadijokani, F.; Jarahiyan, A.; Molavi, H. Magnetic Fe3O4@UiO-66 Nanocomposite for Rapid Adsorption of Organic Dyes from Aqueous Solution. *J. Mol. Liq.* **2021**, *322*, 114910.
(126) Alijani, H.; Noori, A.; Faridi, N.; Bathaie, S. Z.; Mousavi, M. F. Aptamer-Functionalized Fe3O4@MOF Nanocarrier for Targeted Drug Delivery and Fluorescence Imaging of the Triple-Negative MDA-MB-231 Breast Cancer Cells. *J. Solid State Chem.* **2020**, *292*, 121680.
(127) Zhang, C.; Yan, L.; Wang, X.; Zhu, S.; Chen, C.; Gu, Z.; Zhao, Y. Progress, Challenges, and Future of Nanomedicine. *Nano Today* **2020**, *35*, 101008.
(128) Yang, Q.; Zhao, Q.; Ren, S.; Lu, Q.; Guo, X.; Chen, Z. Fabrication of Core-Shell Fe3O4@MIL-100 (Fe) Magnetic Microspheres for the Removal of Cr(VI) in Aqueous Solution. *J. Solid State Chem.* **2016**, *244*, 25−30.
(129) Tregubov, A. A.; Sokolov, I. L.; Babenyshev, A. V.; Nikitin, P. I.; Cherkasov, V. R.; Nikitin, M. P. Magnetic Hybrid Magnetite/Metal Organic Framework Nanoparticles: Facile Preparation, Post-Synthetic Biofunctionalization and Tracking in Vivo with Magnetic Methods. *J. Magn. Magn. Mater.* **2018**, *449*, 590−596.
(130) Li, S.; Bi, K.; Xiao, L.; Shi, X. Facile Preparation of Magnetic Metal Organic Frameworks Core - Shell Nanoparticles for Stimuli-Responsive Drug Carrier. *Nanotechnology* **2017**, *28*, 495601.
(131) García Márquez, A.; Demessence, A.; Platero-Prats, A. E.; Heurtaux, D.; Horcajada, P.; Serre, C.; Chang, J. S.; Férey, G.; De La Peña-O'Shea, V. A.; Boissière, C.; Grosso, D.; Sanchez, C. Green Microwave Synthesis of MIL-100(Al, Cr, Fe) Nanoparticles for Thin-Film Elaboration. *Eur. J. Inorg. Chem.* **2012**, *2012* (32), 5165−5174.
(132) Tsuchida, T.; Fukushima, J.; Takizawa, H. Decrease in the Crystallite Diameter of Solid Crystalline Magnetite around the Curie Temperature by Microwave Magnetic Fields Irradiation. *Nanomaterials* **2021**, *11* (4), 984.
(133) Li, Y.; Lo, W. S.; Zhang, F.; Si, X.; Chou, L. Y.; Liu, X. Y.; Williams, B. P.; Li, Y. H.; Jung, S. H.; Hsu, Y. S.; Liao, F. S.; Shieh, F. K.; Ismail, M. N.; Huang, W.; Tsung, C. K. Creating an Aligned Interface between Nanoparticles and MOFs by Concurrent Replacement of Capping Agents. *J. Am. Chem. Soc.* **2021**, *143* (13), 5182−5190.
(134) Hu, P.; Morabito, J. V.; Tsung, C. K. Core-Shell Catalysts of Metal Nanoparticle Core and Metal-Organic Framework Shell. *ACS Catal.* **2014**, *4* (12), 4409−4419.
(135) Zhuang, J.; Kuo, C.-H.; Chou, L.-Y.; Liu, D.-Y.; Weerapana, E.; Tsung, C.-K. Optimized Metal-Organic-Framework Nanospheres for Drug Delivery: Evaluation of Small-Molecule Encapsulation. *ACS Nano* **2014**, *8* (3), 2812−2819.
(136) Zhang, T.; Zhang, X.; Yan, X.; Kong, L.; Zhang, G.; Liu, H.; et al. Synthesis of Fe3O4@ZIF-8 Magnetic Core - Shell Microspheres and Their Potential Application in a Capillary Microreactor. *Chem. Eng. J.* **2013**, *228*, 398−404.
(137) Yang, J.; Chen, Y.; Li, Y.; Yin, X. Magnetic Resonance Imaging-Guided Multi-Drug Chemotherapy and Photothermal Synergistic Therapy with PH and NIR-Stimulation Release. *ACS Appl. Mater. Interfaces* **2017**, *9*, 22278−22288.
(138) Zhao, M.; Zhang, X.; Deng, C. Rational Synthesis of Novel Recyclable Fe3O4@MOF Nanocomposites for Enzymatic Digestion. *Chem. Commun.* **2015**, *51* (38), 8116−8119.
(139) Deng, Y.; Li, D.; et al. Preparation of Iron-Based MIL-101 Functionalized Polydopamine@Fe3O4Magnetic Composites for Extracting Sulfonylurea Herbicides from Environmental Water and Vegetable Samples. *J. Sep. Sci.* **2018**, *41*, 2046−2055.
(140) Zhao, M.; Deng, C.; Zhang, X. The Design and Synthesis of a Hydrophilic Core-Shell-Shell Structured Magnetic Metal-Organic Framework as a Novel Immobilized Metal Ion Affinity Platform for

https://doi.org/10.1021/acsnanoscienceau.3c00041
ACS Nanosci. Au 2024, 4, 85−114

Phosphoproteome Research. *Chem. Commun.* **2014**, *50* (47), 6228−6231.
(141) Lu, D.; Qin, M.; Liu, C.; Deng, J.; Shi, G.; Zhou, T. Ionic Liquid-Functionalized Magnetic Metal-Organic Framework Nanocomposites for Efficient Extraction and Sensitive Detection of Fluoroquinolone Antibiotics in Environmental Water. *ACS Appl. Mater. Interfaces* **2021**, *13*, 5357−5367.
(142) Zhao, H. X.; Zou, Q.; Sun, S. K.; Yu, C.; Zhang, X.; Li, R. J.; Fu, Y. Y. Theranostic Metal-Organic Framework Core-Shell Composites for Magnetic Resonance Imaging and Drug Delivery. *Chem. Sci.* **2016**, *7* (8), 5294−5301.
(143) He, M.; Zhou, J.; Chen, J.; Zheng, F.; Wang, D.; et al. Fe3O4@carbon@zeolitic Imidazolate Framework-8 Nanoparticles as Multifunctional PH-Responsive Drug Delivery Vehicles for Tumor Therapy in Vivo. *J. Mater. Chem. B* **2015**, *3*, 9033.
(144) Deng, Y.; Qi, D.; Deng, C.; Zhang, X.; Zhao, D. Superparamagnetic High-Magnetization Microspheres with an Fe 3O4@SiO2 Core and Perpendicularly Aligned Mesoporous SiO2 Shell for Removal of Microcystins. *J. Am. Chem. Soc.* **2008**, *130* (1), 28−29.
(145) Ding, H. L.; Zhang, Y. X.; Wang, S.; Xu, J. M.; Xu, S. C.; Li, G. H. Fe3O4@SiO2 Core/Shell Nanoparticles: The Silica Coating Regulations with a Single Core for Different Core Sizes and Shell Thicknesses. *Chem. Mater.* **2012**, *24* (23), 4572−4580.
(146) Hu, Y.; Zheng, S.; Zhang, F. Fabrication of MIL-100(Fe)@SiO2@Fe3O4 Core-Shell Microspheres as a Magnetically Recyclable Solid Acidic Catalyst for the Acetalization of Benzaldehyde and Glycol. *Front. Chem. Sci. Eng.* **2016**, *10* (4), 534−541.
(147) Lajevardi, A.; Sadr, M. H.; Yaraki, M. T.; Badiei, A.; Armaghan, M. A PH-Responsive and Magnetic Fe3O4@silica@MIL-100(Fe)/b-CD Nanocomposite as a Drug Nanocarrier: Loading and Release Study of Cephalexin. *New J. Chem.* **2018**, *42*, 9690−9701.
(148) Lajevardi, A.; Hossaini Sadr, M.; Badiei, A.; Armaghan, M. Synthesis and Characterization of Fe3O4@SiO2@MIL-100(Fe) Nanocomposite: A Nanocarrier for Loading and Release of Celecoxib. *J. Mol. Liq.* **2020**, *307*, 112996.
(149) Jia, Y.; Su, H.; Wong, Y. E.; Chen, X.; Chan, T. D. Thermo-Responsive Polymer Tethered Metal-Organic Framework Core-Shell Magnetic Microspheres for Magnetic Solid-Phase Extraction of Alkylphenols from Environmental Water Samples. *J. Chromatogr. A* **2016**, *1456*, 42−48.
(150) Yang, Q.; et al. Simultaneous Detection and Removal of Organophosphorus Pesticide by A Novel Zr-MOF Based Smart Adsorbent. *J. Mater. Chem. A* **2018**, *6*, 2184−2192.
(151) Huang, L.; He, M.; Chen, B.; Hu, B. Designable Magnetic MOF Composite and Facile Coordination-Based Post-Synthetic Strategy for Enhanced Removal of Hg2+ from Water. *J. Mater. Chem. A* **2015**, *3*, 11587−11595.
(152) Shekhah, O.; Wang, H.; Zacher, D.; Fischer, R. A.; Wöll, C. Growth Mechanism of Metal-Organic Frameworks: Insights into the Nucleation by Employing a Step-by-Step Route. *Angew. Chemie - Int. Ed.* **2009**, *48* (27), 5038−5041.
(153) Shekhah, O.; Wang, H.; Paradinas, M.; Ocal, C.; Schüpbach, B.; Terfort, A.; Zacher, D.; Fischer, R. A.; Wöll, C. Controlling Interpenetration in Metal-Organic Frameworks by Liquid-Phase Epitaxy. *Nat. Mater.* **2009**, *8* (6), 481−484.
(154) Ke, F.; Qiu, L. G.; Yuan, Y. P.; Jiang, X.; Zhu, J. F. Fe3O4@MOF Core-Shell Magnetic Microspheres with a Designable Metal-Organic Framework Shell. *J. Mater. Chem.* **2012**, *22* (19), 9497−9500.
(155) Li, L.; Ke, K.; Fan, L.; Hong, W.; Shun, Z.; Liu, L. Layer by Layer Assembly Synthesis of Fe3O4@MOFs/GO Core-Shell Nanoparticles. *Mater. Lett.* **2014**, *126*, 197−201.
(156) Zhao, M.; Deng, C.; Zhang, X.; Yang, P. Facile Synthesis of Magnetic Metal Organic Frameworks for the Enrichment of Low-Abundance Peptides for MALDI-TOF MS Analysis. *Proteomics* **2013**, *13* (23−24), 3387−3392.
(157) Wu, Y.; Ma, Y.; Xu, G.; Wei, F.; Ma, Y.; Song, Q.; Wang, X.; Tang, T.; Song, Y.; Shi, M.; Xu, X.; Hu, Q. Metal-Organic Framework Coated Fe3O4Magnetic Nanoparticles with Peroxidase-like Activity for Colorimetric Sensing of Cholesterol. *Sensors Actuators B. Chem.* **2017**, *249*, 195−202.
(158) Ke, X.; Song, X.; Qin, N.; Cai, Y.; Ke, F. Rational Synthesis of Magnetic Fe3O4@MOF Nanoparticles for Sustained Drug Delivery. *J. Porous Mater.* **2019**, *26* (3), 813−818.
(159) Fan, J.; Chen, D.; Li, N.; Xu, Q.; Li, H.; He, J.; Lu, J. Adsorption and Biodegradation of Dye in Wastewater with Fe3O4@MIL-100 (Fe) Core-Shell Bio-Nanocomposites. *Chemosphere* **2018**, *191*, 315−323.
(160) Wang, D.; Zhou, J.; Chen, R.; Shi, R.; Xia, G.; Zhou, S.; Liu, Z.; Zhang, N. Q.; Wang, H.; Guo, Z.; Chen, Q. Magnetically Guided Delivery of DHA and Fe Ions for Enhanced Cancer Therapy Based on PH-Responsive Degradation of DHA-Loaded Fe3O4@C@MIL-100(Fe) Nanoparticles. *Biomaterials* **2016**, *107*, 88−101.
(161) Wang, X.; Xu, J.; Yang, D.; Sun, C.; Sun, Q.; He, F.; Gai, S.; et al. Fe3O4@MIL-100(Fe)-UCNPs Heterojunction Photosensitizer: Rational Design and Application in near Infrared Light Mediated Hypoxic Tumor Therapy. *Chem. Eng. J.* **2018**, *354*, 1141−1152.
(162) Ke, F.; Jiang, J.; Li, Y.; Liang, J.; Wan, X.; Ko, S. Highly Selective Removal of Hg2+ and Pb2+ by Thiol-Functionalized Fe3O4@metal-Organic Framework Core-Shell Magnetic Microspheres. *Appl. Surf. Sci.* **2017**, *413*, 266−274.
(163) Chen, X.; Ding, N.; Zang, H.; Yeung, H.; Zhao, R.; Cheng, C.; Liu, J.; Chan, T. D. Fe3O4@MOF Core-Shell Magnetic Microspheres for Magnetic Solid-Phase Extraction of Polychlorinated Biphenyls from Environmental Water Samples. *J. Chromatogr. A* **2013**, *1304*, 241−245.
(164) Zhang, C. F.; Qiu, L. G.; Ke, F.; Zhu, Y. J.; Yuan, Y. P.; Xu, G. S.; Jiang, X. A Novel Magnetic Recyclable Photocatalyst Based on a Core-Shell Metal-Organic Framework Fe3O4@MIL-100(Fe) for the Decolorization of Methylene Blue Dye. *J. Mater. Chem. A* **2013**, *1* (45), 14329−14334.
(165) Ke, F.; Qiu, L.-G.; Zhu, J. Fe3O4@MOF Core-Shell Magnetic Microspheres as Excellent Catalysts for the Claisen-Schmidt Condensation Reaction. *Nanoscale* **2014**, *6*, 1596−1601.
(166) Xiong, Z.; Ji, Y.; Fang, C.; Zhang, Q.; Zhang, L.; et al. Facile Preparation of Core - Shell Magnetic Metal - Organic Framework Nanospheres for the Selective Enrichment of Endogenous Peptides. *Chem. - A Eur. J.* **2014**, *20*, 7389.
(167) Chen, Y.; Xiong, Z.; Peng, L.; Gan, Y.; Zhao, Y.; Shen, J.; Qian, J.; Zhang, L.; Zhang, W. Facile Preparation of Core-Shell Magnetic Metal-Organic Framework Nanoparticles for the Selective Capture of Phosphopeptides. *ACS Appl. Mater. &I nterfaces* **2015**, *7*, 16338−16347.
(168) Ke, F.; Wang, L.; Zhu, J. Multifunctional Au-Fe3O4@MOF Core-Shell Nanocomposite Catalysts with Controllable Reactivity and Magnetic Recyclability. *Nanoscale* **2015**, *7*, 1201−1208.
(169) Yu, S.; Wan, J.; Chen, K. A Facile Synthesis of Superparamagnetic Fe3O4 Supraparticles@MIL-100(Fe) Core-Shell Nanostructures: Preparation, Characterization and Biocompatibility. *J. Colloid Interface Sci.* **2016**, *461*, 173−178.
(170) Zheng, J.; Cheng, C.; Fang, W.; Chen, C.; Yan, R. Surfactant-Free Synthesis of a Fe3O4@ZIF-8 Core-Shell Heterostructure for Adsorption of Methylene Blue. *CrystEngComm* **2014**, *16*, 3960−3964.
(171) Liu, H.; Chen, L.; Ding, J. A Core-Shell Magnetic Metal Organic Framework of Type Fe3O4@ZIF-8 for the Extraction of Tetracycline Antibiotics from Water Samples Followed by Ultra-HPLC-MS Analysis. *Microchim Acta* **2017**, *184*, 4091−4098.
(172) Bian, R.; Wang, T.; Zhang, L.; Li, L.; Wang, C. A Combination of Tri-Modal Cancer Imaging and in Vivo Drug Delivery by Metal-Organic Framework Based Composite Nanoparticles. *Biomater. Sci.* **2015**, *3* (9), 1270−1278.
(173) Chen, R.; Tao, C.; Zhang, Z.; Chen, X.; Liu, Z.; Wang, J. Layer-by-Layer Fabrication of Core-Shell Fe3O4@UiO-66-NH2 with High Catalytic Reactivity toward the Hydrolysis of Chemical Warfare Agent Simulants. *ACS Appl. Mater. Interfaces* **2019**, *11*, 43156−43165.
(174) Li, W.; Li, G.; Liu, D. Synthesis and Application of Core-Shell Magnetic Metal-Organic Framework Composites Fe3O4/ IRMOF-3. *RSC Adv.* **2016**, *6*, 94113−94118.

(175) Miao, Z.; Shu, X.; Ramella, D. Synthesis of a Fe3O4@P4VP@ metal-Organic Framework Core-Shell Structure and Studies of Its Aerobic Oxidation Reactivity. *RSC Adv.* **2017**, *7* (5), 2773−2779.
(176) Jiang, Y. P.; Fang, X. H.; Wang, Q.; Huo, J. Z.; Liu, Y. Y.; Wang, X. R.; Ding, B. Near-Infrared Magnetic Core-Shell Nanoparticles Based on Lanthanide Metal-Organic Frameworks as a Ratiometric Felodipine Sensing Platform. *Commun. Chem.* **2023**, *6* (1), 1−10.
(177) McKinlay, A. C.; Morris, R. E.; Horcajada, P.; Férey, G.; Gref, R.; Couvreur, P.; Serre, C. BioMOFs: Metal-Organic Frameworks for Biological and Medical Applications. *Angew. Chemie - Int. Ed.* **2010**, *49* (36), 6260−6266.
(178) Simon-Yarza, T.; Rojas, S.; Horcajada, P.; Serre, C. The Situation of Metal-Organic Frameworks in Biomedicine. *Compr. Biomater. II* **2017**, 719−749.
(179) Wang, Y.; Yan, J.; Wen, N.; Xiong, H.; Cai, S.; He, Q.; Hu, Y.; Peng, D.; Liu, Z.; Liu, Y. Metal-Organic Frameworks for Stimuli-Responsive Drug Delivery. *Biomaterials* **2020**, *230*, 119619.
(180) Lawson, H. D.; Walton, S. P.; Chan, C. Metal-Organic Frameworks for Drug Delivery: A Design Perspective. *ACS Appl. Mater. Interfaces* **2021**, *13* (6), 7004−7020.
(181) Meng, F.; Zhong, Y.; Cheng, R.; Deng, C.; Zhiyuan, Z. PH-Sensitive Polymeric Nanoparticles for Tumor-Targeting Doxorubicin Delivery: Concept and Recent Advances. *Nanomedicine* **2014**, *9* (3), 487−499.
(182) Barenholz, Y. Doxil® - The First FDA-Approved Nano-Drug: Lessons Learned. *J. Controlled Release* **2012**, *160* (2), 117−134.
(183) Horcajada, P.; Chevreau, H.; Heurtaux, D.; Benyettou, F.; Salles, F.; Devic, T.; Garcia-Marquez, A.; Yu, C.; Lavrard, H.; Dutson, C. L.; Magnier, E.; Maurin, G.; Elkaïm, E.; Serre, C. Extended and Functionalized Porous Iron(Iii) Tri- or Dicarboxylates with MIL-100/101 Topologies. *Chem. Commun.* **2014**, *50* (52), 6872−6874.
(184) Yang, Y.; Xia, F.; Yang, Y.; Gong, B.; Xie, A.; Shen, Y.; Zhu, M. Litchi-like Fe3O4@Fe-MOF Capped with HAp Gatekeepers for PH-Triggered Drug Release and Anticancer Effect. *J. Mater. Chem. B* **2017**, *5*, 8600−8606.
(185) Cheng, C.; Li, C.; Zhu, X.; Han, W.; et al. Doxorubicin-Loaded Fe3O4-ZIF-8 Nano-Composites for Hepatocellular Carcinoma Therapy. *J. Biomater. Appl.* **2019**, *33*, 1373.
(186) Ren, H.; Zhang, L.; An, J.; Wang, T.; Li, L.; Si, X.; He, L.; Wu, X.; Wang, C.; Su, Z. Polyacrylic Acid@zeolitic Imidazolate Framework-8 Nanoparticles with Ultrahigh Drug Loading Capability for PH-Sensitive Drug Release. *Chem. Commun.* **2014**, *50* (8), 1000−1002.
(187) Zheng, H.; Xing, L.; Cao, Y.; Che, S. Coordination Bonding Based PH-Responsive Drug Delivery Systems. *Coord. Chem. Rev.* **2013**, *257* (11−12), 1933−1944.
(188) Fernandes, N.; Rodrigues, C. F.; Moreira, A. F.; Correia, I. J. Overview of the Application of Inorganic Nanomaterials in Cancer Photothermal Therapy. *Biomater. Sci.* **2020**, *8* (11), 2990−3020.
(189) Xue, Z.; Zhu, M.; Dong, Y.; Feng, T.; Chen, Z.; Feng, Y.; Shan, Z.; Xu, J.; Meng, S. An Integrated Targeting Drug Delivery System Based on the Hybridization of Graphdiyne and MOFs for Visualized Cancer Therapy. *Nanoscale* **2019**, *11*, 11709−11718.
(190) Gavilán, H.; Avugadda, S. K.; Fernández-Cabada, T.; Soni, N.; Cassani, M.; Mai, B. T.; Chantrell, R.; Pellegrino, T. Magnetic Nanoparticles and Clusters for Magnetic Hyperthermia: Optimizing Their Heat Performance and Developing Combinatorial Therapies to Tackle Cancer. *Chem. Soc. Rev.* **2021**, *50* (20), 11614−11667.
(191) Avugadda, S. K.; Materia, M. E.; Nigmatullin, R.; Cabrera, D.; Marotta, R.; Cabada, T. F.; Marcello, E.; Nitti, S.; Artés-Ibañez, E. J.; Basnett, P.; Wilhelm, C.; Teran, F. J.; Roy, I.; Pellegrino, T. Esterase-Cleavable 2D Assemblies of Magnetic Iron Oxide Nanocubes: Exploiting Enzymatic Polymer Disassembling to Improve Magnetic Hyperthermia Heat Losses. *Chem. Mater.* **2019**, *31* (15), 5450−5463.
(192) Bilalis, P.; Tziveleka, L. A.; Varlas, S.; Iatrou, H. PH-Sensitive Nanogates Based on Poly(l-Histidine) for Controlled Drug Release from Mesoporous Silica Nanoparticles. *Polym. Chem.* **2016**, *7* (7), 1475−1485.
(193) Minotti, G.; Menna, P.; Salvatorelli, E.; Cairo, G.; Gianni, L. Anthracyclines: Molecular Advances and Pharmacologie Developments in Antitumor Activity and Cardiotoxicity. *Pharmacol. Rev.* **2004**, *56* (2), 185−229.
(194) Beraldo, H.; Garnier-Suillerot, A.; Tosi, L.; Lavelle, F. Iron(III)-Adriamycin and Iron(III)-Daunorubicin Complexes: Physicochemical Characteristics, Interaction with DNA, and Antitumor Activity. *Biochemistry* **1985**, *24* (2), 284−289.
(195) Dalmark, M.; Storm, H. H. A Fickian Diffusion Transport Process with Features of Transport Catalysis. Doxorubicin Transport in Human Red Blood Cells. *J. Gen. Physiol.* **1981**, *78* (4), 349−364.
(196) Nakanishi, T.; Fukushima, S.; Okamoto, K.; Suzuki, M.; Matsumura, Y.; Yokoyama, M.; Okano, T.; Sakurai, Y.; Kataoka, K. Development of the Polymer Micelle Carrier System for Doxorubicin. *J. Controlled Release* **2001**, *74* (1−3), 295−302.
(197) Krishna, R.; Mayer, L. D. Multidrug Resistance (MDR) in Cancer: Mechanisms, Reversal Using Modulators of MDR and the Role of MDR Modulators in Influencing the Pharmacokinetics of Anticancer Drugs. *Eur. J. Pharm. Sci.* **2000**, *11* (4), 265−283.
(198) Cabrera-García, A.; Checa-Chavarria, E.; Rivero-Buceta, E.; Moreno, V.; Fernández, E.; Botella, P. Amino Modified Metal-Organic Frameworks as PH-Responsive Nanoplatforms for Safe Delivery of Camptothecin. *J. Colloid Interface Sci.* **2019**, *541*, 163−174.
(199) Kumar, C. S. S. R.; Mohammad, F. Magnetic Nanomaterials for Hyperthermia-Based Therapy and Controlled Drug Delivery. *Adv. Drug Delivery Rev.* **2011**, *63* (9), 789−808.
(200) Raouf, I.; Khalid, S.; Khan, A.; Lee, J.; Kim, H. S.; Kim, M. H. A Review on Numerical Modeling for Magnetic Nanoparticle Hyperthermia: Progress and Challenges. *J. Therm. Biol.* **2020**, *91* (April), 102644.
(201) Mehdaoui, B.; Meffre, A.; Carrey, J.; Lachaize, S.; Lacroix, L. M.; Gougeon, M.; Chaudret, B.; Respaud, M. Optimal Size of Nanoparticles for Magnetic Hyperthermia: A Combined Theoretical and Experimental Study. *Adv. Funct. Mater.* **2011**, *21* (23), 4573−4581.
(202) Hadadian, Y.; Masoomi, H.; Dinari, A.; Ryu, C.; Hwang, S.; Kim, S.; Cho, B. K.; Lee, J. Y.; Yoon, J. From Low to High Saturation Magnetization in Magnetite Nanoparticles: The Crucial Role of the Molar Ratios between the Chemicals. *ACS Omega* **2022**, *7*, 15996.
(203) Ni, D.; Bu, W.; Ehlerding, E. B.; Cai, W.; Shi, J. Engineering of Inorganic Nanoparticles as Magnetic Resonance Imaging Contrast Agents. *Chem. Soc. Rev.* **2017**, *46* (23), 7438−7468.
(204) Armstrong, P. Magnetic Resonance in Medicine: The Basic Textbook of the European Magnetic Resonance Forum, 3rd ed., Rinck, P.A. (Ed.), Blackwell Scientific Publications, UK (1993). *Clin. Radiol.* **1994**, *49* (11), 842.
(205) Lee, N.; Yoo, D.; Ling, D.; Cho, M. H.; Hyeon, T.; Cheon, J. Iron Oxide Based Nanoparticles for Multimodal Imaging and Magnetoresponsive Therapy. *Chem. Rev.* **2015**, *115* (19), 10637−10689.
(206) Peller, M.; Böll, K.; Zimpel, A.; Wuttke, S. Metal-Organic Framework Nanoparticles for Magnetic Resonance Imaging. *Inorg. Chem. Front.* **2018**, *5* (8), 1760−1779.
(207) Bunzen, H.; Jirák, D. Recent Advances in Metal-Organic Frameworks for Applications in Magnetic Resonance Imaging. *ACS Appl. Mater. Interfaces* **2022**, *14*, 50445−50462.
(208) Rohrer, M.; Bauer, H.; Mintorovitch, J.; Requardt, M.; Weinmann, H. J. Comparison of Magnetic Properties of MRI Contrast Media Solutions at Different Magnetic Field Strengths. *Invest. Radiol.* **2005**, *40* (11), 715−724.
(209) Tang, Y.; Wang, X.; Li, J.; Nie, Y.; Liao, G.; Yu, Y.; Li, C. Overcoming the Reticuloendothelial System Barrier to Drug Delivery with a "Don't-Eat-Us" Strategy. *ACS Nano* **2019**, *13*, 13015.
(210) Osterrieth, J. W. M.; Fairen-Jimenez, D. Metal-Organic Framework Composites for Theragnostics and Drug Delivery Applications. *Biotechnol. J.* **2021**, *16* (2), 2000005 DOI: 10.1002/biot.202000005.

(211) Wen, T.; Quan, G.; Niu, B.; Zhou, Y.; Zhao, Y.; Lu, C.; Pan, X.; Wu, C. Versatile Nanoscale Metal-Organic Frameworks (NMOFs): An Emerging 3D Nanoplatform for Drug Delivery and Therapeutic Applications. *Small* **2021**, *17* (8), 1−26.
(212) Zhang, Y.; Yang, L.; Yan, L.; Wang, G.; Liu, A. Recent Advances in the Synthesis of Spherical and NanoMOF-Derived Multifunctional Porous Carbon for Nanomedicine Applications. *Coord. Chem. Rev.* **2019**, *391*, 69−89.
(213) Yang, P.; Chen, Z.; Liu, S.; Qiao, C.; Xia, Y.; Wang, Z. Recent Progress in Drug Delivery and Cancer Theranostic Built from Metal-Organic Framework. *Biomed. Mater.* **2021**, *16* (4), 042011.
(214) Carrillo-Carrión, C. Nanoscale Metal-Organic Frameworks as Key Players in the Context of Drug Delivery: Evolution toward Theranostic Platforms. *Anal. Bioanal. Chem.* **2020**, *412* (1), 37−54.
(215) Pala, R.; Pattnaik, S.; Zeng, Y.; Busi, S.; Nauli, S. M.; Liu, G. *Functional MOFs as Molecular Imaging Probes and Theranostics*; Elsevier Inc., 2020.
(216) Beg, S.; Jain, A.; Saini, S.; Sharma, T.; Saquib Hasnain, M.; Kazmi, I.; Rahman, M.; Akhter, S.; Singh, B. *Metal-Organic Frameworks as Expanding Hybrid Carriers with Diverse Therapeutic Applications*; Elsevier Inc., 2018.
(217) Zheng, Q.; Liu, X.; Zheng, Y.; et al. The Recent Progress on Metal - Organic Frameworks for Phototherapy. *Chem. Soc. Rev.* **2021**, *50* (8), 5086−5125.
(218) Nappini, S.; Fogli, S.; Castroflorio, B.; Bonini, M.; Baldelli Bombelli, F.; Baglioni, P. Magnetic Field Responsive Drug Release from Magnetoliposomes in Biological Fluids. *J. Mater. Chem. B* **2016**, *4* (4), 716−725.
(219) De Paoli, V. M.; De Paoli Lacerda, S. H.; Spinu, L.; Ingber, B.; Rosenzweig, Z.; Rosenzweig, N. Effect of an Oscillating Magnetic Field on the Release Properties of Magnetic Collagen Gels. *Langmuir* **2006**, *22* (13), 5894−5899.
(220) Liu, T. Y.; Hu, S. H.; Liu, K. H.; Liu, D. M.; Chen, S. Y. Study on Controlled Drug Permeation of Magnetic-Sensitive Ferrogels: Effect of Fe3O4 and PVA. *J. Controlled Release* **2008**, *126* (3), 228−236.
(221) Nappini, S.; Bonini, M.; Bombelli, F. B.; Pineider, F.; Sangregorio, C.; Baglioni, P.; Nordèn, B. Controlled Drug Release under a Low Frequency Magnetic Field: Effect of the Citrate Coating on Magnetoliposomes Stability. *Soft Matter* **2011**, *7* (3), 1025−1037.
(222) Nappini, S.; Bonini, M.; Ridi, F.; Baglioni, P. Structure and Permeability of Magnetoliposomes Loaded with Hydrophobic Magnetic Nanoparticles in the Presence of a Low Frequency Magnetic Field. *Soft Matter* **2011**, *7* (10), 4801−4811.
(223) Nappini, S.; Bombelli, F. B.; Bonini, M.; Nordèn, B.; Baglioni, P. Magnetoliposomes for Controlled Drug Release in the Presence of Low-Frequency Magnetic Field. *Soft Matter* **2010**, *6* (1), 154−162.
(224) Okada, T.; Fujimoto, K.; Fushimi, Y.; Akasaka, T.; Thuy, D. H. D.; Shima, A.; Sawamoto, N.; Oishi, N.; Zhang, Z.; Funaki, T.; Nakamoto, Y.; Murai, T.; Miyamoto, S.; Takahashi, R.; Isa, T. Neuroimaging at 7 T: A Pictorial Narrative Review. *Quant. Imaging Med. Surg.* **2022**, *12* (6), 3406−3435.
(225) Wu, M. X.; Gao, J.; Wang, F.; Yang, J.; Song, N.; Jin, X.; Mi, P.; Tian, J.; Luo, J.; Liang, F.; Yang, Y. W. Multistimuli Responsive Core-Shell Nanoplatform Constructed from Fe3O4@MOF Equipped with Pillar[6]Arene Nanovalves. *Small* **2018**, *14* (17), 1704440−170445.
(226) Zhang, H.; Li, Y.; Chen, Y.; Wang, M.; Wang, X.; Yin, X. Fluorescence and Magnetic Resonance Dual-Modality Imaging-Guided Photothermal and Photodynamic Dual-Therapy with Magnetic Porphyrin-Metal Organic Framework Nanocomposites. *Sci. Rep.* **2017**, *7*, 44153.

https://doi.org/10.1021/acsnanoscienceau.3c00041
ACS Nanosci. Au 2024, 4, 85−114